The Pennsylvania State University

The Graduate School

SYNAPSE-INSPIRED MAGNETO-RESPONSIVE MATERIAL

A Thesis in

Mechanical Engineering

by

Amal Mohamed Badri

Submitted in Partial Fulfillment
of the Requirements
for the Degree of

Master of Science

August 2021

The thesis of Amal Mohamed Badri was reviewed and approved by the following:

Zoubeida Ounaies
Professor of Mechanical Engineering
Thesis Co-Advisor

Joseph Najem
Assistant Professor of Mechanical Engineering
Thesis Co-Advisor

Paris Von Lockette
Associate Professor of Mechanical Engineering

Karen Thole
Department Head of Mechanical Engineering

ABSTRACT

Learning and memory have inspired the research and discovery of materials that can mimic brain synapses, with applications in signal processing and computing. Synapses are junctions that allow neurons to transfer chemical and electrical signals among each other and are integral to the function of the brain. This study aims to fabricate and characterize artificial synapses using magneto-responsive materials, consisting of oleic acid-coated magnetic iron oxide microparticles dispersed in an organic solvent matrix. The broad goal is to design these materials so that they can emulate short-term synaptic plasticity via voltage-dependent changes in conductance. An optimum iron oxide to oleic acid weight ratio of 0.45 and mechanical stirring was employed to enhance dispersion and control the sedimentation rate of the material. Effects of other parameters such as volume fraction and carrier fluid viscosity were also investigated. In general, it was found that an increase in volume fraction of the particle and increase in viscosity of the carrier fluid resulted in a reduction in sedimentation rate, due to the higher drag forces experienced by the particles. Once the fabrication method was determined, the next step focused on the effect of the external magnetic field on the particle assembly. Application of a low-strength continuous and cyclic magnetic field leads to the formation of chain-like assemblies of iron oxide microparticles within the insulating matrix, which results in analog and hysteretic changes in conductance. Our work demonstrates that the application of a magnetic field increases the viscosity of the insulating matrix, which impacts the rates of chain formation and decay. Low, medium and high viscosities of the material were fabricated and characterized to understand the impact of viscosity on electrical conductance changes. Under the application of a continuous magnetic field, as viscosity increases, chain formation and changes in conductance with time slow down. Further, we find that a cyclic application of the magnetic field leads to changes in electrical conductance dependent on the viscosity of the carrier fluid. The resulting changes in conductance are driven by the interplay

between drag and magnetic dipole-dipole forces acting on the material. Both low and high viscosity samples exhibited the synaptic plasticity state of facilitation, while medium viscosity samples displayed depression. The results of this research demonstrate promise and potential in terms of enabling artificial synapses and their functions using magneto-responsive material. By conducting further theoretical and experimental work such as using a larger viscosity range, different cycle times, and focusing on the fluids mechanics of the system, the material can be tailored to mimic artificial synapses.

TABLE OF CONTENTS

LIST OF FIGURES

LIST OF TABLES

ACKNOWLEDGEMENTS

I wish to express my sincere appreciation to my advisors, Dr. Zoubeida Ounaies and Dr. Joseph Najem for their continuous mentorship and support throughout my master's journey. I am especially grateful for the opportunity to work with Dr. Ounaies, an inspiring leader and role model to women in STEM. Her mentorship, guidance, advice, and support taught me how to succeed as a female leader in engineering. I would also like to recognize the Foreign Fulbright program and the United Arab Emirates Ministry of Higher Education for funding my master's program. Without their financial support, the goals of this project could not have been accomplished. The technical support and expertise from my lab members at the EMClab and AIMSlab, as well as Dr. Amira Meddeb, Dr. Paris Von Lockette, Ebrahim El Hag Ali, and Saeed Saifaee are truly appreciated. I wish to also bring to light the boundless support and love of my parents and siblings, Khalid, Shahad, and Farah, who always believed in me and constantly kept me going when challenges seemed too difficult to overcome. I would not be where I am if it was not for my family setting an amazing example of the impact of hard work and encouraging me to always pursue my goals and dreams. I am immensely indebted to have my parents as role models in my life and my siblings as my inspiration and support system. Finally, I would like to extend my deepest gratitude to Yasmeen AlAwadhi and Hamad Aljaberi for their endless emotional and mental support throughout my journey and particularly on trying days. Their enthusiasm and motivation led me to successfully complete my thesis away from home and during a pandemic.

1 Introduction

1.1 Motivation

In recent years, there has been a surge of research focused on materials and devices that emulate biological synapses and exhibit synaptic plasticity, called artificial synapses [1]–[4] . Synapses are junctions that allow neurons to transfer chemical and electrical signals among each other and are integral to the function of the brain. Artificial synapses are a step towards achieving engineered materials that demonstrate brain-like properties, such as efficiency and adaptability. Synaptic plasticity plays a vital role in the brain's ability to adapt and learn via the alteration of the strength and efficiency of synaptic transmission [5]–[7]. Such brain-inspired devices and materials show promising applications that go far beyond computing. By learning from their environment and adapting accordingly, artificial synapses can be used to enhance the efficiency of everyday applications that require sensing and actuation (see section 1.2.2).

Magneto-responsive materials can be manipulated to approximate the biological activity of the synapse and emulate their function. Chemical composition and property changes of a magneto-responsive material show similarities to the conformation and functioning of the synapse. Under the influence of one external stimulus, namely magnetic field, magneto-responsive materials can exhibit multiple changes in properties including electrical conductivity, viscosity, and stiffness. Similarly, the brain uses one frequency-dependent stimulus to generate several varying plasticity states in the synapse. The motion of magnetoactive particles in the material resembles the movement of neurotransmitters across synapses, while the base fluid resembles the medium that allows neurotransmitters to move. Moreover, the formation and redistribution of conducting paths of magnetic particles under the influence of an external magnetic field lead to property changes in

the material. The strength and speed of chain formation in the material correlate to the concentration and speed of neurotransmitters moving between neurons, responsible for different plasticity states in the brain (see section 1.2.1).

Currently, magneto-responsive materials are being used in various industries such as automobile, health, defense, and aerospace, with applications including vibration control, brakes, clutches, control valves, power steering pumps, artificial joints, engine mounts, and drug delivery [8]–[10]. Despite the many functions of these materials, and to the best of our knowledge, there is currently no research that is looking into relating the property changes of magneto-responsive materials to synaptic functions.

The broad goal of this thesis is to further the advancement of magneto-responsive materials as potential artificial synapses. By altering the composition of magneto-responsive materials, the response of the material under an external magnetic field can change to achieve varying synaptic functions.

1.2 Background

1.2.1 Biological Synapses and Functions

Synapses are junctions that connect neurons in the brain and allow the transmission of information in the form of action potentials through highly specific chemicals known as neurotransmitters [5], [8]. Even though there are different types of synapses present in biological systems, the fundamental process of synaptic transmission is the same. A change in voltage called an action potential, allows the presynaptic membrane potential to depolarize and initiate synaptic functions [9]. Sufficient current is needed to raise the voltage in the neurons above the threshold value and generate an action potential. The action potential activates channels, releasing

neurotransmitters that travel from the presynaptic neuron to the postsynaptic neuron via the synaptic cleft as shown in figure **1-1**. The concentration, type, and timing of the release of neurotransmitters differ, resulting in the phenomenon of short-term presynaptic plasticity.

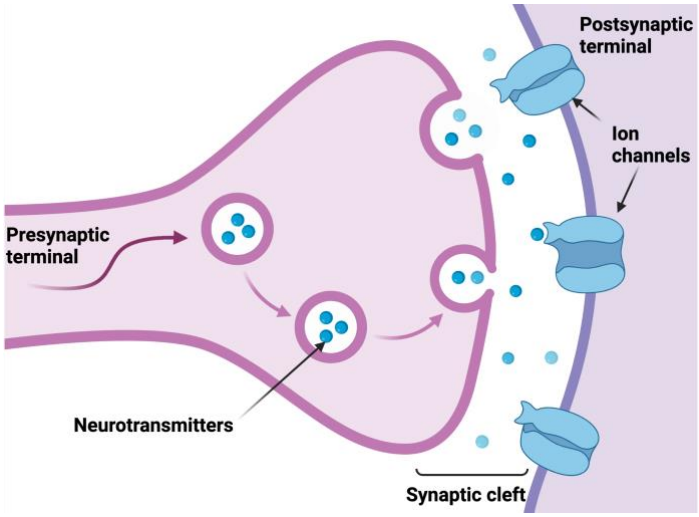

Figure 1-1: Schematic of the main parts of a synapse

Synaptic plasticity is the primary mechanism for learning and memory in the brain. The mechanism can be described as the change in the synaptic strength between neurons in response to voltage patterns of the presynaptic action potential. Synaptic strength can be explained as the connection strength between two neurons, which is dependent on the concentration, speed, and timing of neurotransmitters released. The connection also referred to as synaptic weight, is static and reformed in both the short-term and long-term [6], [11]–[13]. Important synaptic functions include long-term plasticity (LTP) and short-term plasticity (STP) [10]. Long-term plasticity is essential in forming memory in the brain and the activity-dependent changes can last from hours to days. The effect of plasticity on the synaptic weight and extent of neurotransmitters released can be seen in figure 1-2. Long-term plasticity can be classified into potentiation and depression. Potentiation results in a long-lasting increase in synaptic strength as repeated stimulation lead to more neurotransmitters being released over a long period of time. Long-term depression results in

the weakening of the synapse for extended periods as repeated simulation leads to fewer neurotransmitters being released over a longer period of time as shown in figure [6], [10], [14]–[16].

In contrast, short-term plasticity plays a crucial role in synaptic computation and information processing [17], [18]. This form of plasticity occurs when the change in synaptic weight lasts from an order of milliseconds to at most a few minutes [11], [19]. Short-term plasticity can be categorized into two main categories: facilitation and depression [15], [18]. Short-term depression occurs when multiple spaced stimuli are evoked consecutively, leading to fewer neurotransmitter releases and a weaker response after the second spike compared to the first spike [19]. Short-term depression is correlated to a low pass filter, reducing postsynaptic response and overall synaptic weight [9], [20] as shown in figure 1-2 and 1-3. Short-term facilitation occurs when multiple spaced stimuli are evoked consecutively, leading to a greater concentration of neurotransmitter release and an enhanced response after the second spike compared to the first spike [19]. Short-term facilitation is correlated to a high pass filter, augmenting postsynaptic response and overall synaptic strength as shown in figure 1-2 and 1-3 [21][17].

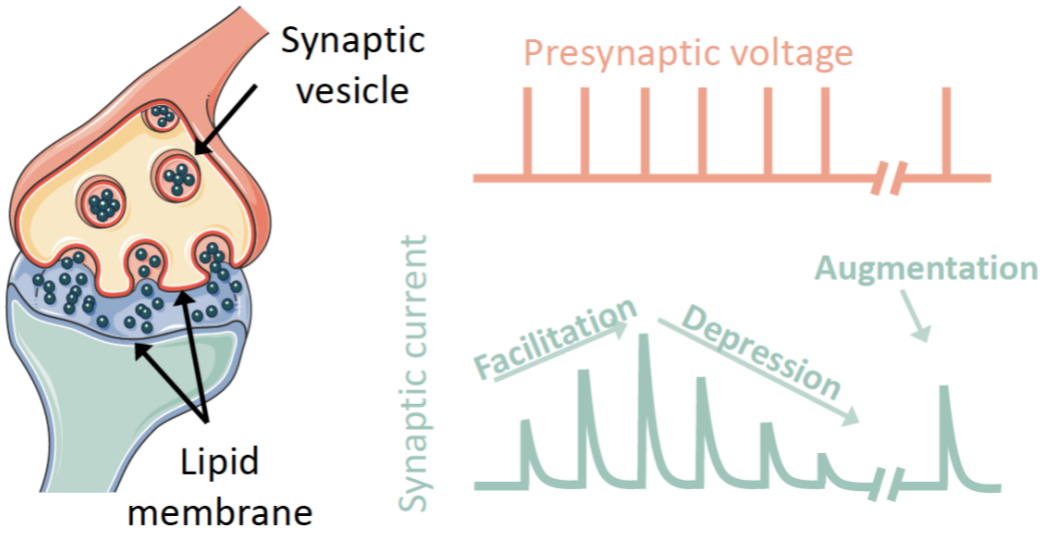

Figure 1-2: Facilitation and depression states in the synapse correlating to stronger and weaker synaptic current respectively

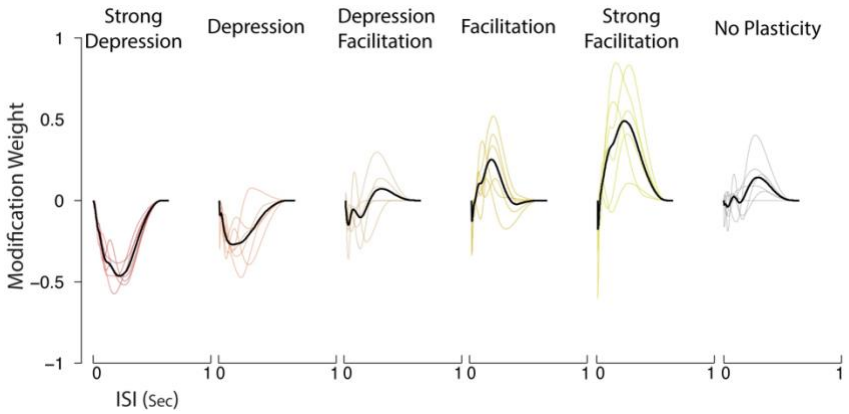

Figure 1-3: Effect of depression and facilitation on synaptic weight [21]

1.2.2 Artificial Synapses and Memristors

Memristors are resistance switches that display a variable and non-volatile or volatile electrical resistance, dependent on the history of the applied voltage and current. The four fundamental two-terminal circuit elements include resistors, capacitors, inductors, and memristors as shown in figure 1-4 (a). Each element relates two primary circuit variables to each other: electric current (*i*), voltage (*v*), charge (*q*) and flux (φ) [22] . Memristors exhibit a unique feature called a "pinched hysteresis loop" at (0,0) as shown in figure 1-4 (b) [23], which makes the devices distinct from other two-terminal electronic components [24], [25]. Many materials and devices hold potential in exhibiting the distinctive characteristics of a memristor. Examples of memristors currently investigated in the literature, using both organic and inorganic materials, include magnetic tunnel junctions [3], polymers, donor-acceptor complexes, ferroelectric materials, phase change materials [26], vacancy migration-based materials, and conductive filament-based devices [22], [27]–[29]. Memristors are explored as potential artificial synapses because of their ability to emulate the plasticity behavior of a synapse and are currently seen as the best approach to realize artificial synapses by researchers in the field [5], [6], [8], [24], [26], [30].

Artificial synapses are devices that simulate the function of the synapses in the brain. Existing literature on artificial synapses provides inspiration for the development of model materials that can exhibit variable resistance states controlled by one external stimulus. Artificial synapses researched include, but are not limited to, complementary metal-oxide-semiconductor circuits [1], resistive and conductance switching memory [30], oxide-based devices [8], [25], [31], charge trap memory [32], renewable materials [6], electrochemical devices [24], carbon-nanotube based memory elements [2], and Ag_2S inorganic synapse [15]. Resistance switching behavior and synaptic plasticity can potentially be shown more simply using magnetoactive particles dispersed in an insulating matrix. The magneto-responsive material will allow access to multiple synaptic states via the property changes it exhibits from the external stimulus, thus demonstrating synaptic plasticity using a single device.

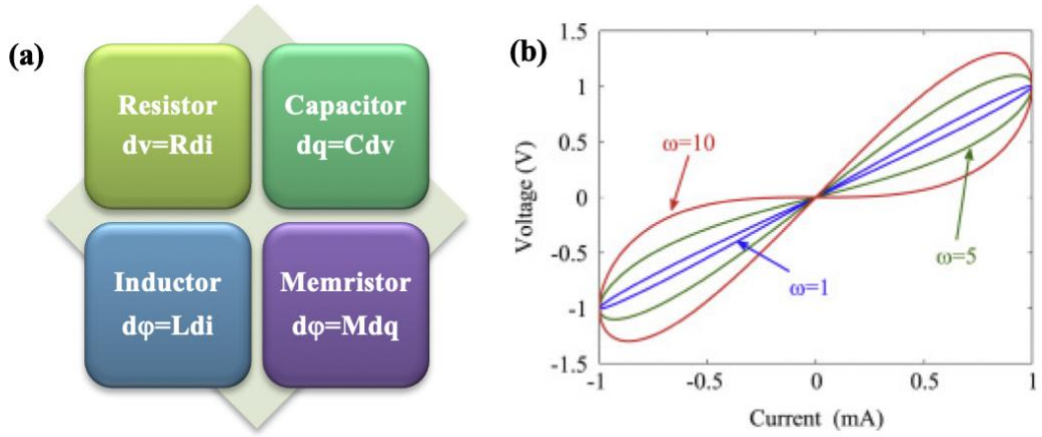

Figure 1-4: (a) Fundamental circuit elements and the respective variables, (b) Pinched hysteresis loop characteristic of a memristor [23]

1.2.3 Magneto-Responsive Materials

Smart materials are materials that change one or more of their properties when exposed to an external stimulus such as temperature, stress, light, electric, or magnetic fields, and are currently used to fabricate artificial synapses [8], [15], [33], [34]. Examples of smart materials include, but are not limited to magnetorheological fluid, ferrofluids, electrorheological fluid, piezoelectric materials, and shape memory alloy [35]. A magneto-responsive material is a type of smart material that changes its properties when exposed to an external magnetic field. Under a magnetic field, magneto-responsive materials exhibit overall structural and property changes. Magnetoactive particles create a complex dense structure of chains that reduce motion in the carrier fluid and increase the viscosity and stiffness of the material. Complete chains also provide conductive paths that reduce the resistance of the material. The rheological changes and non-Newtonian behavior of the material occur on a millisecond timescale. The changes in properties under a fast response time make magneto-responsive materials widely studied and researched to develop state-of-the-art technologies.

Magneto-responsive materials are made of ferromagnetic particles that respond to an external magnetic field by magnetizing and changing their macroscopic properties. Atoms in ferromagnetic particles group together into domains separated by domain walls, where unpaired electrons spin parallel to each other and hold the same magnetic orientation. Domain walls are boundaries between domains and are transition zones that change direction with magnetization [36]. Depending on the size of the magnetic particles, they either have a single domain or multidomain structures as shown in figure 1-5. The domain size is important to understand the physical, chemical, and magnetic properties of the particle. At the microscale, the particles exhibit a multidomain structure. As the particle size reduces to the nanoscale regime, the particles modify

to achieve a single domain structure [37]. The critical radius value to achieve a single domain structure is 30 – 60nm for iron oxide particles. When the size of the particle is reduced below the critical radius, the particle becomes superparamagnetic, which occurs at around 4-20nm for iron oxide particles [38].

Superparamagnetism occurs in sufficiently small magnetic particles with single domains. Thermal fluctuations can randomly flip the orientation of the magnetic moment of the particle between its two most stable states. Instantaneously, a superparamagnetic particle is very magnetized because the thermal energy is sufficient to flip the moment of all the particles and compel a new conformation[39]. The time in between two flips is called the Neel relaxation time. However, over a period of time much longer than the Neel relaxation time, the magnetization of the particles averages to zero. This is termed the superparamagnetic state. Under the influence of an external magnetic field, the magnetic force causes the spin of the particles to align towards the direction of the magnetic flux, leading to the particles in their magnetized state. When the external magnetic field is removed, the particles return to random spin orientation, completely demagnetizing [40]. This leads to zero coercivity and remanence of the particle (see section 2.3). A single domain particle, outside of the superparamagnetic range, however, can exhibit some coercivity and remanence.

On the other hand, multidomain structures involve many domain groups within the same particle. As the particle size increases, refer to figure 1-5 [38], domain walls become energetically favorable creating the multidomain state. Each domain contains magnetic moments aligned in the same direction. Within the same domain group, a magnetic field exists. However, in the bulk sample, the overall magnetic moments are randomly orientated with respect to each other, rendering the bulk material macroscopically non-magnetic. When an external magnetic field is applied, most of the magnetic moments in the domain align parallel to the magnetic field lines. This leads to the

particles magnetizing. When the external magnetic field is removed, the particles tend to maintain some magnetization and thus exhibit both remanence and coercivity (see section 2.3).

Magnets can be categorized into either soft or hard magnets depending on coercivity as shown in figure 1-6 (see section 2.2.2). Figure 1-6 displays the difference in the hysteresis loop and coercivity between hard and soft magnets. It is important to note that the remanence magnetization, or the B^r value, between hard and soft magnets are not the same. Hard Magnets have higher remanence magnetization values than soft magnets. Figure 1-6 is used to demonstrate the difference in coercivity in soft and hard magnets. Soft magnets retain lower values of magnetization in the absence of an external field, and so require a lower coercive force to demagnetize. However, this also means they have high permeability and can be easily magnetized. Magnetic material is soft when its magnetic domains can easily migrate. On the other hand, if the domain walls are difficult to migrate, a higher magnetic field is required to align magnetic moments, and the magnet is considered hard [36]. Hard magnets possess a high coercivity value implying that they retain their magnetization more and require a larger force to demagnetize [41], as shown by their H_c value in figure 1-6[42].

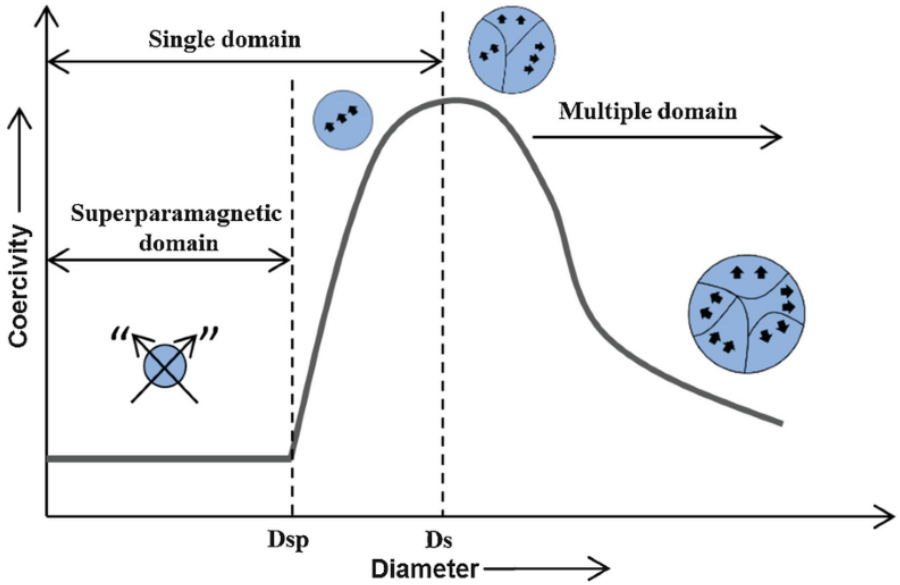

Figure 1-5: Effect of particle size on domain structure of magnetic iron oxide particles [38]

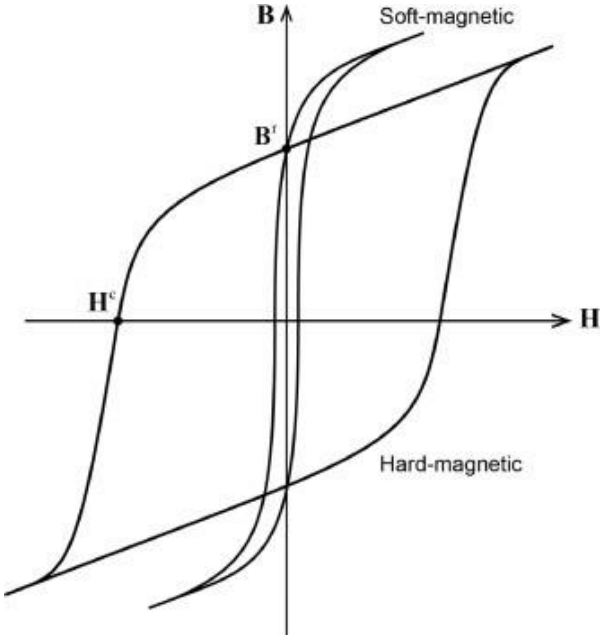

Figure 1-6: Magnetization curve shows the difference between the hysteresis loop and coercivity of a hard vs soft magnet [42]

1.2.4 Composition of Magneto-Responsive Materials

Magneto-responsive materials are a two-phase system made up of magnetic particles, functionalized using a stabilizing additive, dispersed in a non-magnetic carrier fluid [35]. This thesis focuses on using micron-sized iron oxide (Fe_3O_4) magnetite particles as the magnetic particles dispersed in motor oil and silicone oil of various viscosities. Iron oxide microparticles are soft magnets, non-toxic, widely available, bio-friendly, and cheap [43]. Iron oxide particles tend to agglomerate because of magnetic dipole-dipole forces, Van der Waal forces, and high surface energy. The iron oxide particles are hydrophobic without surface coating and the attractive magnetic forces lead to clusters of the particles, reducing its stability and use.

Different factors can reduce sedimentation of particles such as mixing method, temperature, pH, type of carrier fluid, particle size, additive type, and ratio [44]–[46]. The most

common method to reduce sedimentation is by attaching a surfactant to the surface of the particles [47]–[49]. The surfactant consists of both hydrophilic and lipophilic groups making it interactive with both the particles and carrier fluid. The hydrophilic end absorbs on the particle surface and the lipophilic end interacts with the carrier fluid. This functionalization prevents particle sedimentation and improves the polarizability of the magnetoactive particles [50]. In addition to improving stability, the surfactant plays an important role in determining the physicochemical and magnetic properties of the particle[49]. Moreover, the carrier fluid provides the insulating medium to disperse the particles and makes up the majority composition of the magneto-responsive material. The type of carrier fluid, volume, and initial viscosity state also affect both the extent of the property changes of the material and the stability of the suspension.

1.2.5 Magnetic and Fluidic Forces

In its initial state, when no external stimulus is applied, the particles are randomly distributed in the non-magnetic medium and the material behaves like the carrier fluid as shown in figure 1-7. Under the influence of an external magnetic field, the magneto-responsive material undergoes a reversible transformation from liquid to a semi-solid state [41], [51], [52]. The particles form a chain-like columnar structure parallel to the magnetic field flux line as shown in figure 1-8. The particle is influenced by two external forces; magnetic and fluidic. The magnetic force is generated by the gradient of the external magnetic field and the fluidic force by the insulating medium on the moving particle. Each particle carries a magnetic moment and adjacent particles interact via both van der Waal forces and a long-range dipole-dipole interaction potential that is directional in nature [53].

The changes in a magneto-responsive material properties is the result of a magnetic dipole induced in each particle by the application of the external magnetic field and the interaction

between the dipole and the magnetic field. The dipoles are represented by magnetic moment vectors. Under no magnetic field application, the particles are randomly orientated and dispersed in the carrier fluid, due to Brownian motion. Upon application of a magnetic field, there comes a moment where the interaction energy between the magnetic moment and the magnetic field exceeds the Brownian thermal energy. Past this moment, the dipole aligns head to tail and nearby particles are dragged in proximity, minimizing potential magnetic energy and forming chains. The external magnetic field induces a magnetic dipole in the particles which enhances the attractive dipole-dipole interaction between them. This causes the self-assembly of the particles into a columnar structure.

The attractive dipole-dipole forces depends on the configuration of the two dipole. Because the dipole force has components along the radial and orthoradial axis, a force momentum and torque aligns particles in a head to tail configuration in the direction of the applied magnetic field [54] . The force is attractive up to a critical angle and then it becomes repulsive. That is why separate chains are forming along the magnetic moment axis and not across the axis. The angle is between the direction of the external magnetic field and the center line that connects two particles. As shown in figure 1-9 below, when the center line that connects the particles and the magnetic flux lines are parallel, an attractive force forms between the particles. However, when the center line of adjacent particles are perpendicular to the flux lines, the force between the particles are repulsive. This phenomenon causes the chains to form along the flux lines. Chain structures causes the the change in properties between the on-state and off-state condition of the material, as well as the flow behavior of the fluid [55].

In addition, the viscosity of the material under no external stimulus, or the off viscosity, is affected by both the inherent viscosity of the carrier fluid and the volume fraction of the suspension [41]. The off viscosity of the carrier fluid impacts the fluidic forces acting on the particle. Choosing a high starting viscosity will lead to both high viscosity of the suspension

without a magnetic field and a smaller and slower response of the material to changes in the external stimuli. The reduced response is due to larger viscous forces acting on the particles and opposing the attractive magnetic forces, decreasing the overall motion of the particle and slowing down chain formation. Meanwhile, a low viscosity carrier fluid will lower the viscous forces on the particles, leading to sedimentation problems that make the material inapplicable, but also a faster response and overall motion of the particle.

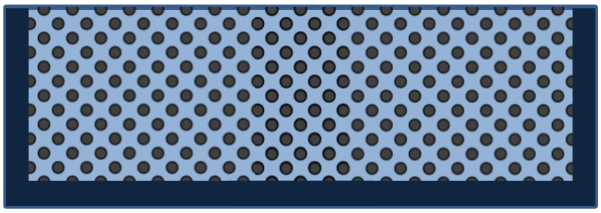

Figure 1-7: Magnetoactive particles dispersed uniformly in a carrier fluid under no external magnetic field

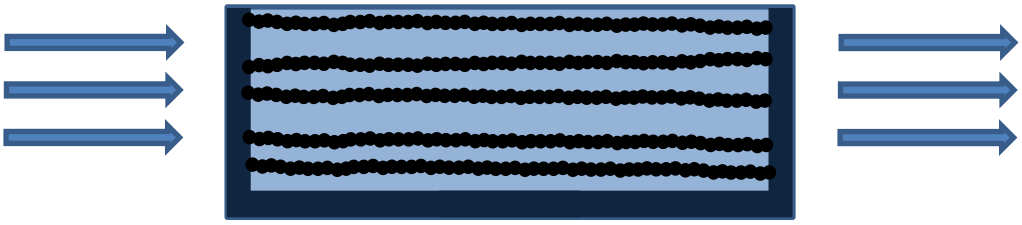

Figure 1-8: Chain formation of particles under the influence of an external magnetic field

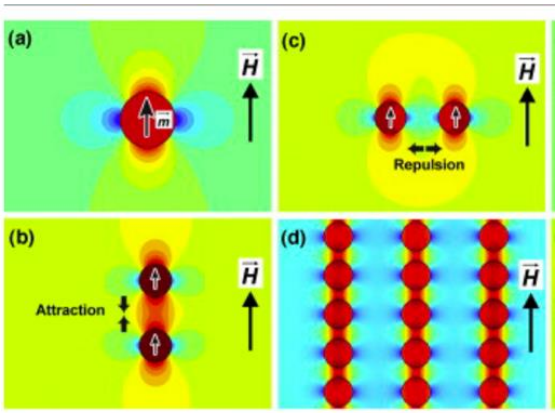

Figure 1-9: (a) Particle magnetic moment aligned with the magnetic flux, (b) Attractive force between adjacent particles with magnetic moment parallel to magnetic flux, (c) Repulsive force between adjacent particles with magnetic moment perpendicular to magnetic flux, (d), 1D chain structures [55]

1.3 Literature Review

1.3.1 Particle Phase

Different types of metals and alloys can make up the particle phase of a magneto-responsive material. The type and size of magnetoactive particles impact the stability, rheology, electrical response, and application of magneto-responsive materials. Many literature papers focus on maximizing the response and property changes of the material by altering factors related to the magnetoactive particles. Commonly used particles include but are not limited to carbonyl iron [41], [56]–[62] and iron oxide particles [46], [63]–[69]. Both types of particles fall under the soft magnet category, which means they act as temporary magnets and can be magnetized and demagnetized under the ON and OFF state of the external magnetic field respectively. The domain structure of the particles causes their reversible magnetization, hence leading to mutable property changes of the material under the application of an external stimulus [43].

Carbonyl iron particles are commonly employed to prepare magneto-responsive materials for various reasons. First, the particles exhibit high magnetic saturation which means the material will experience its maximum response and property change within a broader range of magnetic field strength. Carbonyl's high magnetic saturation led to many commercial and industrial applications such as dampers, brakes, and vibration control [43], [70], [71]. However, their high density causes quick sedimentation of the magneto-responsive material, limiting its long-term application. Many researchers investigated different methods to reduce the sedimentation rate of carbonyl-based suspensions. For example, Lim et al [59] stabilized the carbonyl iron-based suspension by adding fumed silica, whilst Choi et al [60] encapsulated the particles with poly(methyl methacrylate) to improve dispersion and stability of the material. Despite their

limitations, carbonyl particles are utilized more frequently than iron oxide particles as magnetic particles in magneto-responsive materials.

Over the past years, the focus on using iron oxide for the particle phase in magneto-responsive materials declines. The recent lack of interest in using iron oxide particles for magneto-responsive materials is mainly due to their low magnetic saturation [43], implying that the particles have a low maximum moment per unit volume for a magnetic particle [72]. Similar to carbonyl, iron oxide particles agglomerate and initiate sedimentation in the material. Although both challenges limit the application of magneto-responsive materials for commercial uses, for the purpose of this thesis, the benefits outweigh the limitations. Iron oxide particles show promising opportunities because of their low cost, availability, resistance to oxidation, biocompatibility, soft magnetism, polymorphic properties, and non-toxicity [43], [73]. Iron oxide also has high physical and chemical stability and lower sedimentation rates compared to carbonyl particles [50], [51]. As a result, iron oxide particles are significantly used in the biomedical and health industry for heat transfer applications, biosensing, drug delivery, therapeutic targets in chemotherapy, and contrast agents for MRI [46], [63], [65], [68], [74]–[76].

Magnetic iron oxide can be divided into two main size categories, microparticles and nanoparticles [46], [69], [73], [74], [77]–[80]. Ali et al [65] summarized the benefits of using iron oxide nanoparticles which include superparamagnetism, zero coercivity, zero remanence, higher surface area to volume ratio, lower sedimentation rate, and easier dispersion compared to microparticles [81]. However, findings by Deshmane et al [82] portray that the magnetic saturation of iron oxide particles increases with their size. Thus, microparticles will have a higher magnetic saturation than nanoparticles making micron-sized particles more applicable and sensitive to changes in the magnetic field [83]. Moreover, Caterino et al [83] concluded that decreasing the particle size, although enhances stability, brings about the degradation of the rheological effect of

the material. This limiting factor will reduce the performance and the extent of property changes exhibited by the magneto-responsive material when an external stimulus is applied.

Another reason to choose iron oxide microparticles is thoroughly described in findings by Them et al [40]. A mathematical model was utilized to rationalize the positive correlation between the size of the particle's core radius, and the strength of the magnetic dipole-dipole force induced on adjacent particles. Thus, iron oxide microparticles can achieve greater magnetic dipole-dipole forces between neighboring particles compared to nanoparticles. Stronger interparticle forces will result in faster chain formation and a greater change in the properties of the magneto-responsive material. Moreover, due to the multidomain structure of iron oxide microparticles, they can remember their magnetic history. Unlike nanoparticles that possess zero remanence, micron-sized particles can retain some of their magnetization after the removal of an external magnetic field. The remanence advantage iron oxide microparticles hold makes using them in magneto-responsive material to achieve synaptic functions very promising. Owing to the several properties mentioned above and the goals of this research, iron oxide microparticles will be selected to fabricate the magneto-responsive material.

1.3.2 Sedimentation and Stability

One of the most pursued topics related to magneto-responsive materials is techniques to slow down or overcome sedimentation of the material. Sedimentation renders the material inoperable and poses a huge challenge to researchers and commercial users [35], [52], [81], [84], [85]. Different researchers develop various methods to observe changes in sedimentation and measure related data. Simple visual observations are commonly practiced to monitor sedimentation rates and evaluate the extent of the material's stability. For example, Wang et al [86] and Imran et al [73] observed samples over a long period of time and qualitatively recorded results using images.

The limitation of employing a simple observation method is that rigor is difficult to assess and maintain. Trends can be problematic to conclude on and data characterization becomes challenging, as the approach used by researchers becomes subjective. Besides, qualitative data is usually not well understood or accepted compared to quantitative data [87].

As a result, many researchers employ quantitative methods to measure sedimentation rate [47], [48], [88]–[90]. For example, Truong et al [91] and Shah et al [92] measured the volume of the separated carrier fluid and divided it by the total volume of the suspension over a period of time. Whilst Cruze et al [70], Jang et al [62], and Yang et al [56] measured the change in height of the sediment over time as the boundary between the particle and carrier fluid increased. The height change method will be used in this research to measure the stability of all samples synthesized. Due to the objective and accurate nature of quantitative data, assessing sedimentation rates quantitively will allow for easier comparison between different data, and findings will be understood better.

In addition to measuring sedimentation rates, researchers constantly focus on finding new techniques to slow down sedimentation. Common approaches include adding surfactants and additives [50], [60], [71], [74], [88], [91], increasing the viscosity of the carrier fluid [73], and using different particle sizes in the same material [61], [83], [92], [93]. Iron oxide particles are prone to sedimentation because of the attractive magnetic dipole-dipole forces that cause adjacent particles to cluster. It is essential to find a technique to slow down sedimentation rates of iron oxide-based magneto-responsive materials, to execute the goals of this thesis. One commonly practiced technique is using a high viscosity carrier fluid. Imran et al [73] and Hajiyan et al [78] dispersed iron oxide particles in high viscosity motor oil and glycerol respectively and concluded that there was long-term stability of the suspensions. Depending on carrier fluid viscosity to reduce sedimentation rate, limits the range of carrier fluid viscosity that the particles can be dispersed in. Also, high viscosity fluid can mitigate the response of the material to an external magnetic field.

The initial high viscosity of the carrier fluid will reduce the on/off state ratio of the resistance and viscosity of the material, limiting the performance and application of the material.

Another method implemented is adding nano-sized particles to magneto-responsive materials composed of micron-sized particles. The addition of nanoparticles of lower density and higher surface area to volume ratio will help reduce the sedimentation rate of larger particles. This improvement can be further supported by Iglesias et al [94] which established the effect of adding iron nanoparticles to a suspension made of iron microparticles. The results revealed that nanoparticles form a cloud around each microparticle, increasing repulsion between adjacent particles and enhancing the stability of the suspension. However, this method can increase the off-state viscosity of the material and reduce their response to an external stimulus, limiting its applications [95].

Due to the limitations that occur with high viscosity fluid and different particle sizes, the most common method to achieve stability is adding a surfactant to the material. Soares et al [49] employed optical absorbance to study the influence of surfactant on the stability of iron oxide nanoparticles. UV-VIS absorbance of samples with and without a surfactant was measured. The UV-VIS spectrum of pristine iron oxide particles confirmed that their sedimentation occurs much faster than those coated with a surfactant. According to Wang et al. [93], a surfactant should be selected based on two main factors. First, the surfactant should have a strong affinity with the particle and good intermiscibility with the carrier fluid to ensure proper interaction between all components of the suspension. Another factor is that the surfactant should have is a broad operating temperature range and thermal stability to avoid decomposition of the material. A commonly used surfactant that targets both factors is oleic acid. In addition to meeting the thermal stability requirements, Soares et al. [49] confirmed that oleic acid chains possess a negatively charged terminal carboxylic acid that has a high affinity for magnetic particles.

After selecting oleic acid as the stabilizer, it is imperative to find an optimum amount of the acid to use with iron oxide microparticles. Using too much or too little oleic acid can affect the response of the material as well as increase sedimentation rate. Many articles discuss using oleic acid with iron oxide microparticles to reduce sedimentation rate [41], [46], [56], [66], [69], [75], [77]. The limitation of all these articles is the lack of study on finding an optimum oleic acid to 1-5 micron-sized iron oxide particle ratio to reduce sedimentation rate. For example, Fonseca et al [64] used an iron oxide/oleic acid ratio of 1/1.5 in volume when fabricating the magneto-responsive material. However, this paper is limited in that it did not study the impact different ratios of iron oxide to oleic acid have on sedimentation. On the other hand, Yang et al [56] experimented with five different oleic acids to carbonyl particle mole ratio and measured the sedimentation rate of each sample to obtain the optimum ratio. No similar study has been made on iron oxide microparticles of size 1-5 micrometer. Thus, this research will vary the oleic acid to iron oxide microparticle ratio and measure sedimentation rate to obtain an optimum ratio that maximizes stability and lowers cost.

1.3.3 Continuous Phase

Over the years, many researchers strove to synthesize a mixture that achieves a reasonable compromise among conflicting objectives. Choosing the carrier fluid can impact both the stability of the material and its response to an external magnetic field. As mentioned in the background section, magneto-responsive materials are widely studied because of their ability to change their properties almost instantaneously under a magnetic field. Using a high viscosity carrier fluid can limit particle settling and increase long-term use of the material compared to a low viscosity carrier fluid. However, unlike a low viscosity carrier fluid, using a high viscosity fluid will lead to slower chain formation and response of the material to a magnetic field. Thus, understanding the impact

of carrier fluid viscosity on the property changes of the magneto-responsive material is crucial in selecting a carrier fluid that will fit the purpose of this thesis.

There is a lack of literature focus on magneto-responsive materials made of iron oxide microparticles dispersed in high viscosity fluid. Imran et al [73] experimented with oleic acid-coated iron oxide nanoparticles dispersed in three different fluid viscosities; paraffin oil, sunflower oil, and motor oil. The study examined the effect of using high viscosity fluid on the stability and thermal conductivity of the suspension. After 180 days, the fluid with the highest viscosity, motor oil, showed no signs of particle aggregation. The suspension also demonstrated a 77% enhancement in thermal conductivity. Achieving an increase in conductivity and stability shows the promising opportunities of using high viscosity carrier fluid. However, Imran et al [73] experimented with nanoparticles instead of microparticles which impacts the stability and response of the material. In addition, there was no measurement of the electrical conductivity behavior of the suspension. Examining the electrical conductivity changes in the material with and without an external stimulus is necessary to emulate synaptic functions. Thus, this research will attempt to disperse iron oxide microparticles in motor oil and explore stability, electrical conductivity behavior, and viscosity changes of the material in response to an external magnetic field.

To further study the effect of carrier fluid viscosity, Yang et al. [56] dispersed carbonyl micron particles in silicone oil of viscosities 200cst,350cst, and 500cst. A magnetic field ranging from 100mT to 900mT was applied to all samples, and resistance measured at each every 100mT. All the resistances of the samples dropped to zero by 400mT. However, for high viscosity fluids, the resistance reached zero at a higher magnetic field strength than low viscosity fluid, owing to drag forces and slower chain formation. Thus, by controlling the viscosity of the carrier fluid, the response of the material can be tuned to meet different material objectives. The limitation of this paper is the lack of data on the effect of carrier fluid viscosity on the sedimentation rate of the suspension. Such data is important to ensure an operable and stable material that allows for accurate

experimenting and long-term use. In addition, Yang et al [56] plotted minimum resistance at different field strengths. In contrast, this thesis will display how resistance changes over time for constant magnetic field strength, in an attempt to exhibit synaptic behavior.

Furthermore, it is important to study the response of the material at a broad range of viscosities to recognize the role carrier fluid viscosity plays on the property changes and response of the material. By doing so, a cutoff viscosity range can be chosen that allows for a reasonable compromise between stability and desired response. Another advantage of experimenting with a wider range of viscosities is that the speed chain formation and thus property changes will vary. The speed of response varies because of the fluidic forces that become more dominant at higher viscosities (see section 1.2.5). Thus, the response of the magneto-responsive material can be controlled by tuning the viscosity to achieve desired objectives for the material. Unlike Yang et al [56] paper that only experimented with three types of viscosities, this thesis will explore a wider range of carrier fluid viscosities. Iron oxide microparticles will be dispersed in silicone oil viscosities of 10cst,100cst,350cst,1000cst, and 5000cst, and both the sedimentation rate and resistance changes will be recorded over time. Therefore, a clearer trend can be established on the effect of carrier fluid viscosity on the property changes of the magneto-responsive material.

1.3.4 Literature Gaps

Building on the literature review, iron oxide microparticles show encouraging potential as components of magneto-responsive materials can exhibit synaptic plasticity. Achieving a stable dispersion of iron oxide microparticles in oil is challenging due to density contrast and poor interaction that leads to sedimentation. To the best of our knowledge, no study was conducted on dispersing iron oxide microparticles (1-5 micrometer in diameter) in oils with a broad range of viscosities, such as motor oil and silicone oils, and then evaluating the property changes under an

external magnetic field. Specifically, no study explored the electrical resistance changes over time in response to low-strength uniform and cyclic magnetic field conditions. The use of low-strength magnetic fields will display how the interplay of magnetic and viscous forces impacts the property changes of the magneto-responsive material. By observing changes in resistance at different viscosities and magnetic field conditions, the material can exhibit synaptic plasticity. The changes in resistance of the magneto-responsive material over a short period of time can be correlated to short-term depression and facilitation, a study currently lacking in the literature.

1.4 Problem Statement and Research Objectives

This research aims to explore, fabricate, and characterize a stable magneto-responsive material that exhibits synaptic functions and can be classified as an artificial synapse, for sensing and signal processing applications. In nature, voltage-driven changes in synapses lead to the rise of different synaptic plasticity states. Voltage pulses are regarded as the presynaptic spike and the concentration of neurotransmitters flowing between neurons is the synaptic weight. In this model material, the presynaptic spikes are correlated to the applied magnetic field and the conducting channels are the particle chains forming conducting paths under the applied field. By controlling the external stimulus and fabrication process, the response of the material and property changes can potentially emulate synaptic functions. The research questions this study raises are as follows:

(1) What components and synthesis method are most suitable to fabricate a stable magneto-responsive material?

(2) How can the composition of a stable magneto-responsive material be altered to emulate short-term synaptic behavior and become more intelligent and complex?

(3) How can the response of the material under different external magnetic field conditions mimic short-term facilitation and depression states of plasticity?

To answer the research questions and move forward with the development of new materials as artificial synapses, several objectives and experimental tasks are in place:

1. A fabrication process is developed to disperse magnetoactive particles in a carrier fluid medium and create a stable magneto-responsive material. Various material components affect the responsiveness and properties of the material under the application of the external magnetic field. The components (summarized below) is investigated through literature review and experimentation to develop a stable material that can exhibit synaptic behavior.
    a. Determine an appropriate particle, carrier fluid, and surfactant type to potentially emulate synaptic behavior
    b. Identify a suitable fabrication method to ensure proper dispersion
    c. Evaluate the effect of surfactant to particle weight ratio, carrier fluid viscosity, and volume fraction on the stability of the suspension
    d. Quantify sedimentation rates of all samples fabricated
2. The material is characterized before and after applying an external magnetic field to assess the changes in the distribution of the magnetoactive particles and study the changes in the electrical (conductance/resistance) and rheological properties(viscosity) of the material.
    a. Create a magnetic and electrical setup for magnetic field application on the material and response evaluation
    b. Identify range and time for low strength uniform and cyclic magnetic field application on the materials to emulate voltage spikes in synapses
    c. Plot resistance changes over time for low, medium, and high viscosity of the material
    d. Characterize distribution of the particles and viscosity changes before and after magnetic field application to theoretically explain results

3. The changes in material properties and responsiveness measured in part 2 is analyzed to portray memory and be correlated to synaptic functions. The material will then be further developed to accomplish a pinched hysteresis loop; a feature of a memristor and increase the level of complexity of the material
    a. Demonstrate short term plasticity in the magneto-responsive material by analyzing property changes in the material
    b. Evaluate the effect of viscosity on simulating short term facilitation and depression
    c. Understand the role of magnetic dipole forces, remanence, and viscous forces on emulating synaptic plasticity
    d. Expand on the analytical and theoretical part of a memristor and link it to the model material
    e. Provide next steps for further development of the material to enhance its difficulty and complexity

2 Experimental Methods

2.1 Materials

The materials used to make up the magneto-responsive material include magnetoactive particles, carrier fluid, and stabilizing additive. In this study, silicone oil of different viscosities and motor oil was used as the carrier fluid (see figure 2-1(a)). The range of viscosities used was 10 cst (Clearco Products) and 100cst, 350cst,1000cst, and 5000cst (Synco Chemical Corporation). The motor oil used was the Castoral GTX 20W-50 Conventional Motor Oil whilst the stabilizing additive used was 90% oleic acid (Sigma Aldrich) (see figure 2-1(b)). Iron oxide particles of the order 1-5 μm, 99.9% purity, and a cubic structure were used (Atlantic Equipment Engineers) for the particle phase (see figure 2-1(c)).

Figure 2-1: (a) Samples of silicone oil of different viscosities and motor oil in a glass vial and their vendors, (b) Sample of oleic acid in a glass vial and its respective vendor, (c) Sample of iron oxide particles stored in an aluminum container and their vendor

Motor oil is composed of hydrocarbons derived from crude oil, with additives to improve its properties. This base fluid is advantageous because it provides an initial high viscous state for the material that ensures a stable magneto-responsive material, and is stable under high temperatures. Silicone oil is a hydrophobic polymeric compound that is a straight-chained

polydimethylsiloxane fluid. It has a wide range of viscosities depending on the molecular weight and length of the polymer [96]. This carrier fluid is stable at a wide range of temperatures and pressures, environmentally friendly, chemically inert, nontoxic, shows low polarizability, and has good heat transfer characteristics [97]. It is used to ensure a stable magneto-responsive material and to study the effect of initial viscosity on the response of the material.

Moreover, long-term stability is an important goal when fabricating the material. Thus, the use of oleic acid is needed to stabilize the material by coating the surface of iron oxide microparticles. Oleic acid creates a core-shell structure with the iron oxide microparticles. The functionalized structure decreases the density of the particle which reduces the mismatch of density between the particle and continuous phase. The resulting new structure also increases static repulsion between adjacent particles, thus improving dispersion[98].

2.2 Particle Characterization

2.2.1 Scanning Electron Microscopy

A scanning electron microscope was utilized to study the microscopic size and structure of the iron oxide particles. Figure 2-2 (a) and (b) show the images of the iron oxide microparticles. Figure 2-2 (a) is a larger overview of the particles that shows clustering of the particles which is common due to the particle's attractive dipole forces. During the fabrication process, the particles were sieved and coated with a surfactant to reduce agglomeration and the rate of sedimentation. Figure 2-2 (b) is a magnified image of the particles, exhibiting their cubic structure and particle size. Cubic structures compared to spherical ones display a higher magnetic saturation, which will allow for faster response of the particle to the external magnetic field [79] (see section 2.2).

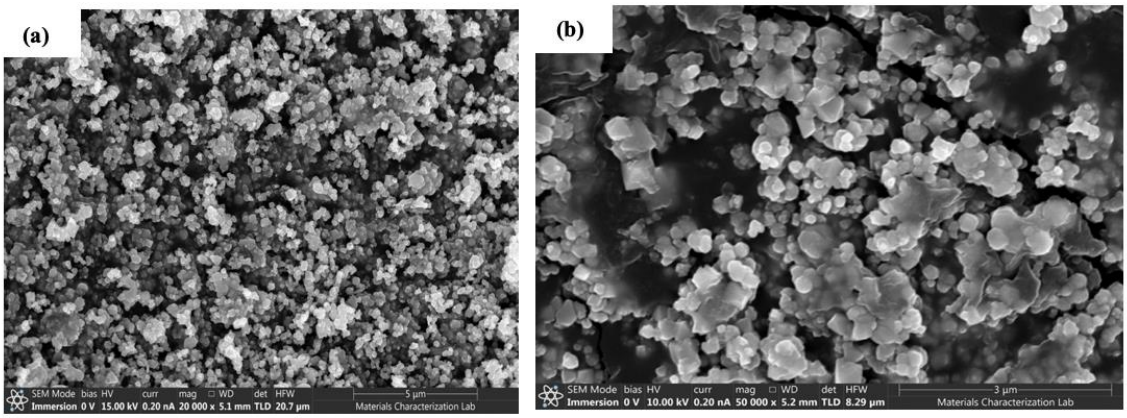

Figure 2-2: (a) Overview of the iron oxide microparticles showing multiple points of clustering of particles. (b) Magnetified view of the particles exhibiting their cubic structure

2.2.2 Vibrating Sample Magnetometer

A vibrating sample magnetometer was used to study the macroscopic magnetic properties of iron oxide microparticles. Important parameters include remanence magnetization (M_r), coercivity (H_c), and saturation magnetization (M_s). The curves in figure 2-3 portray the relationship between induced magnetization and applied magnetic field strength. The size and type of particles affect the values of the parameter in the curve. Some magnetic particles are able to retain memory by maintaining their magnetization upon removal of the magnetic field, dictated by M_r. Saturation magnetization is an important parameter to consider when selecting particles because it determines the maximum magnetization that can be induced in the material [36]. The curvature of the magnetic hysteresis, or hysteresis loop, is characteristic of the type, size, and shape of the material. The loop displays the path taken by the magnetic material when an external magnetic field is applied and then removed. When a magnetic force is directed at the material, induced magnetization increases up to saturation magnetization. Upon reaching saturation magnetization, all the magnetic dipole

moments are aligned in the direction of the magnetic field, and the material cannot be magnetized further. When the magnetic field is removed, some remanence magnetization remains, which is indicated by M_r on the orange curve in figure 2-3. To completely demagnetize the material, a magnetic field is applied in the opposite direction to cancel the dipole moments [36]. To remove remanence magnetization, a coercivity force is applied in the opposite direction, leading to a hysteresis loop forming shown by the orange curve in figure 2-3. When the material shows no hysteresis loop, coercivity, or remanence, as shown by the dashed blue line in figure 2-3, the material is said to be superparamagnetic.

The plots in figure 2-4 portray the magnetization curves of different iron oxide particle sizes. Both sieved and non-sieved iron oxide microparticles displayed a higher magnetic saturation than nano-sized iron oxide particles as shown in figure 2-4. The saturation magnetization of iron oxide particles increases with diameter size [82]. According to figure 2-4 (a), the saturation magnetization of sieved iron oxide microparticles is 111emu/g, of non-sieved iron oxide microparticles is 97.8 emu/g and of iron oxide nanoparticles is 50.6 emu/g. Moreover, by analyzing the hysteresis curve of the particles in figure 2-4 (b), the micron-sized particles showed a hysteresis curve and higher remanence, and are thus more resistant to changes in magnetization, as expected from their multidomain structure (see section 1.2.3). The nano-sized particles, on the other hand, displayed no hysteresis curve or remanence, exhibiting superparamagnetic behavior. Also, the sieved particles have a narrower and more uniform size distribution, thus resulting in a higher magnetic saturation, higher remanence, and wider hysteresis curve compared to the non-sieved particles. This magnetic feature implies that sieved particles are harder and can retain more memory than non-sieved particles. The sieved particles have a remanence magnetization value of 9.66 oersted and non-sieved particles have a remanence magnetization value of 8.06 oersted as shown in figure 2-4 (b). The higher saturation magnetization is due to greater true particle interaction between the external magnetic field and the individual particles. Also, the reduction of clustering

of particles due to sieving, means that the particles in the aggregates are more likely to align their moments with the magnetic field, thus increasing saturation magnetization.

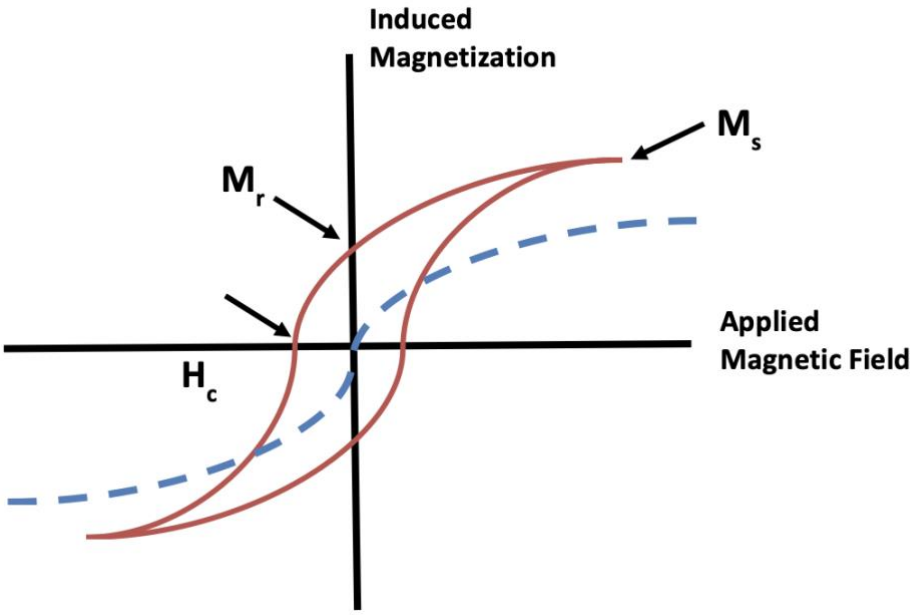

Figure 2-3: Magnetization curve exhibiting important parameters that can indicate magnetic properties of a sample

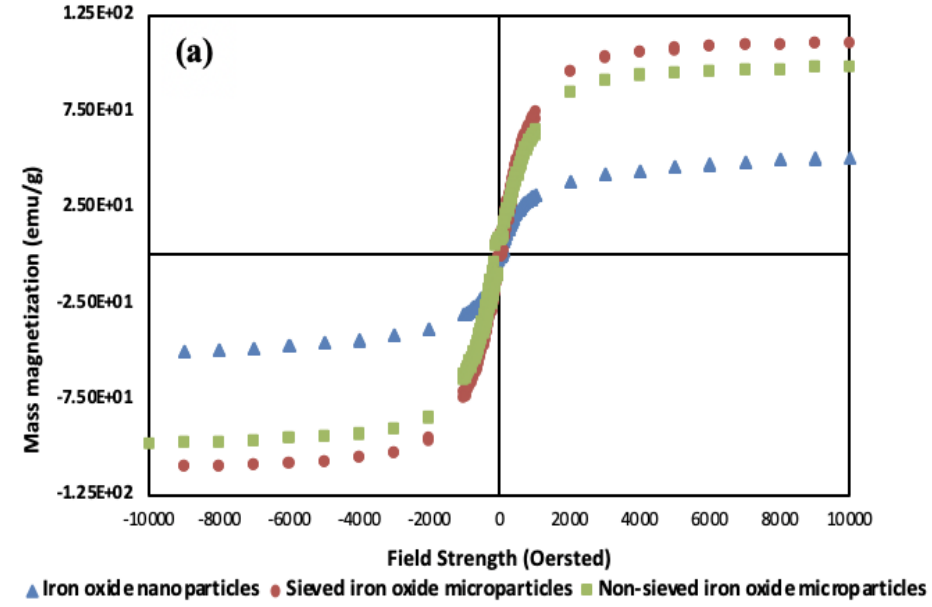

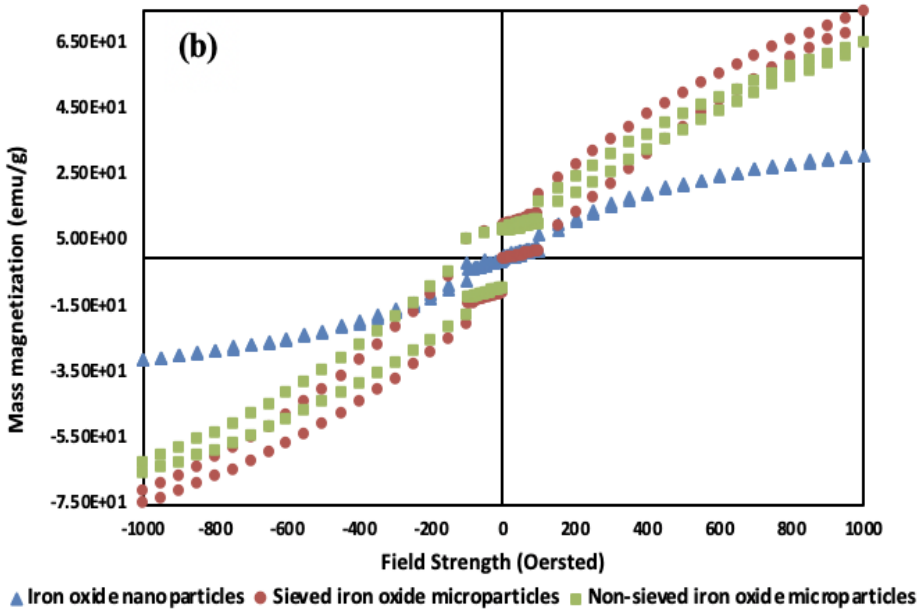

Figure 2-4: (a) Magnetization curve of different sizes of iron oxide particles exhibiting their respective saturation magnetization, (b) Magnetization curve of different sizes of iron oxide particles exhibiting their respective hysteresis loop, remanence magnetization

2.2.3 Chain Formation Observation

The fundamental property changes exhibited by magneto-responsive materials are caused by chains forming under an external magnetic field. To better understand chain formation, iron oxide microparticle powder dispersed in different carrier fluids was placed in an electromagnet of strength 50mT to observe the macroscopic motion of particles. A glass vial filled with iron oxide powder was placed on the edge of the electromagnet led to particles magnetizing and instantaneously collecting near the edge, as shown in figure 2-5 (a). When the particle was placed at 2.5cm as opposed to 3cm, there were more visible and uniform chains forming indicating a more uniform flux. This observation was crucial to select a position between the electromagnet to investigate the rheological and electrical properties of the magneto-responsive material.

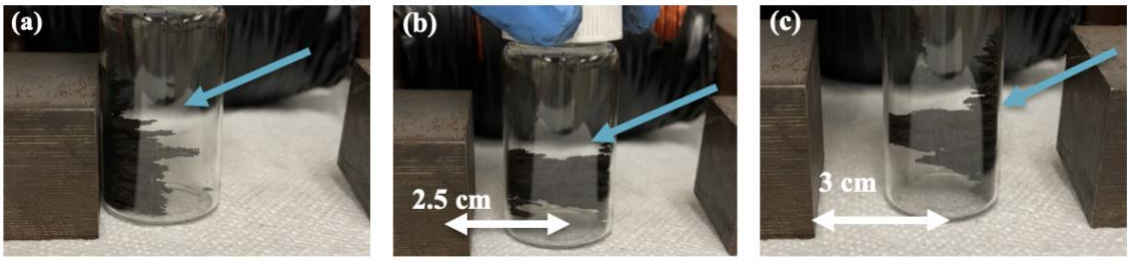

Figure 2-5: (a) Iron oxide microparticles placed by electromagnet edge, (b) Iron oxide microparticles placed 2.5cm from the electromagnet edge, (c) Iron oxide microparticles placed 3 cm from the electromagnet edge

Next, iron oxide microparticle powder was added to 10cst silicone oil in a glass vial and dispersed via shaking. The glass vial was then placed in an electromagnet with a magnetic field strength of 50mT. It was placed on the edges to macroscopically observe chain formation under the effect of a magnetic field, as shown in figure 2-6. Particles dispersed in 10cst silicone oil moved towards the edge of the electromagnet and held their position, displaying similar behavior to the sample in figure 2-5. Placing the vial against the edge of the electromagnet also demonstrated that no chains were extending from one end of the glass vial to the other, indicating a lack of chain formation if the magneto-responsive sample is to be placed by the edge.

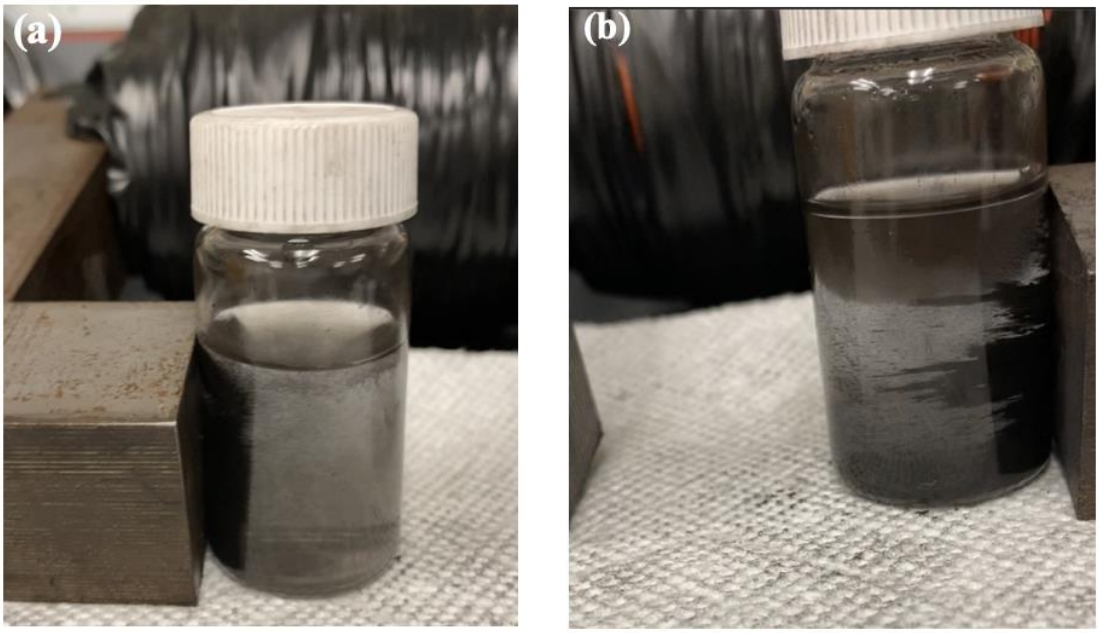

Figure 2-6: Iron oxide microparticles dispersed in silicone oil instantaneously clustered at the (a) the left end of the electromagnet (b) the right end of the electromagnet

Moreover, a glass vial filled with iron oxide microparticles dispersed in 10cst silicone oil was placed 2.5cm from the edge of the electromagnet. Snapshots of chain formation were recorded over 13 seconds as shown in figure 2-7. At 0 seconds, the sample was fully dispersed and the magnetic field was turned on. The particles quickly separated from the carrier fluid and formed chains that extended across the glass vial.

Figure 2-7: A map of iron oxide microparticles dispersed in silicone oil, placed in the centre of an ON electromagnet, displays macroscopic motion of particles and chain formation over 13 seconds. At 0 seconds, the magnetic field was applied

Furthermore, iron oxide microparticle powder dispersed in high viscosity motor oil was studied to observe chain formation as shown in figure 2-8 and figure 2-9. Particle movement in motor oil as opposed to 10cst silicone oil, portrayed the difference in speed of chain formation between low and high viscosity fluids. This observation is crucial to understand the microscopic changes that occur in the magneto-responsive material when a magnetic field is applied. By understanding the effect of the magnetic field on chain formation and redistribution, the rheological and electrical responses of the material can be analyzed and explained theoretically and experimentally. The high viscosity fluid is also important to study the effect of viscous forces on the particle motion, which will lead to different electrical and rheological responses of the material. Figure 2-8 and figure 2-9 showed how slowly the particles migrated towards the edge of the electromagnet as opposed to almost immediately in low viscosity silicone oil. As shown in figure 2-9, because of the high viscosity fluid slowing down particle motion, intermediate chains were forming as the particles migrated to the edge of the electromagnet. The chain collection was getting thinner and less visible with time as particles moved closer to the electromagnet edge and clustered there.

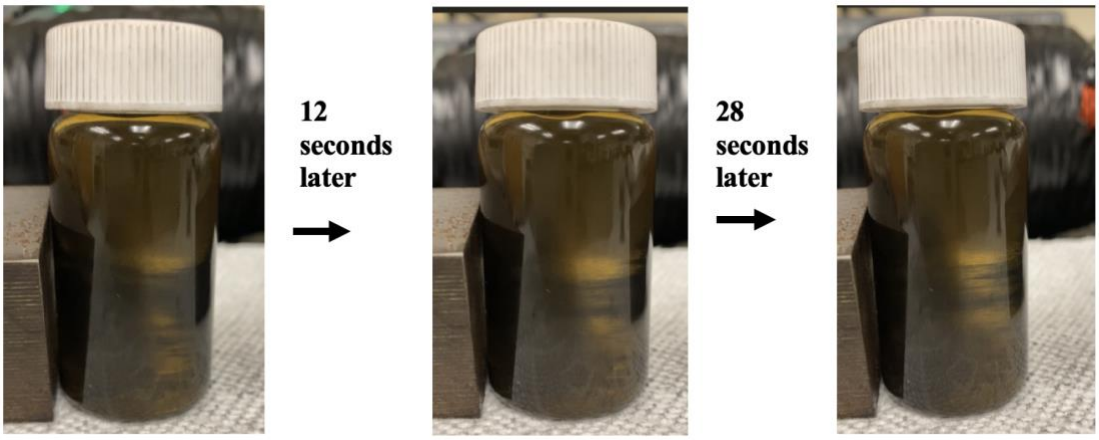

Figure 2-9: Iron oxide microparticles slowly migrate towards the electromagnet end, forming and breaking intermediate chains in the process

2.3 Processing of Iron Oxide-Oil Solutions

Different synthesizing methods were explored to fabricate iron oxide-oil solutions which included altering the type and amount of surfactant, size and volume fraction of iron oxide particles, volume and type of carrier fluid, and mixing method. Iron oxide microparticles (Atlantic Equipment Engineers), motor oil (Castoral), silicone oil (Synco Chemical Corporation and Clearco products), and oleic acid (Sigma Aldrich) were used to fabricate the magneto-responsive material. The fabrication steps are explained thoroughly below and summarized in the flowchart shown in figure 2-10.

Step 1: The required amount of iron oxide particles were sieved. This step is necessary to achieve a narrow size distribution of particles and physically separate the particles to reduce clustering and enhance dispersion. It is important to lower clustering so the particles are evenly coated with oleic acid. Moreover, sieved particles have a higher saturation magnetization and better particle interaction with each other and the external magnetic field, as clusters can inhibit particles in the aggregate from aligning their magnetic moment with the external field.

Step 2: A digital weighing scale was used to weigh the required amount of the sieved iron oxide particles. Depending on the desired volume fraction, the mass of iron oxide was determined, see table 2-1.

Step 3: The iron oxide microparticles were transferred to a round bottom flask and oleic acid was added to the powder. A ratio of 10g:5ml of iron oxide to oleic acid was chosen after carrying out sedimentation tests on different ratios and finding an optimum ratio that will lead to the best dispersion (see section 2.3 and 3.3).

Step 4: The flask was placed in an ultrasonic bath sonicator set at 40C and the sample was mechanically stirred for one hour at 290rpm. After extensive experiments with different mixing methods (see section 3.1), mechanical stirring was the most ideal mixing method when

working with micron-sized iron oxide particles. The timing and temperature of the mixing method were based on the paper by Imran et al. [73] that shows a synthesis method for fabricating a long-term stable ferrofluid suspension with a motor oil base. The method was adapted to iron oxide microparticles for this research.

Step 5: The required volume of carrier fluid was added to the flask. Depending on the desired volume fraction or viscosity, refer to table 2-1, the required type and volume of carrier fluid were measured and added to the solution. For example, if a 10 Vol% sample in 100cst silicone oil was needed, then looking at table 2-1, 95ml of 100cst silicone oil was added to the solution in the flask.

Step 6: The flask was placed in an ultrasonic bath sonicator set at 70C and the sample was mechanically stirred for one hour at 290rpm.

Step 7: The final suspension was transferred to a glass jar for storage at room temperature.

Table 2-1: Amount of each composition for various volume fractions

Volume %	**Iron oxide microparticles (g)**	**Oleic acid (ml)**	**Carrier fluid (ml)**
5	10	5	195
10	10	5	95
20	20	10	90

Step 1: Sieve iron oxide microparticles

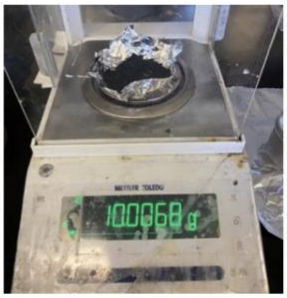

Step 2: Weigh the iron oxide microparticles and add to a round bottom flask

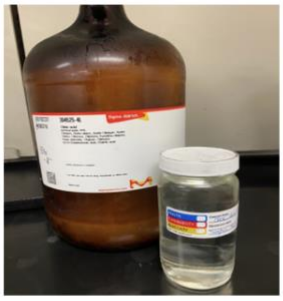

Step 3: Add oleic acid to the particles in the flask

Step 4: Mechanically stir for one hour at 290rpm at 40C

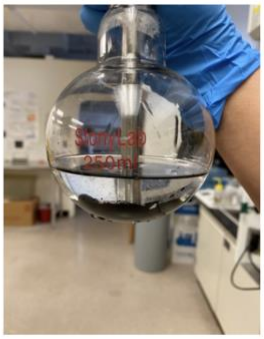

Step 5: Add carrier fluid to the flask

Step 6: Mechanically stir for one hour at 290rpm at 70C

Step 7: Transfer the suspension to a glass jar for storage

Figure 2-10: Flowchart summarizing the steps to synthesize the magneto-responsive material

2.4 Sedimentation test

Sedimentation is a major challenge faced by magnetoactive particles dispersed in a carrier fluid medium. Due to the attractive forces between the particles as well as the mismatch in density between the particles and the carrier fluid medium, the particles tend to agglomerate, rendering the material inoperable. Figure 2-11 and equation 1 illustrate how sedimentation of suspensions was recorded during the study. As soon as the sample was synthesized, 10ml of the sample was transferred to a test tube. As particles sedimented, a color boundary appeared in the test tube because the oil was separating from the carrier particles. The test tube was fixed in the same position until the suspension fully sedimented, which is when h_2 no longer changed. Using a ruler, h_2 was recorded at different intervals as shown in figure 2-11 (b). The changes in h_2 were recorded until there was no longer any change in h_2, thus achieving h_{2max}. Using equation 1, the % change of sedimentation was calculated.

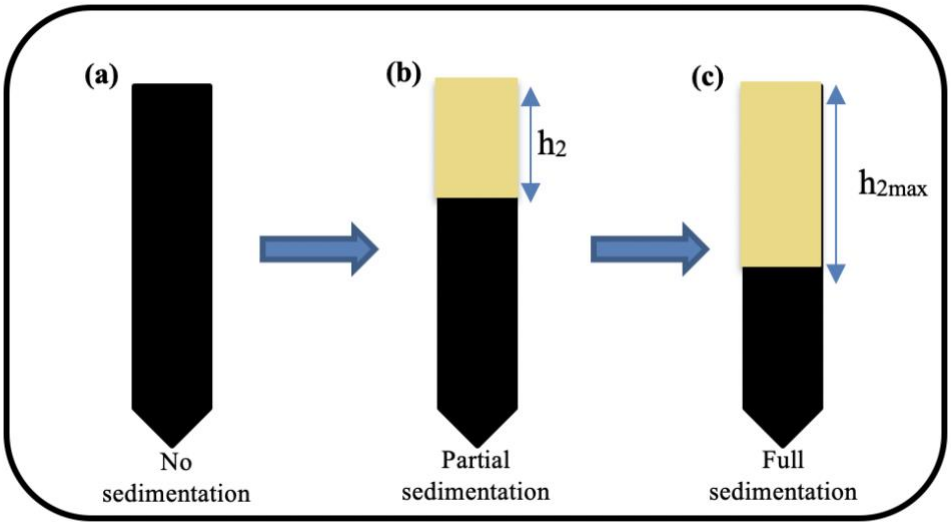

Figure 2-11: Method to measure sedimentation of the samples (a) No sedimentation shows no color boundary in the sample (b) partial sedimentation as particle separate from the oil and (c) full sedimentation shows maximum sedimentation of the sample

$$Sedimentation\ Ratio\ = \frac{h_2}{h_{2max}} \qquad (equation\ 1)$$

2.5 Magnetic Setup

The magnetic field strength of three different magnets was measured using a gauss meter and mapped to understand the field strength applied to the material. The mapping is important to determine points of maximum magnetic field strength and select a position to place the sample. This study worked with two permanent magnets and one electromagnet, with varying magnetic field strengths.

2.5.1 Permanent Magnet Mapping

A gauss meter was used to measure the magnetic field strength of a low-strength and high-strength permanent magnet. A magnetic field reading was taken of the top, middle, and bottom plane as shown in figure 2-12. Each plane was divided evenly into a grid of dimensions 1x1 cm. Figure 2-13 shows how the sample will be placed in the permanent magnet for testing. Tables 2-2, 2-3, and 2-4 summarize the magnetic mapping of the low-strength permanent magnet on different planes. Tables 2-5, 2-6, and 2-7 summarize the magnetic mapping of the high-strength permanent magnet on different planes.

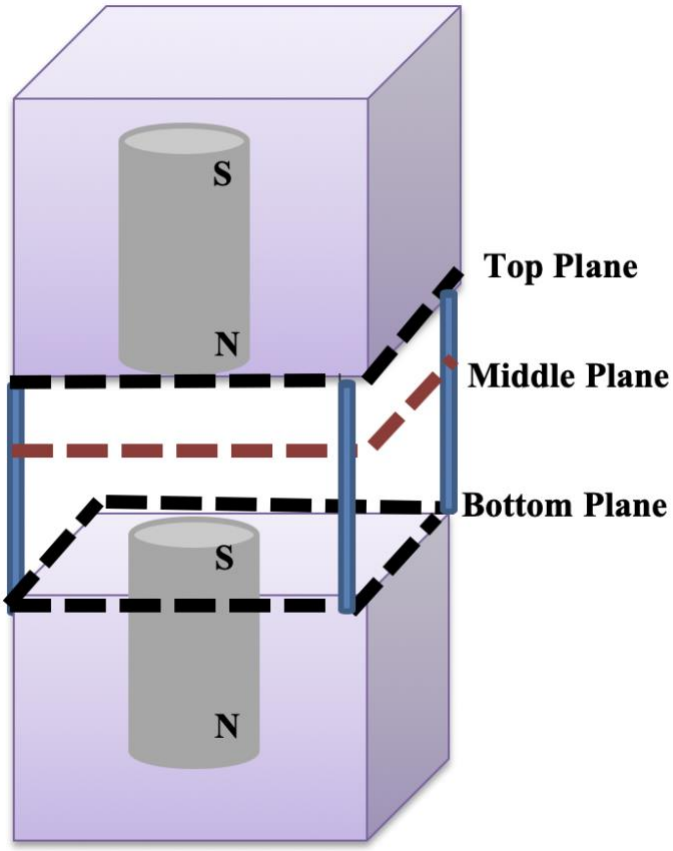

Figure 2-12: Schematic of two symmetrical permanent magnets held in place using separators and rods

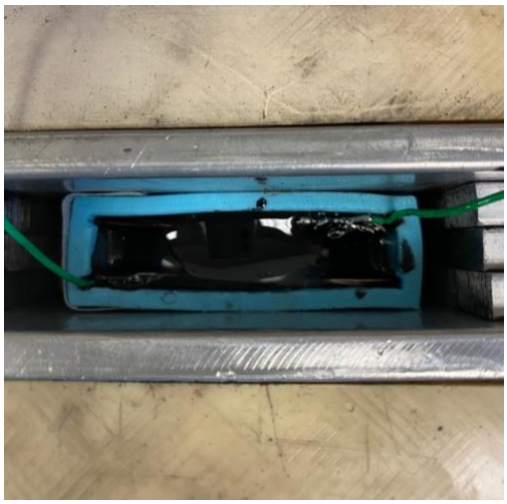

Figure 2-13: The material placed in the low strength permanent magnet

Legend of the low-strength permanent magnet					
>300 mT	250-299mT	200-249mT	100-199mT	50-99mT	0-49mT

Table 2-2: Top plane magnetic field mapping of the low-strength permanent magnet

0	*4*	*13*	*23*	*12*	*11*	*3*
14	42	62	95	73	54	11
42	96	185	242	227	130	42
73	206	292	302	310	257	76
90	279	305	298	305	281	136
123	229	304	305	306	264	132
112	134	305	307	308	195	113
57	47	206	240	211	94	52
19	19	70	83	72	39	14
3	2	32	26	25	11	2

Table 2-3: Middle plane magnetic field mapping of the low-strength permanent magnet

4	*9*	*16*	*22*	*10*	*5*	*1*
16	37	67	73	59	36	17
49	105	163	197	158	99	47
97	260	289	302	261	173	90
176	303	318	315	301	230	98
180	302	324	316	305	237	134
131	257	307	319	290	195	113
56	171	225	215	172	98	60
26	73	96	96	18	37	23
7	21	31	31	21	18	6

Table 2-4: Bottom plane magnetic field mapping of the low-strength permanent magnet

3	*7*	*12*	*15*	*11*	*0*	*2*
14	38	70	76	55	30	15
42	146	218	206	172	83	36
81	279	317	320	220	155	70
200	333	320	321	316	244	108
219	340	325	327	325	276	120
135	319	339	335	314	224	64
70	210	275	280	217	126	36
27	69	93	108	67	36	8
0	20	27	32	18	10	1

Legend of the high-strength permanent magnet				
>700 mT	500-699mT	300-499mT	100-299mT	0-99mT

Table 2-5: Top plane magnetic field mapping of the high-strength permanent magnet

18	10	3	15	5	4
6	46	157	235	156	64
16	194	588	668	625	330
172	546	771	790	771	435
220	689	807	830	806	538
230	608	785	805	782	645
108	430	686	709	712	417
30	99	187	305	212	60
8	7	22	28	8	5
21	19	16	14	14	17

Table 2-6: Middle plane magnetic field mapping of the high-strength permanent magnet

16	7	3	11	0	11
1	44	64	138	50	26
57	231	615	688	682	359
94	620	738	797	766	577
470	663	788	815	813	639
160	371	737	794	775	545
66	177	329	367	335	107
7	20	71	97	96	32
13	1	3	9	8	10
21	20	17	12	13	17

Table 2-7: Bottom plane magnetic field mapping of the high-strength permanent magnet

20	1	5	4	0	14
15	70	149	124	100	40
168	432	677	630	400	200
331	680	808	820	717	440
263	664	828	870	783	536
325	696	870	878	820	346
62	295	634	656	389	153
24	98	242	275	131	24
8	9	25	25	1	9
20	16	15	13	18	18

2.5.2 Electromagnet Mapping

An electromagnet was connected to a power source. A gauss meter was used to take readings of the magnetic field at the center, at various distances and voltages as summarized in table 2-8. All distances were measured from the edge of the left side of the electromagnet (see figure 2-14).

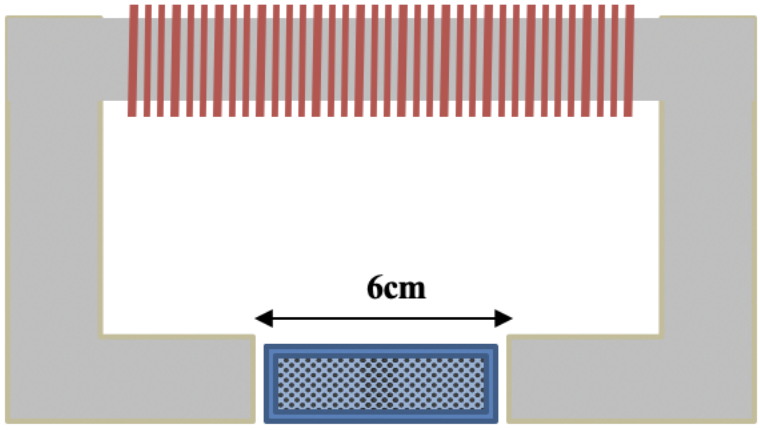

Figure 2-14: Schematic of the electromagnet with a 6cm gap between the electromagnet edges, where the sample will be placed

Table 2-8: Electromagnetic mapping, in mT, at different voltages and distances

	Distance (cm)						
Voltage (V)	0	1	2	3	4	5	6
0	0	0	0	0	0	0	0
1V	6.6	5.2	4.2	4	4.6	5.4	7.7
2V	15.1	11.7	9.2	8.41	4.9	11.5	14
3V	23.6	18.1	14.2	13.5	15	18.1	24
4V	30.5	24.5	19.6	18	19.7	23.3	32.3
5V	40	30.8	24.3	23.2	25.1	29.6	38.1
6V	47.1	37.2	30.2	27.9	31.1	37.3	48.6
7V	59.5	47	38.3	34.5	37.8	44.3	58.5
8V	70.2	57.4	43.6	39.3	41.3	49.2	73.1
9V	75.2	59.5	46.7	43.9	48.6	57.2	76.7
10V	80.2	64.2	57.2	45.7	47.2	52	75.3
11V	82.4	70.1	55.3	48.3	50.3	56.3	83.5
12V	83.7	71.3	53.4	48.5	51.3	64.3	84.7
13V	86.8	72.1	55.8	49.9	53.3	63.8	86
14V	89.2	67.2	55.8	50.2	58	61.7	88.9
15V	91.3	68.5	56.1	51.2	54.8	66	90

An empty sample holder (see section 2.7) was placed between the electromagnet to map the magnetic field at different points. Figure 2-15 (a) shows how the sample holder was positioned between the electromagnet and figure 2-15 (b) shows a zoomed-in view of the sample holder with the nine different locations a magnetic reading was taken labeled. Figure 2-16 demonstrates the magnetic field strength experienced by the material in the sample holder at different distances from the edge of the electromagnet at 15V. It is color coded according to the points in figure 2-15 (b).

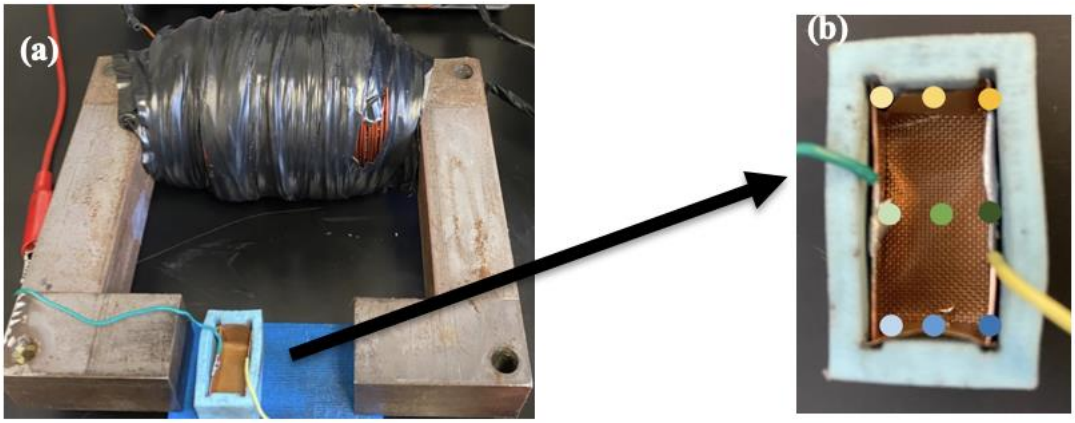

Figure 2-15: (a) Electromagnet setup with the sample holder, (b) Points where a magnetic field strength reading was taken inside the holder

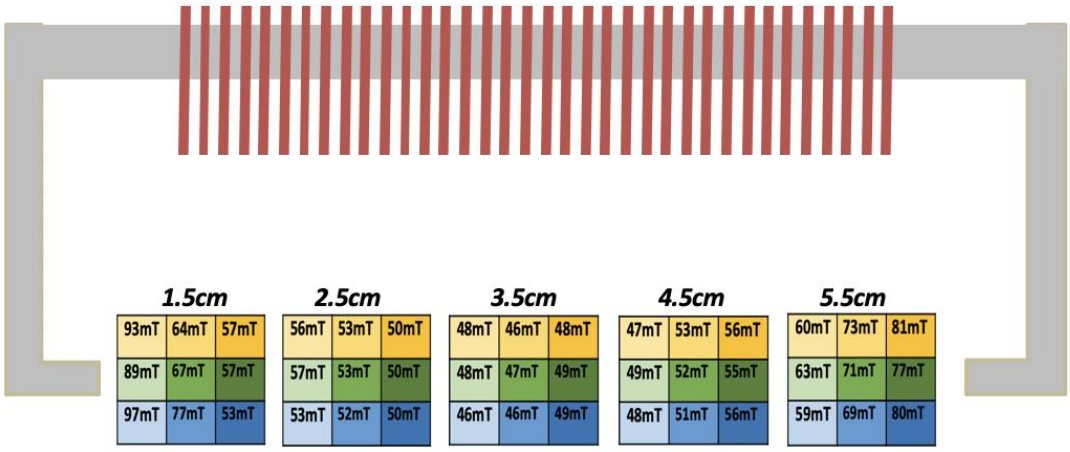

Figure 2-16: Electromagnetic mapping of different points in the sample holder, at different positions from the edge of the electromagnet

2.6 Electrical Setup

Two different electrical setups were used to measure the changes in resistance and evaluate the electrical conductivity properties of the magneto-responsive material with and without an external magnetic field. The first electrical setup used a current sensing circuit to measure low resistance values as shown in figure 2-17. The schematic of the circuit model is shown in figure 2-17 (a) and was designed and simulated online using the Multisim software. The variable R4 in the online circuit schematic represents the model material, and R3 is varied according to the resistance range of R4. The myDAQ provided a voltage source of 5V and measured voltage output. Figure 2-17 (b) shows the actual electrical setup using an electromagnet, with the circuit attached to the electrodes in the sample. Figure 2-17 (c) shows the same circuit used with the permanent magnet and a faraday cage around the setup to reduce noise. LabView was used to record the output voltage (V_{out}) in real-time. Figure 2-18 (a) demonstrates the coded block diagram to plot data from the myDAQ, and figure 2-18 (b) shows the waveform chart that plots the output voltage which is then exported into Matlab. The resistance was calculated using equation 2 to equation 6, where V_{out} is the measured voltage output, V_{in} is the voltage input at points 2 and 3 in figure 2-17(a), R_{model} is the resistance of the sample and, R_1 and R_2 are the gains resistance, which is 20kΩ and 1kΩ respectively as shown in figure 2-17 (a).

$$\frac{V_{out}}{V_{in}} = 1 + \frac{R_1}{R_2} \qquad (equation\ 2)$$

$$\frac{V_{out}}{(1 + \frac{R_1}{R_2})} = V_{in} \qquad (equation\ 3)$$

$$\frac{V_{in}}{R_3} = I \qquad (equation\ 4)$$

$$R_{model} = \frac{5V - V_{in}}{I} \qquad (equation\ 5)$$

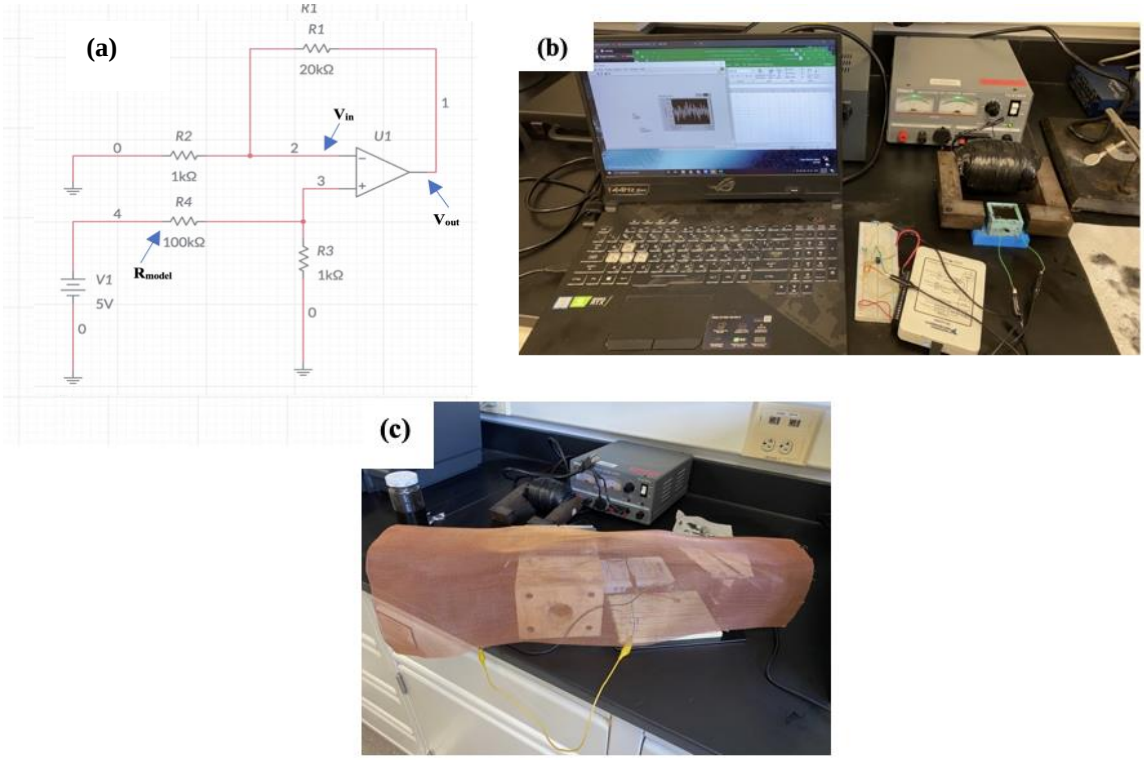

Figure 2-17: (a) Schematic of an online simulation of the current sensing circuit, (b) Electrical setup measuring Vout from the sample, in an ON magnetic field provided by the electromagnet (c) Electrical setup covered with a faraday cage, measuring Vout from the sample, in an ON magnetic field provided by the low-strength permanent magnet

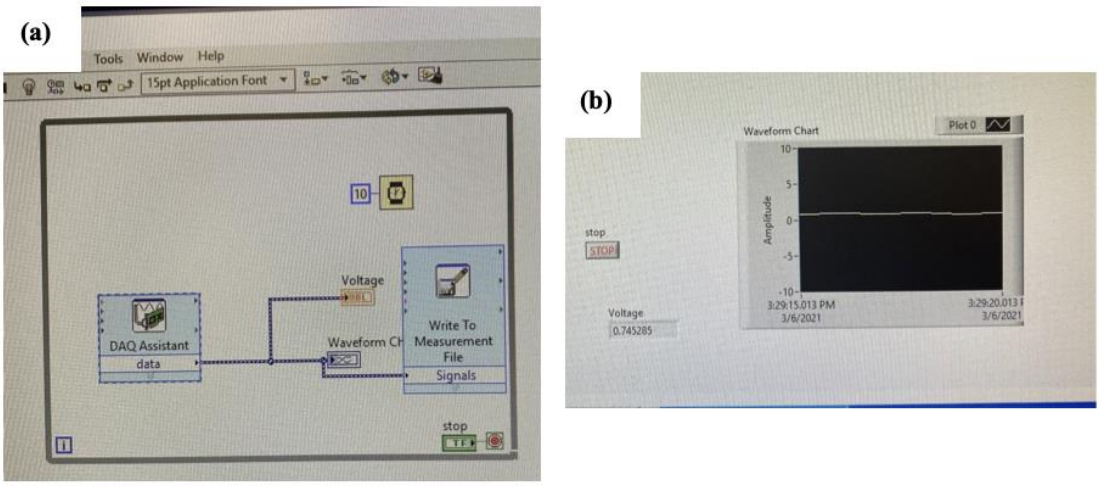

Figure 2-18: (a) Block diagram of the circuit using LABVIEW (b) Waveform chart displaying the recorded voltage output from the sample

For high resistance readings, larger than 200kΩ, a Keithley 6517A source meter was used to measure resistance values of the material (see figure 2-19). The Keithley meter was set up to provide an internal voltage and grounding of the device. The wires from the meter were connected to the electrodes in the sample to measure resistance.

Figure 2-19: Resistance reading of the sample with a Keithley source meter, under a magnetic field applied using an electromagnet

2.7 Sample Holder Design

To fabricate the sample holder, a negative mold was first designed on Solidworks and then 3D printed. The negative printed piece was sprayed using a rapid-release agent. A positive mold was made using part A, the V-340 mold making silicone rubber, and part B, the CA-45 Silicone Catalyst. Part A and part B were mixed using a weight ratio of 10A:1B. The mold was poured into the negative piece and left to set overnight at room temperature. Pure copper sheets with wires soldered on them were used as electrodes. The bottom of the sample holder was covered with a Teflon sheet to reduce the mismatch of surface tension between the holder and the magneto-

responsive material. The process is summarized in figure 2-20. Three different sizes of the mold were fabricated as shown in figure 2-21 with the dimensions summarized in table 2-9.

Holder A was made to fit inside the high-strength permanent magnet (see section 2.5.2). Due to the narrow opening inside the magnet, holder A had to be made very small. The same Holder B was tailored to fit inside the low-strength permanent magnet (see section 2.5.1). The small holder sizes allowed the material to be exposed to a uniform distribution of the magnetic flux, to ensure particles can align in the direction of the magnetic field and form chains. Holder size C was tailored to span the electromagnet vertically and also be big enough to observe changes in the sample's rheological behavior. The height of holder C was chosen to ensure that chains will form across the holder so that changes in the sample's electrical properties can be observed.

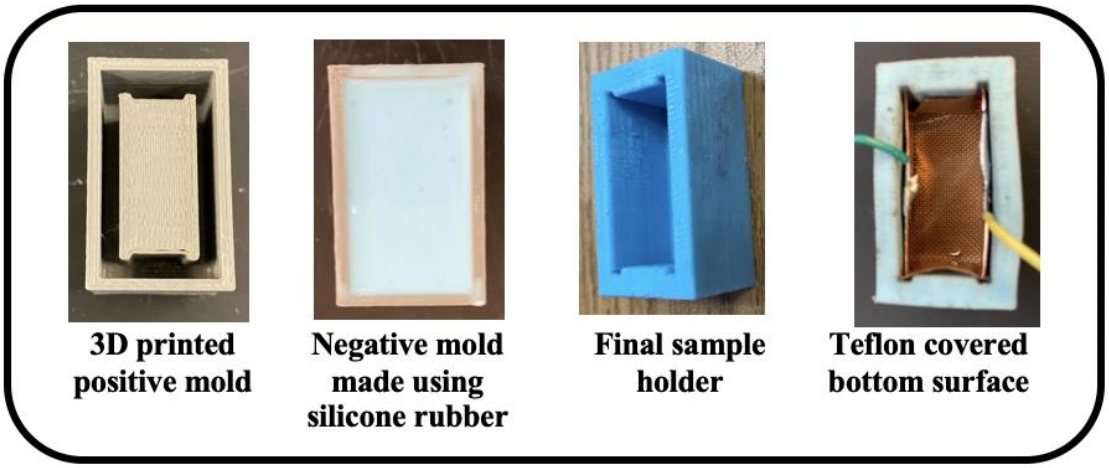

Figure 2-20: Flow chart summary to fabricate the sample holder

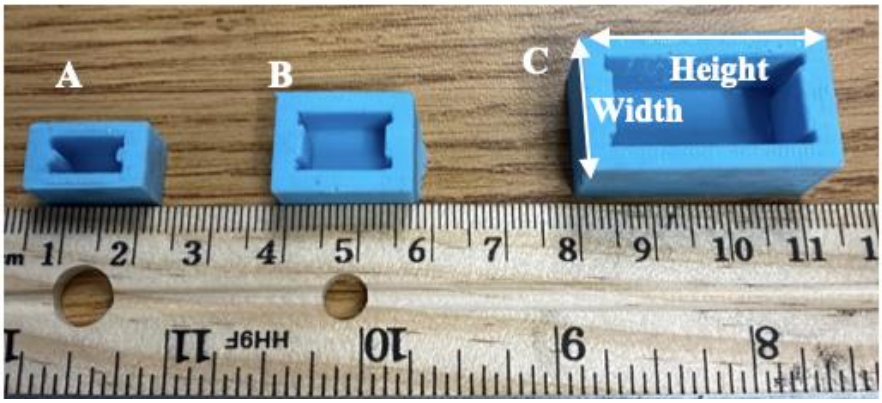

Figure 2-21: Different sample holder sizes to fit into the magnets

Table 2-9: Dimensions of sample holders A, B and C

Holder Type	Height	Width	Thickness
A	0.6cm	1cm	0.6cm
B	0.8cm	1.3cm	0.6cm
C	1.2cm	2.6cm	1.2cm

3 Dispersion and Solution Stability Assessment

3.1 Dispersion Method

3.1.1 Mixing Technique

The synthesis and preparation of magneto-responsive material was investigated using several methods summarized in figures 3-3, 3-4, and 3-7 . The mixing technique, particle size range and iron oxide to surfactant weight ratio were varied independently to find a method that leads to the most stable suspension. The fabrication method was adapted from the works of Imran et al [73], where iron oxide nanoparticles were dispersed in motor oil using a two-step mixing method; mechanical mixing and ultrasonication. This project works with iron oxide microparticles which have a smaller surface area to volume ratio compared to nanoparticles. Thus, different mixing techniques were experimented with for the second mixing step to ensure better dispersion at the microscale.

Three different mixing methods investigated to choose the most appropriate mixing method; sonicator, homogenizer and mechanical mixing[81]. Ultrasonication transmits sound energy to the sample to agitate the particles. There are two main types of sonicator experimented with to fabricate the magneto-responsive suspension. An ultrasonic bath provides a weaker sonication than probe sonicator, while also leading to non-uniform distribution of energy. The probe sonicator uses a more direct method of sonication by providing a more focused and uniform power input (see figure 3-1(a)). The probe sonicator is also more controllable, reproducible, and more intense [81]. The use of sonication in dispersing magnetite particles in carrier fluid occurs more frequently with nano-sized particles [65], [68], [73][66],[99]. The homogenizer used is called a Polytron homogenizer and is a form of an immersion dispenser that uses a rotor/stator technology.

It works by applying a focused high shear force to homogenize samples via particle size reduction which eases dispersion in the carrier fluid (see figure 3-1 (b)). Mechanical mixing, specifically a motor-driven stirring blade, was used to evenly coat the magnetic particles with oleic acid in the first step, similar to the first step in Imran et al [73] method. It was also experimented with for the second step to disperse the coated iron oxide microparticles in the carrier fluid (see figure 3-1 (c)).

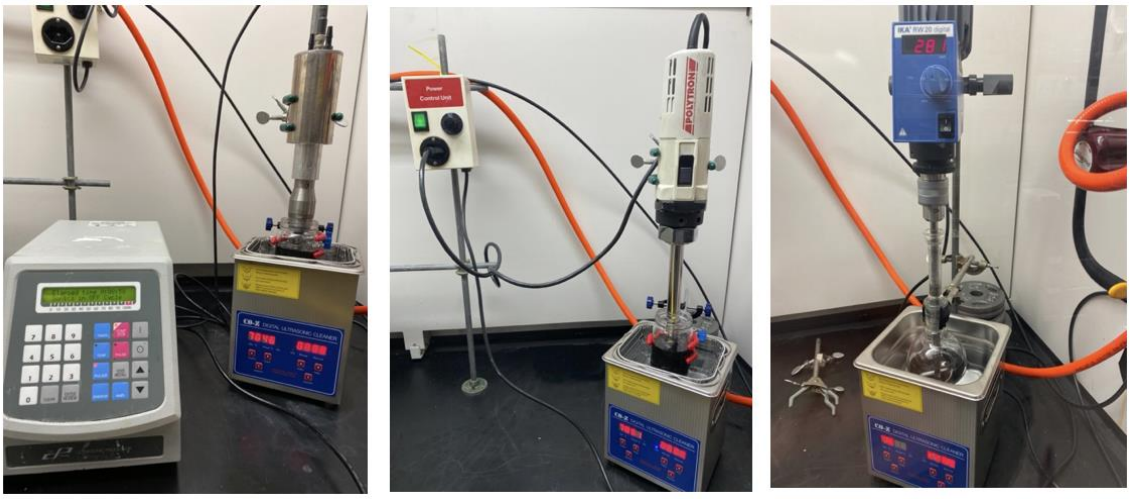

Figure 3-1: (a) Probe sonication, (b) Polystron homogenizer, (c) Mechanical Stirring

3.1.2 Fabrication Methods

Method 1: 10g of iron oxide microparticles were added to 20ml of oleic acid. This specific amount of particles was used to ensure that the particles were properly mixed using the mechanical stirrer when placed in the round bottom flask shown in figure 2-10. If a smaller number of particles were used then, the stirrer wouldn't be able to properly mix the components. Larger amounts of particles were unnecessary because the sample holders used are very small (see figure 2-21 and table 2-9), leading to a waste of resources and material. The mixture was mechanically stirred at

40°C for 1 hour at 290 rpm. The initial oleic acid to iron oxide ratio, volume fraction, temperature and mixing time was adapted from the works of Imran et al [73].

Next, 180ml motor oil was added to the mixture and an ultrasonication method was used to disperse the particles in the oil. An ultrasonication method was used for the second mixing step in an attempt to replicate the work of Imran et al [73], given the same carrier fluid type and viscosity used, surfactant and particle type as well as relevant amount of each composition. The flask was placed in an ultrasonic bath set at 70°C and for 1 hour [73]. The probe sonicator was set at 40% power with a 5 on/ 15 off pulsing. The bath sonicator and probe sonicator were used simultaneously to maintain the temperature at 70°C. High power intensity and long on time of the probe sonication will quickly heat up the sample and exceed the desired temperature of 70°C. Thus a 40% power was used in addition to extra sonication from the bath sonicator. Also, whilst the probe sonicator was off, the bath sonicator provided a weak form of sonication to keep the particles suspended in the oil and not settle to the bottom of the flask.

However, there was particle residue left behind in the flask when transferring the solution for storage. This is indicative of either insufficient mixing time or inadequate incorporation of the microparticle phase with the continuous phase using ultrasonication. Since this project works with microparticles instead of nanoparticles, which is the particle size range in Imran et al [73], another mixing method should be investigated at a one hour time frame . In addition, method one showed quick sedimentation within the first hour, as shown by the color boundary in figure 3-2. Given the high viscosity of motor oil, and the slow sedimentation rate found in the results section of Imran et al [73] work, a better mixing method should be explored. If this method demonstrated quick sedimentation at high viscosity, then at low viscosities such as 10cst and 100cst of silicone oil, the stability will be very low.

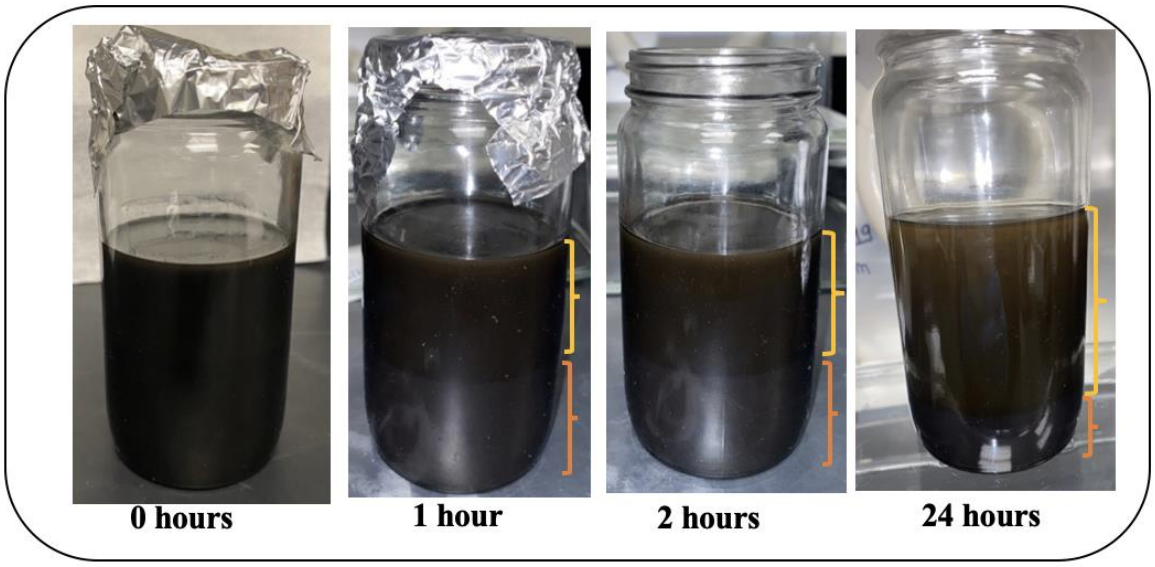

Figure 3-2: The sample fabricated using method one over a period of 24 hours. The orange and yellow bracket shows a color boundary as particles separate from the oil and settle to the bottom

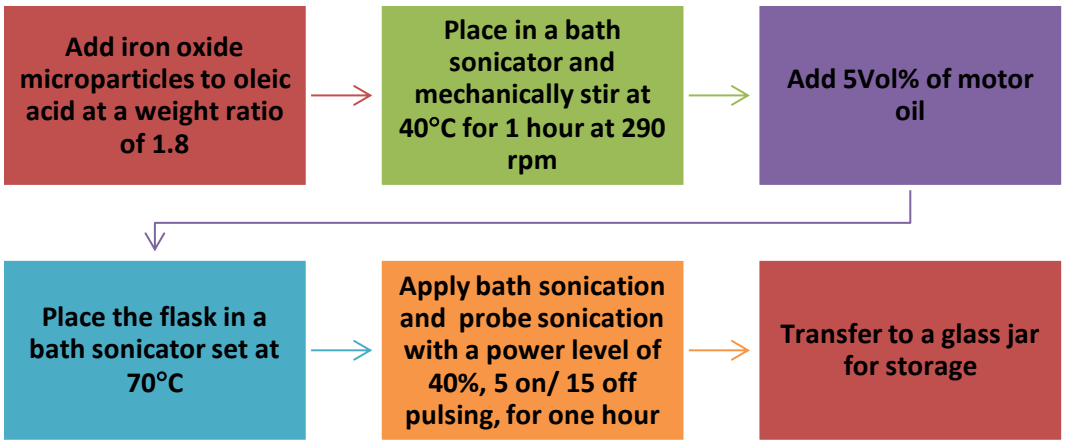

Figure 3-3: Summarized step by step process of method one

Method 2: 10g of iron oxide microparticles were added to 20ml of oleic acid. The mixture was mechanically stirred in a water bath at 40°C and 290 rpm for one hour. Next, 180 ml motor oil was added to the mixture and a homogenizer and water bath sonicator were used to mix the solution

for one hour. The homogenizer and bath sonicator were turned on and off and the power varied to both reduce foaming in the solution and attempt to reduce high temperature fluctuations.

First, the homogenizer was set at power level four for thirty seconds, then followed by two minutes at power level three. The temperature increased to 76°C, so the power level was then dropped to two to reduce the temperature and foaming that was taking place. The bath sonicator was turned on for three minutes to keep the solution mixing. When the temperature reduced to 73°C, the homogenizer was set at power level 4 for thirty seconds, then power level five for five minutes. Meanwhile, the bath sonicator was turned off as temperature increased rapidly to 77°C. Thus, the homogenizer was decreased down to level four for one minute, then back to power level two again with no bath sonicator for nine minutes, maintaining a temperature of 72°C. The homogenizer was then set at a power level of four and a half for fifteen seconds then back to a power level of three for six minutes, causing a temperature drops to 69°C. Then, the power level was set to four and a half for fifty seconds, followed by a power level of three with the bath sonicator on for five minutes. This led to a temperature of 75.5°C. Finally, a power level of five was applied for one minute, followed by a power level of three, with the bath sonicator on. The final temperature of the solution was 73°C.

Method 2 displayed a slower sedimentation rate based on qualitative assessment offered by pictures takes as a function of time compared to method one (figure 3-4). However, there was a lot of temperature fluctuations due to the high temperature inflicted by the demulsfier which affects synthesis of the material and makes the method difficult to reproduce. Also, turning the homogenizer and bath sonicator on and off, as well as changing the power based on observation of the temperature fluctuations and trail would be very difficult to replicate. Thus, a new, more replicable mixing method needs to be determined.

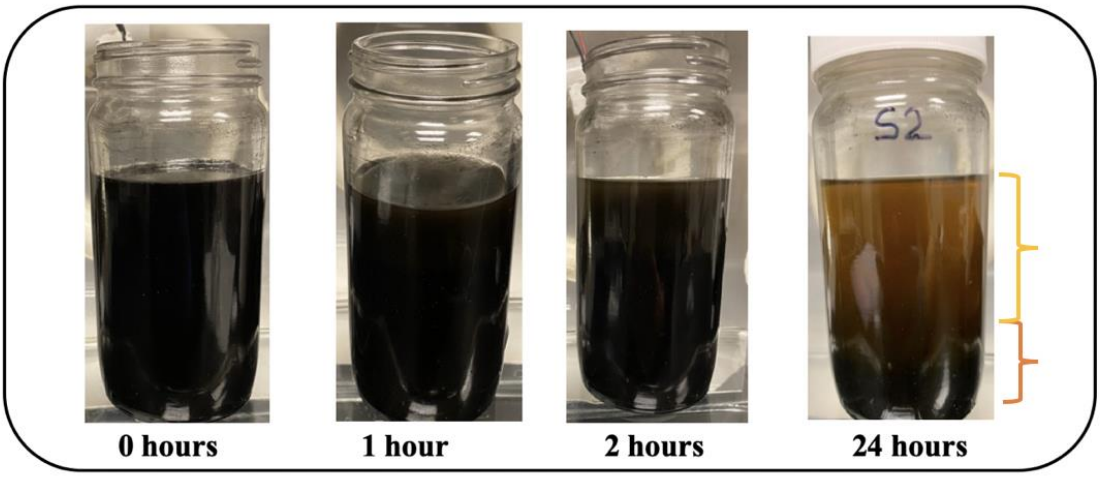

Figure 3-5: The sample fabricated using method two over a period of 24 hours. The orange and yellow bracket shows a color boundary as particles separate from the oil and settle to the bottom

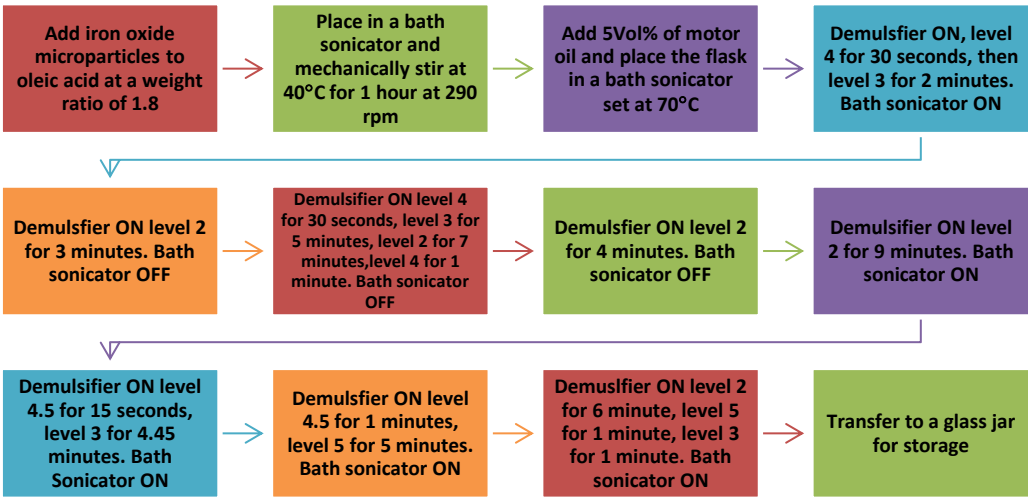

Figure 3-4: Summarized step by step process of method two

Method 3: 10g of iron oxide microparticles were added to 20ml of oleic acid. In many literature papers, regardless whether it was microparticles and nanoparticles, mechanical stirring was used to coat the particles with the additive [56], [73], [77].

The mixture was then mechanically stirred at 40°C for 1 hour at 290 rpm. Next, 180ml of motor oil was added and the solution was mechanically stirred for 1 hour at 70°C. Method three, compared to method one, showed much better dispersion shown by no sedimentation in the first

hour (figure 3-6). Moreover, the method maintained a temperature of 70°C, was easily reproducible and led to better mixing in one-hour which would be shorter than ultrasonication. It also resulted in no particle residue left in the flask upon transferring within the one hour time frame, which is important in gaining an accurate volume fraction, but also indicative of better dispersion of the solution in general.

The result of this method indicates that mechanical stirring is more suitable than ultrasonication for microparticles in producing stable material within a shorter time frame. This finding is confirmed by literature paper such as that by Yang et al [56] that used mechanical stirring to disperse microparticles in silicone oil, whilst findings by Imran et al [73], and Hajiyan et al [78] showed the effective use of ultrasonication for dispersing nanoparticles in carrier fluid.

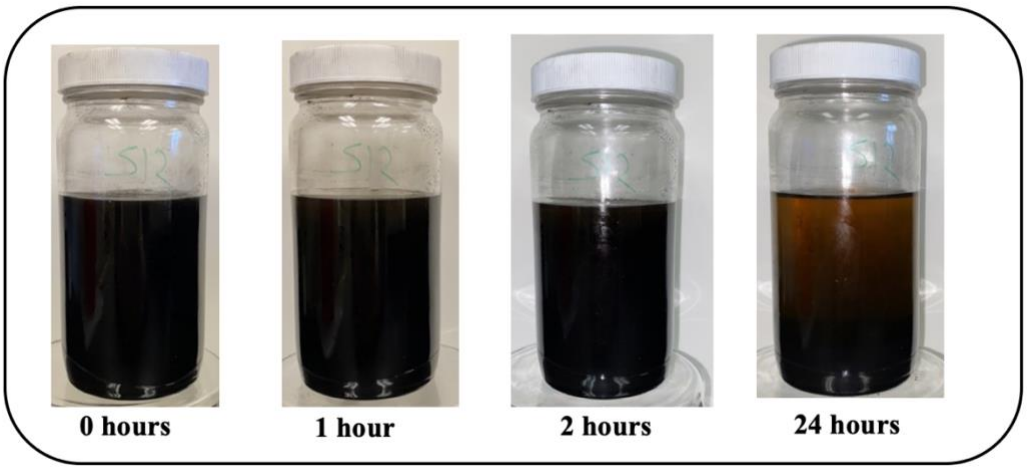

Figure 3-6: The sample fabricated using method three over a period of 24 hours

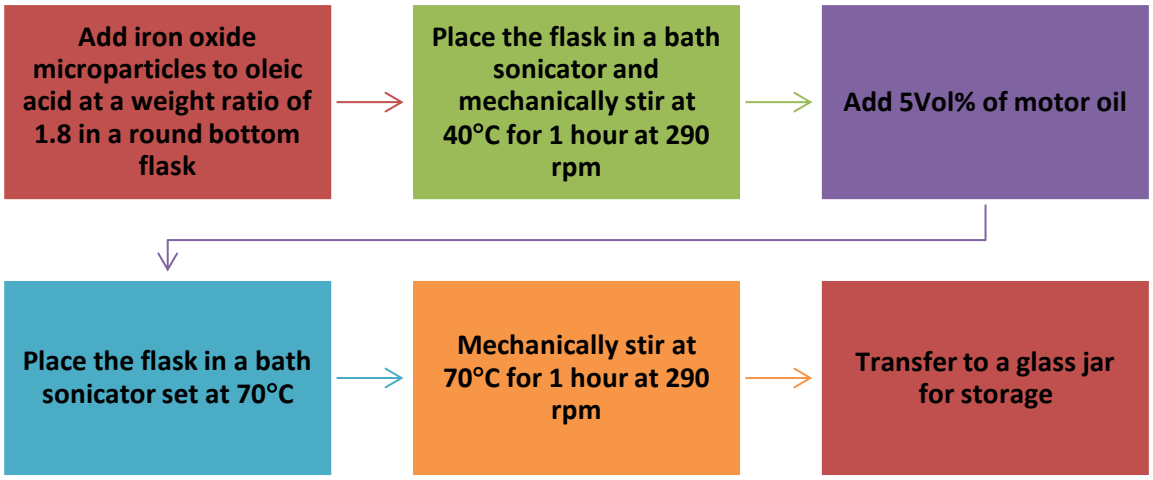

Figure 3-7: Summarized step by step process of method three

3.2 Surfactant ratio

After identifying the most suitable mixing method, it is important to find an appropriate surfactant to iron oxide mass ratio to enhance stability of the suspension and reduce sedimentation rate. Oleic acid coats the iron oxide microparticles to increase electrostatic repulsion between adjacent particles and reduce clustering (refer to section 1.2.4 and 1.3.2 on surfactant's role on stability). As mentioned in section 1.3.2, there is a lack of study on finding a suitable iron oxide to oleic acid ratio for particle sizes in the range of 1-5μm. Nanoparticles have a larger surface area to volume ratio compared to microparticles and thus might require different amounts of surfactant to improve dispersion, when adapting the work of Imran et al[73] to microparticles. Given the need to coat the particles' surface with the surfactant, the smaller surface area to volume ratio of microparticles indicates the potential need for lower amounts of oleic acid compared to nanoparticles. At very low ratios, there is not enough electrostatic repulsion provided by the oleic acid to overcome the attractive magnetic dipole-dipole interparticle attraction that causes clustering of the particles. At very high ratios, excess oleic acid starts separating from the solution and

sedimentation ratio increases, similar to sedimentation findings by Yang et al [56]. Similarly, Gupta et al. [66] demonstrated that using high amounts of oleic acid can lead to oversized agglomerates which enhances sedimentation ratio. Thus, it is important to find an optimum oleic acid quantity to improve dispersion and reduce sedimentation rate.

To determine an optimum ratio, a starting ratio of 1.45 was chosen and investigated, and then subsequent ratios were selected accordingly. Six different ratios were examined (0.225, 0.45,0.89, 1.45, 1.8 and 2.7) and the samples were fabricated using method three which constitutes motor oil as a base fluid and 5vol% (see figure 3-7). A 5Vol% was used for two main reasons, the first is to save materials and cost. The second reason is because at higher volume fractions, the viscosity of the sample will increase due to a higher concentration of particles being suspended in the carrier fluid. If a suitable ratio is determined for 5Vol% , then at higher volume fractions, suspension stability will be better as viscosity keeps the particles suspended in the fluid longer. However, if a ratio is determined for higher volume fraction, then both viscosity and surfactant play a role in the sedimentation results of the sample and the stability. Thus, the results might not be extended to lower volume fractions where the role of viscosity is less significant.

Figure 3-4 compares the six different ratios at 5vol% of iron oxide microparticles dispersed in motor oil. The measurement technique used to record changes in sedimentation over time is explained thoroughly in section 2.4. The changes in height were recorded until there was no longer any change (h_{max}), which is when the sample achieved full sedimentation. The height measured at different time intervals for each sample was divided by the maximum height to calculate the sedimentation ratio. The sedimentation ratio allows for easier comparison between each surfactant ratio and find an optimum amount. A sedimentation ratio of 0 indicates no sedimentation, whilst a sedimentation ratio of 1 denotes full sedimentation. The sedimentation ratio over a period of time for each iron oxide to oleic acid mass ratio was plotted in figure 3-8. There are two important indicators of a suitable ratio. The first marker is the time it takes for the particles to start settling

and the material to show sedimentation, or “start to sediment”. Understanding the time it took for the sample to start showing sedimentation is important because experiments carried out in the off magnetic field state needs to be done within the period of no sedimentation to ensure stability is not affecting results. Another crucial marker is the time it takes for the particle to reach “full sedimentation”, as it provides insight into the effect of the surfactant ratio on the long-term stability of the sample (figure 3-9).

As shown in figure 3-8, the sedimentation ratio increased gradually in the beginning and then much more rapidly as it reaches full sedimentation. As the particles agglomerate and cluster during sedimentation, their magnetic dipole-dipole interaction increases because their overall size increases. The larger interparticle force augments the sedimentation ratio as it dominates the electrical repulsion caused by the surfactant coating and the viscous forces acting on the particle from the carrier fluid.

The findings in figure 3-8 portray that a ratio of 0.45 has the lowest sedimentation rate and took the longest time to attain full sedimentation, which ensures long term stability. As seen in figure 3-8 and 3-9, lower ratios (0.225, 0.45 and 0.89) took longer to start showing sedimentation compared to higher ratios of 1.45,1.8 and 2.7. Ratio 0.225 started showing sedimentation after five hours, and 0.45 and 0.89, started showing sedimentation after 4 hours. At higher ratios, the sample started showing sedimentation after two hours. In terms of full sedimentation, ratio 0.45 took the longest time to reach full sedimentation, whilst ratio 1.45 took the shortest time to reach full sedimentation. Although a ratio of 0.225 seems more suitable in terms of taking longer to start showing sedimentation, 0.45 was selected as a compromise because it took 3.5 more hours before

it reached full sedimentation. Long term stability of the suspension is an important characteristic of magneto-responsive materials.

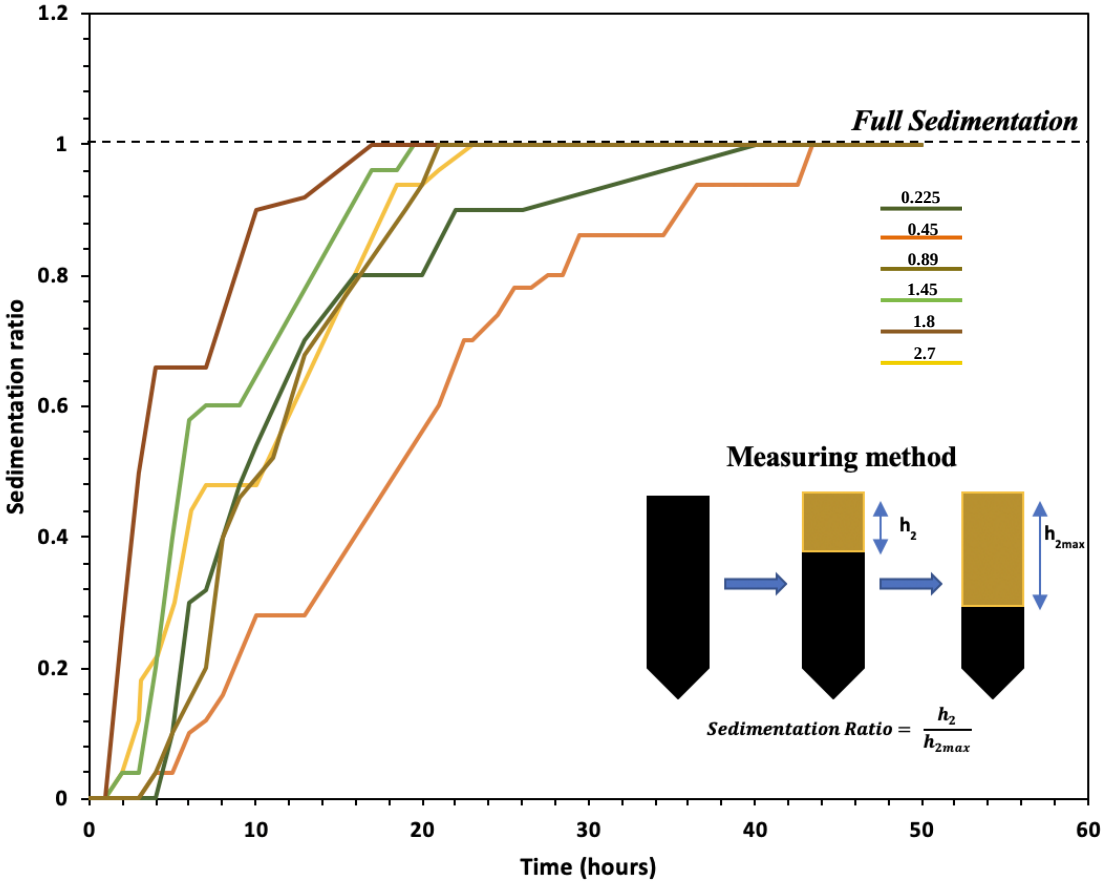

Figure 3-8: The sedimentation ratio for six different weight ratios of iron oxide to oleic acid, at 5Vol% and using motor oil as a carrier fluid

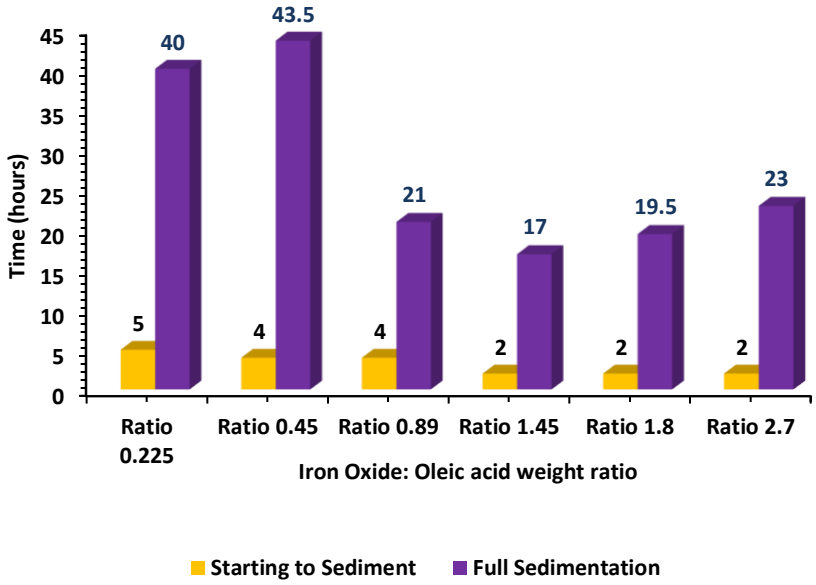

Figure 3-9: The time it takes for six different weight ratios of iron oxide to oleic acid to start to sediment and reach full sedimentation, at 5Vol% and using motor oil as a carrier fluid.

3.3 Viscosity effect on Stability

Samples with different viscosities of silicone oil (10cst, 100cst, 350cst, 1000cst, 50000cst) were prepared to analyze the effect of viscosity on the overall stability of the iron oxide-oil suspension. Those specific viscosities were chosen because they provide a large range to understand the effect on sedimentation. Silicone oil is commonly used as a carrier fluid when fabricating magneto-responsive materials [43], [56]. Table 3-1 summarizes some of the chemical properties of silicone oil, whilst section 2.1 provides insight into why silicone oil was employed as a carrier fluid.

All factors including synthesis method, surfactant to iron oxide microparticles weight ratio, measuring technique, volume of carrier fluid, and volume fraction were kept constant when varying the viscosity of the carrier fluid to ensure reliability. This study is important to understand the effect

of carrier fluid viscosity on the stability of the material, as well as determine a suitable time range to perform experiments, so that the results are not affected by sedimentation. The method summarized in figure 3-10, adapted from method three (figure 3-7), was followed to prepare the suspensions with the different carrier fluid viscosities. The measurement technique and experimental set up used to record changes in sedimentation is described in section 2.4 and is similar to the procedure carried out in section 3.2.

The plot in figure 3-11 portrays the changes in sedimentation ratio over time at different carrier fluid viscosities. There is a positive correlation between the viscosity of the carrier fluid and the time it takes for the suspension to sediment. As viscosity of the carrier fluid increases, so does the drag forces experienced by the particles suspended in the solution. The drag forces slow down the particles, which means it takes them longer to migrate towards adjacent particles and cluster. When the particles cluster, their overall weight increases, which enhances the gravitational force acting on it, thus overcoming the drag forces and settling to the bottom of the test tube. At higher viscosities of carrier fluid, 350cst, 1000cst and 5000cst, the sedimentation ratio increases gradually in the beginning and then faster towards full sedimentation. In the beginning, the viscous forces are very high and they slow down motion of particles which means they take a long time to migrate and attach to adjacent particles. However, as the particles agglomerate and cluster during sedimentation, their magnetic dipole-dipole interaction increases because their overall size increases. The larger interparticle force augments the sedimentation ratio as it dominates the electrical repulsion caused by the surfactant coating. Also, the clusters experience a higher gravitational force than individual particles due to their larger mass, which speeds up settling of the particles.

Moreover, the time it takes for sedimentation to start is important to ensure that the sample, under no magnetic field application, is being tested before any settling occurs so that results are not affected by sedimentation. For example, for the 100cst, the sample is tested in the first three hours.

As shown in figure 3-12, for an increase in viscosity of the order of 10, from 10cst to 100cst, led to a 12 times increase in time for sedimentation to start, and 24 times increase in time for full sedimentation to occur. Whilst an increase in viscosity of the order of 100, from 10cst to 1000cst, led to a 272 times increase in time for sedimentation to start, and 77.5 time increase in time for full sedimentation to occur. These values portray the significant role viscosity plays in reducing sedimentation ratio and overcoming clustering due to magnetic dipole interaction.

Table 3-1: Chemical properties of Silicone oil

Chemical Name	Polydimethylsiloxane Silicone Oil
Linear Formula	$[\text{-Si}(CH_3)_2\text{O-}]_n$
Dielectric strength	14 kV/mm
Refractive index	1.4

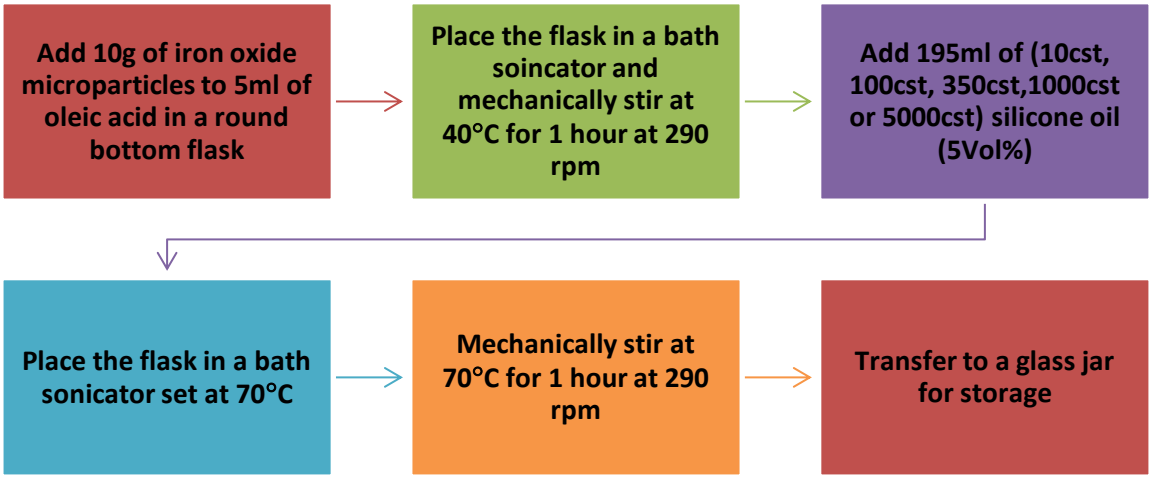

Figure 3-10: Summarized step by step process to test the effect of silicone oil viscosity on stability using the optimum iron oxide to oleic acid mass ratio of 0.45

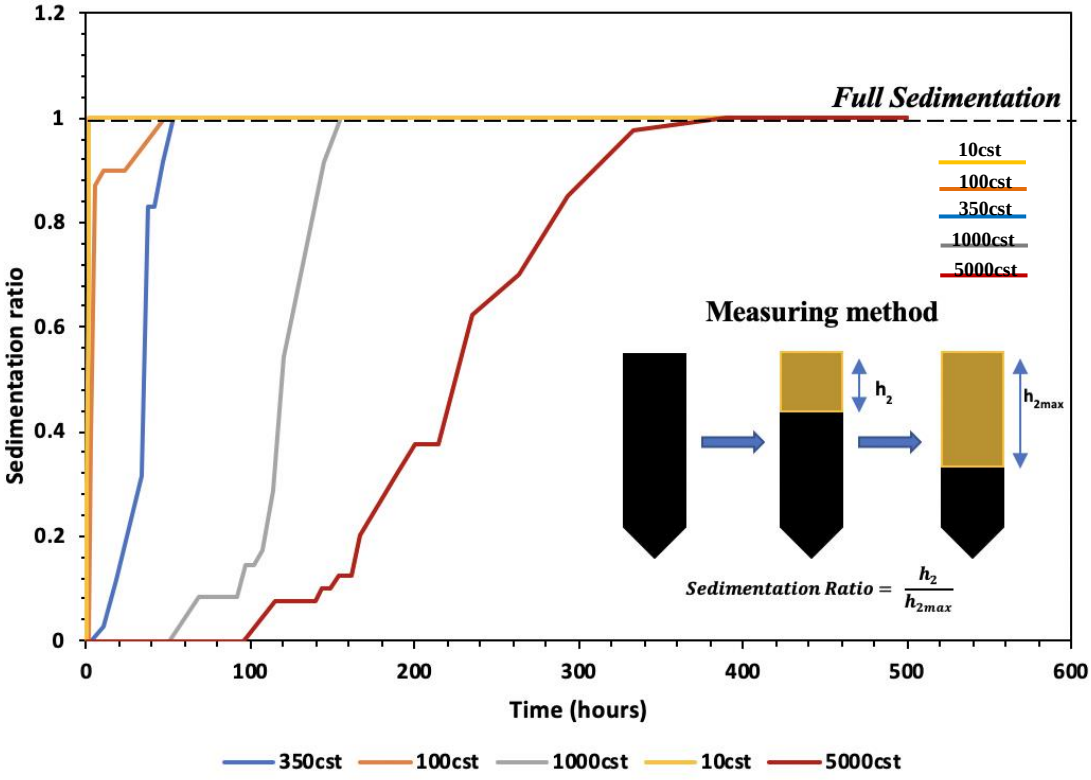

Figure 3-11: Sedimentation ratio using iron oxide to oleic acid weight ratio of 0.45, 10Vol%, and silicone oil of various viscosities

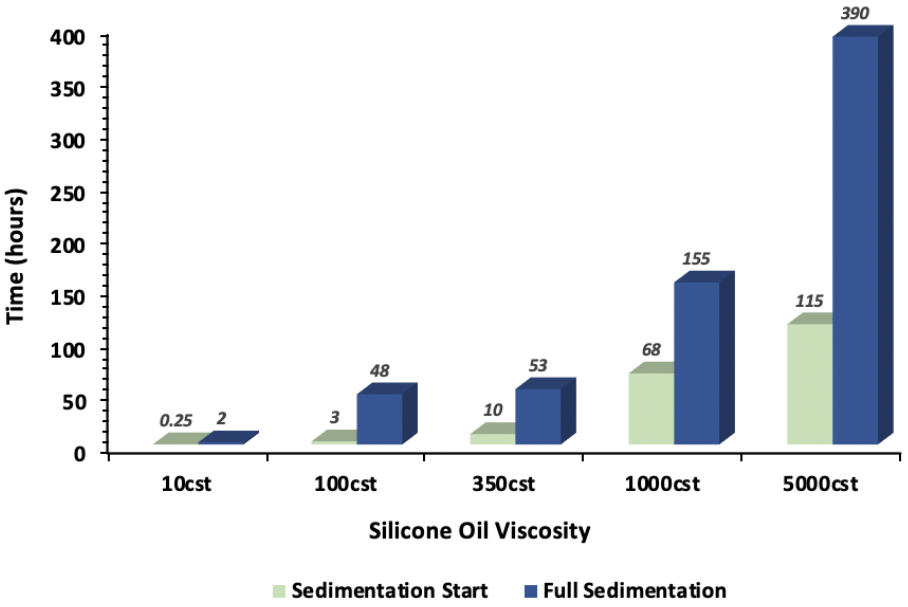

Figure 3-12: The time sedimentation starts and time it reaches full sedimentation using iron oxide to oleic acid weight ratio of 0.45, 10Vol%, for silicone oil of different viscosities

3.4 Volume Fraction Effect on Stability

The effect of volume fraction on sedimentation ratio with motor oil as the carrier fluid was investigated. The method used to prepare iron oxide-oil with the different volume fractions is shown in figure 3-13 with the respective amount of each composition summarized in table 3-2. Due to the high viscosity of motor oil, it provides an initial stable material to test the effect of volume fraction on stability [73]. The other benefits of using motor oil is discussed in section 2.1. Three different volume fractions (5%, 10% and 20%) provides a range to investigate with and understand its effect on stability. After preparing the suspensions, the changes in sedimentation were measured for each volume fraction during different time intervals, and the sedimentation ratio plotted in figure 3-14. Figure 3-15 portrays the time it took for each suspension to start to sediment as well as the time it took it to reach full sedimentation.

As shown in figure 3-14 and 3-15, increasing the volume fraction, decreases the sedimentation ratio, and improves stability. At higher volume fractions, the overall viscosity of the magneto-responsive material increases, which increases the viscous drag acting on the particles, maintaining their suspension in the solution longer. As the volume fraction increases, the time it takes for the sedimentation to start increases. This is because at higher volume fractions, the drag forces are stronger and more dominant, especially in the beginning of the process. This slows down particle migration towards adjacent particles.

Interestingly, the time it takes for the sedimentation to reach full sedimentation decreases from 5Vol% to 10Vol% and then increases at 20Vol%. As shown in figure 3-14, up to 28 hours, sedimentation at 5Vol% is faster than 10Vol%, consistent with lower viscous forces acting on the particles, however at 28 hours, the 5Vol% and 10Vol% overlaps, with the 10Vol% increasing its sedimentation rate to be higher than the 5Vol%. 20 Vol% took the longest time to sediment throughout. The trends exhibit the interplay of viscous and dipole forces in the material. For the

5vol% and 20Vol%, there is a slower and more gradual transitions than the 10vol%, which is explained by the conflicting viscous and dipole forces acting in parallel on the particles. However, in the 10vol% there is a sudden change in sedimentation rate, as the dipole forces become more obviously dominant than the viscous forces that aims to slow down sedimentation.

At 5Vol%, the viscous forces are still most dominant towards full sedimentation even with particles clustering, keeping the particles suspended in the solution longer before attaining full sedimentation. At 10Vol%, the particles are closer together because there are more particles in the same volume space, which means that particles will experience dipole-dipole forces. However, initially the viscous forces are larger than in the 5Vol% which explains the slower sedimentation rate. However, as the particle cluster and grow in size, their magnetic dipole-dipole increases which speeds up agglomeration. Larger agglomeration means the acting gravitational force is bigger, quickening sedimentation. The dipole-dipole forces are more dominant than the viscous forces which is why the sedimentation rate overcomes that of the 5Vol%.

For the 20Vol%, the particles are closer in proximity compared to the 10Vol%, which means the dipole forces are larger. However, the viscous forces are much stronger than the 10Vol% and thus play a more dominant role than the magnetic dipole-dipole forces. This explains the slower sedimentation rate despite the higher attractive forces in the suspension. Over time, the particles slowly sediment because they slowly move and get attracted to adjacent particles, clustering and increasing their attractive forces, hence settling to the bottom.

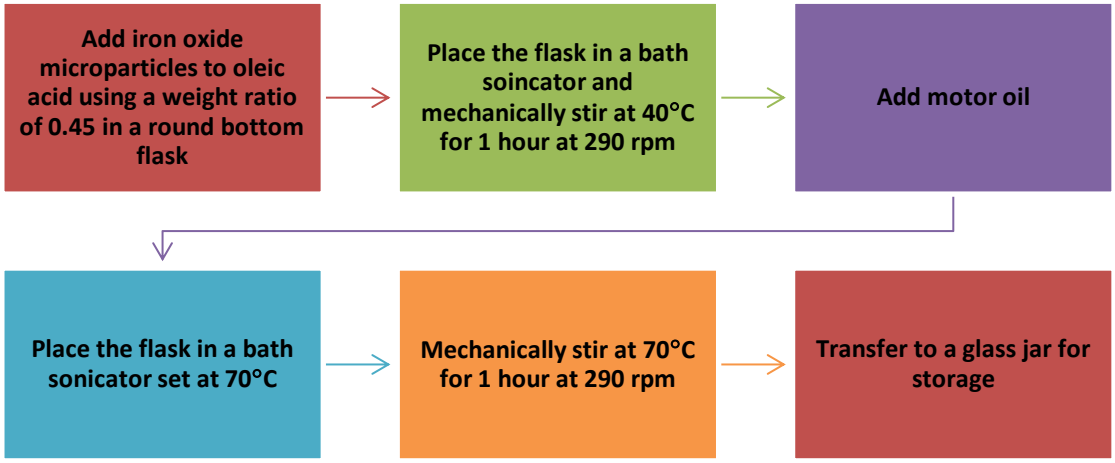

Figure 3-13: Summarized step by step process to test the effect of volume fraction on stability

Table 3-2: Amount of each composition to prepare samples with different volume fractions

Volume Fraction	Mass of Iron Oxide (g)	Oleic Acid Volume (ml)	Carrier Fluid Volume (ml)
5Vol%	10	5	195
10Vol%	10	5	95
20Vol%	20	10	90

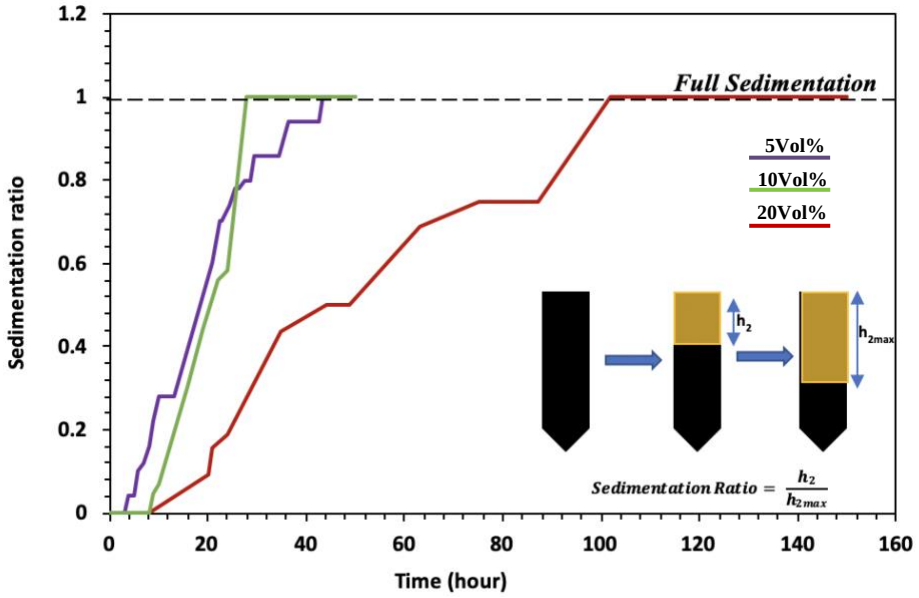

Figure 3-14: Sedimentation ratio using iron oxide to oleic acid weight ratio of 0.45 at different volume fractions, using motor oil as the carrier fluid

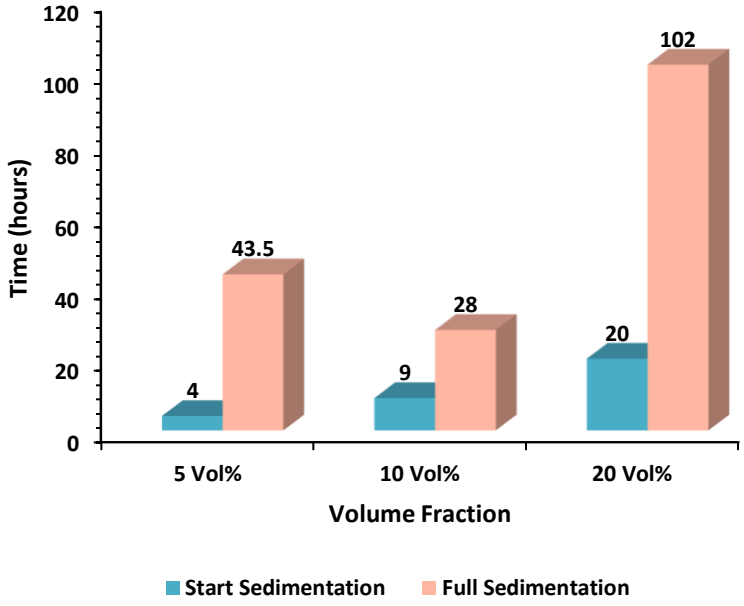

Figure 3-15: The time sedimentation starts and time it reaches full sedimentation using iron oxide to oleic acid weight ratio of 0.45, at different volume fractions, using motor oil as the carrier fluid

3.5 Summary of Significant Results

Various mixing methods were investigated to determine a suitable process to disperse iron oxide microparticles in oil. Ultrasonication was more effective for nanoparticles, whilst mechanical mixing resulted in lower sedimentation rates for microparticles. The stability of the material was investigated by preparing the materials and plotting sedimentation ratio over time. Sedimentation ratio was calculated by measuring the changes in height over time as particles settle to the bottom, then dividing it by the maximum change in height achieved during full sedimentation.

One method to overcome sedimentation is by coating the particles with a surfactant to increase electrostatic repulsion between particles and reduce clustering. It is important to find a suitable amount of oleic acid to use when fabricating the material, as too little and too much surfactant can increase clustering. Six different iron oxide to oleic acid weight ratios were investigated and sedimentation ratio over time was recorded. A ratio of 0.45 led to the most stable suspension and thus used when investigating the effect of volume fraction and carrier fluid viscosity on stability.

Magneto-responsive material with five different silicone oil viscosities were fabricated using mechanical mixing and a surfactant ratio of 0.45 to test the effect of carrier fluid viscosity on stability. In addition, magneto-responsive material with three different volume fractions and motor oil were fabricated using mechanical mixing and a surfactant ratio of 0.45 to test the effect of volume fraction on stability. As the viscosity of the carrier fluid or volume fraction increased, sedimentation rate decreased due to higher drag forces keeping the particles suspended in the solution longer. By changing factors in the fabrication method such as the carrier fluid viscosity and volume fraction, the role of dipole and viscous forces varied, resulting in different extents of stability.

Both volume fraction and viscosity impact the electrical and rheological response of the material under the application of an external magnetic field. To study their effect on the material's properties, experiments discussed in chapter four must be run on stable suspensions so that sedimentation doesn't affect results. Thus, it is important to both find a suitable fabrication method to increase stability and identify the time it takes to start showing sedimentation and reach completion.

4 Electrical Properties of Magneto-Responsive Material

The changes in electrical properties of magneto-responsive materials under a magnetic field make them widely applicable and useful. Under no external stimulus, the resistance of the magneto-responsive material is of the order of the high resistance of the insulating carrier fluid. Under an external magnetic field, particles align in the direction of the magnetic flux, forming chains. The resulting paths, or chains, ease the transfer of electrons across, thus increasing the electrical conductance of the material. This chapter will discuss the effect of various parameters, such as carrier fluid viscosity, particle concentration, and duration of external field on the resistance changes of the material and synaptic plasticity demonstration (see table 4-1). The material was placed in holder C (see section 2-7) and positioned 2.5cm from the edge of the electromagnet (see figure 2-18). By applying both a low strength, 50mT, constant and cyclic magnetic field on the material, the resistance change of the material over time was recorded using a high resistance source meter (see section 2.6)

Table 4-1: Summary of different case studies conducted to investigate effect of carrier fluid viscosity and cycle time on electrical conductance

Viscosity	Vol%	Cycle time	Short-term synaptic plasticity
10cst	10	3 minutes 5 seconds 3 seconds	Facilitation
100cst	10	1 minute 30 seconds	Depression
5000cst	10	15 minutes	Facilitation

4.1 Low Viscosity Carrier Fluid

4.1.1 Continuous Condition

A 10Vol% iron oxide solution was fabricated using 10cst silicone oil and a 0.45 iron oxide to oleic acid weight ratio, to test the effect of low viscosity carrier fluid on the electrical properties of the magneto-responsive material. This particular suspension started to sediment after 15 minutes as shown in figure 3-12 , and thus experiments were conducted on the sample before it started to show sedimentation. A continuous magnetic field of strength 50mT was applied to the sample and the changes in resistance and conductance over time are displayed in figures 4-1 and 4-2 respectively. Under no magnetic field, the resistance of the sample averaged at 157GΩ. After the magnetic field was turned on, the resistance of the sample dropped to 20GΩ, corresponding to an overall decrease of 87.2% within milliseconds (see figure 4-1). In terms of conductance, under no magnetic field, the conductance of the material was 0.006 nS. Within milliseconds, the conductance value increased to 0.043 nS when the magnetic field was applied, analogous to a 616.6% increase (see figure 4-2).

The role of carrier fluid viscosity is displayed by the changes in resistance and conductance over time. For a carrier fluid with low viscosity, the magnetic dipole-dipole forces induced in the particles are more dominant than the viscous forces. The magnetic force provided by the electromagnet causes the magnetic moment of the particles to align parallel to the flux. Particles induce magnetic dipoles in adjacent particles, creating a force of attraction between them. This leads to chain formation under the application of an external magnetic field, which acts as conducting paths that enhance the conductance of the material. The chains formed by particles attracted to each other, allow electrons to move across, conducting a current.

When the magnetic field is turned off, the particles lose most of their magnetization, but maintain some due to remanence magnetization (see section 2.2.2). This removes the attractive forces, causing the particles to re-disperse in the solution. The viscous forces act opposite to the motion of the particles as they move to form and break chains. Under no magnetic field, the viscous forces are too low to keep the particles in chains. Thus, due to the very low viscous forces acting on the particles and dominating magnetic dipole forces, the particles form chains and break within milliseconds.

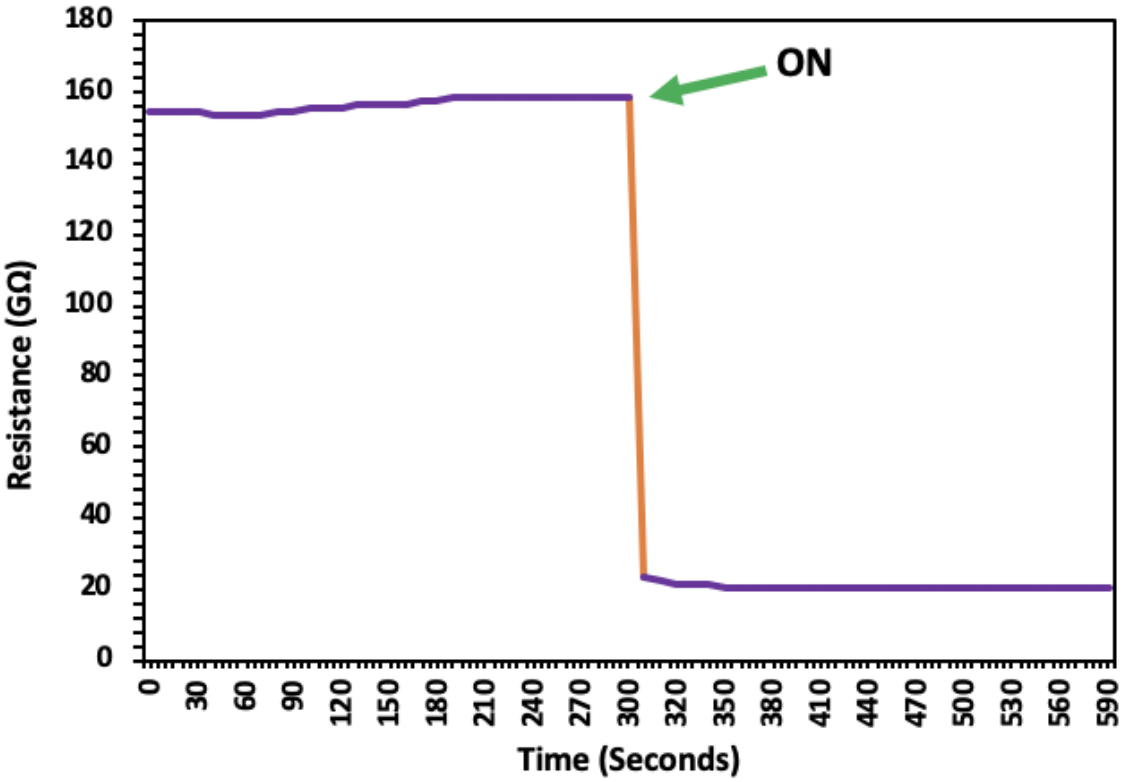

Figure 4-1: Resistance change over time for a low viscosity sample under the constant application of a uniform 50mT magnetic field with the magnetic field turned on at 300 seconds, or as indicated by the ON label

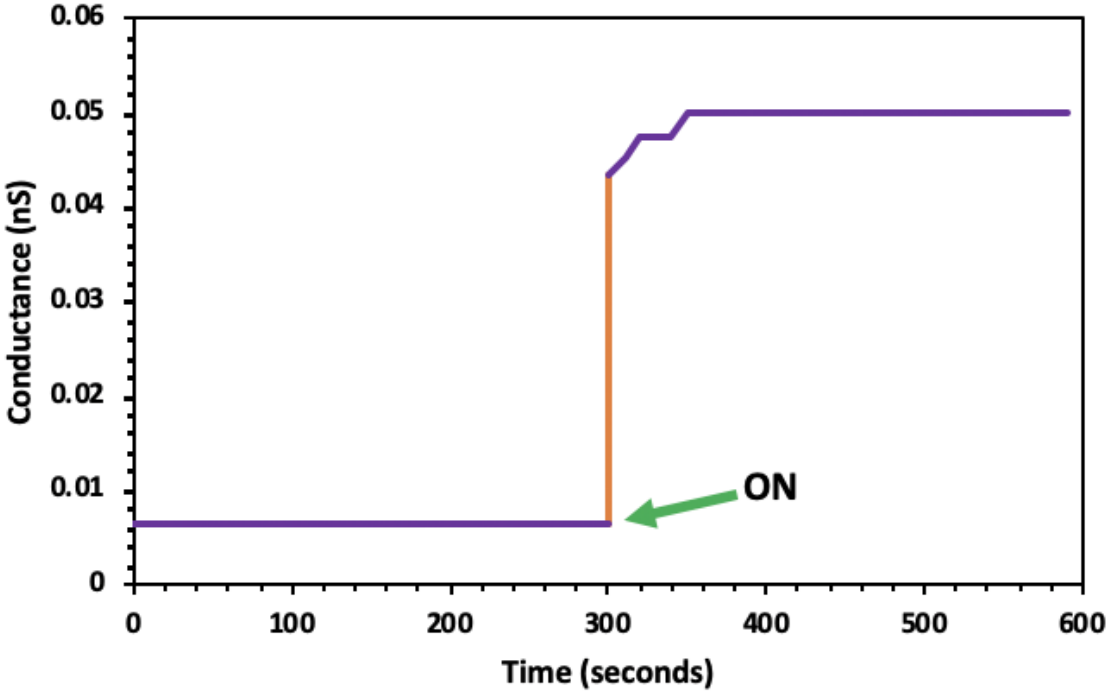

Figure 4-2: Conductance change over time for a low viscosity sample under the constant application of a uniform 50mT magnetic field with the magnetic field turned on at 300 seconds, or as indicated by the ON label

4.1.2 Cyclic Condition

Moreover, the sample was investigated using cyclic field conditions to understand the effect of repeated stimulus on the material. The repeated stimulus provided by the magnetic field is similar to the reiterated spikes experienced by synapses that give rise to short-term facilitation and depression. To the best of our knowledge, there are no past literature paper that performed a similar experiment on magneto-responsive material using low magnetic field cyclic conditions on different viscosities of carrier fluid. Thus, the time selected to apply the cycles were based on trial and observation of the material's response to the continuous magnetic field application. Different

cycle timings were experimented with to understand its effect on the material's conductance and find a suitable cycle time.

For low viscosity fluids, first a long cycle time was used to understand its effect on the material's conductance. This means the magnetic field was turned on, data was collected every ten seconds for three minutes, and then the magnetic field was turned off and data was collected for ten seconds for three minutes, and so on (see figure 4-3). During the periods when the magnetic field was on, as shown by the green ON label in figure 4-3, the conductance increased rapidly first as chains form and then more steadily. This can be supported by figure 4-2, where chains form within milliseconds due to the low drag forces acting on the particles. When the magnetic field was off, shown by the red OFF label in figure 4-3, the conductance dropped rapidly as well as chains break and particles re-disperse. To better understand the changes that occurred within the three minutes ON cycle, each ON cycle was plotted in figure 4-4. The figure showed that the biggest change in conductance and most dynamic response for each cycle occurred within the first ten seconds due to the low viscosity of the carrier fluid. Thus, cycles within a ten second time frames were also experimented with.

For the three minutes cycle, as the number of cycles increased, the overall conductance increased (see figure 4-5). This change is due to the remanence experienced by the iron oxide microparticles. With each magnetic field cycle, the particles maintained some magnetization, thus displaying higher conductance values with each cycle. When the magnetic field is turned off, chains break, and the majority of the particles disperse forming no attractive forces with each other. However, some form of attraction remains in between particles as they memorize their previous state, allowing them form stronger chains and display higher conductance values with increasing cycle numbers. Due to the low drag forces present, particles form and break chains rapidly, with

the most dominant force being magnetic dipole-dipole. Thus, as the number of cycles increase, the magnetic dipole and the remanence magnetization led to higher conductance.

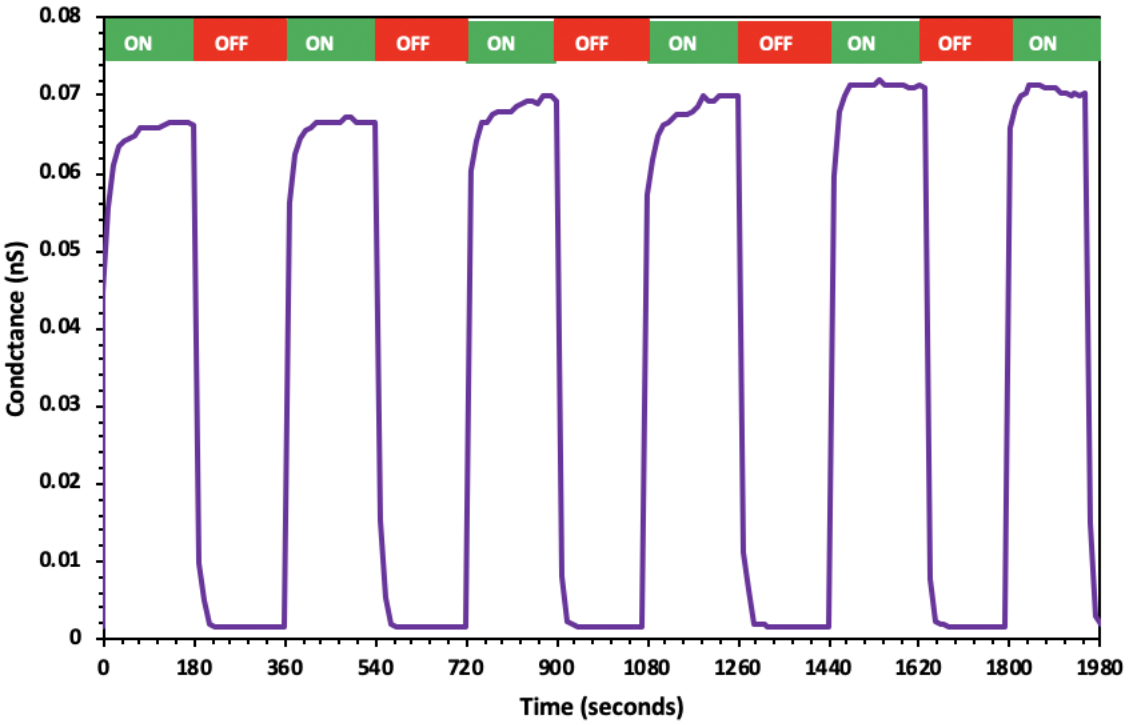

Figure 4-3: Conductance change of a low viscosity sample during three minute cycles, with an on magnetic field indicated by the ON label and an off magnetic field off indicated by the OFF label

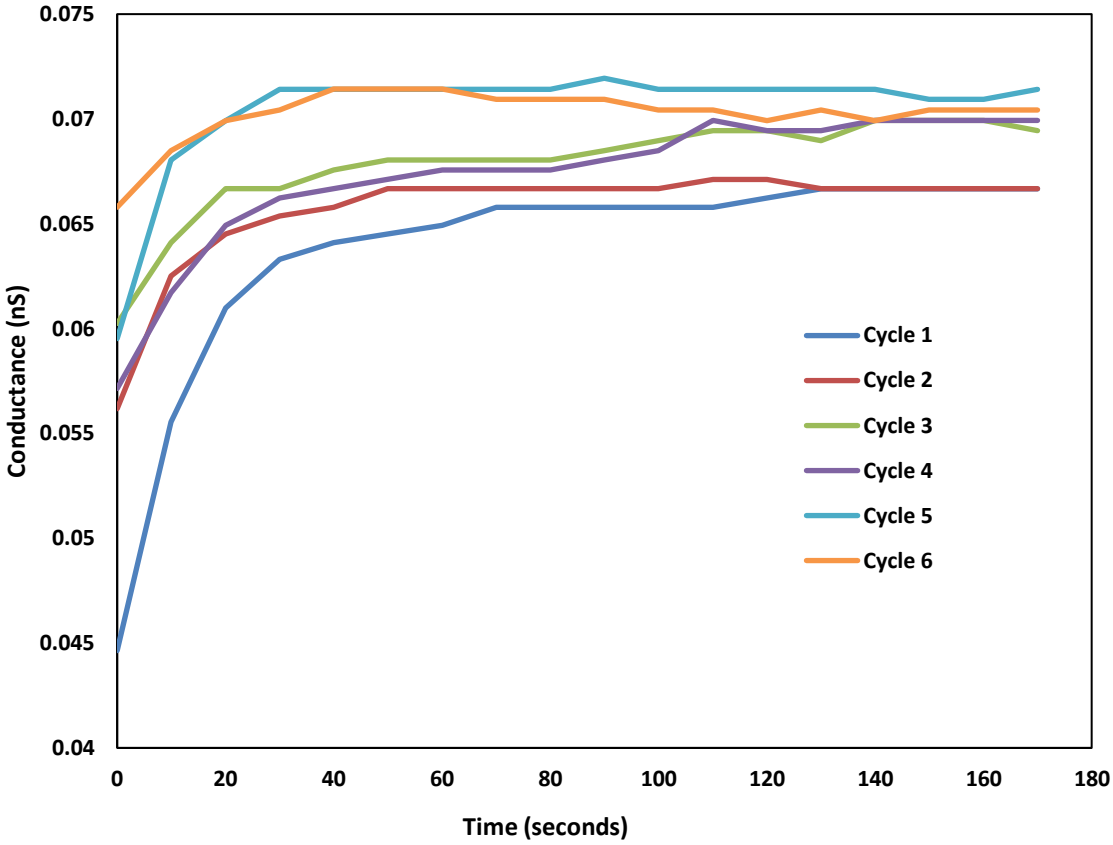

Figure 4-4: The conductance of a low viscosity sample during an ON magnetic field state at each three minute cycle

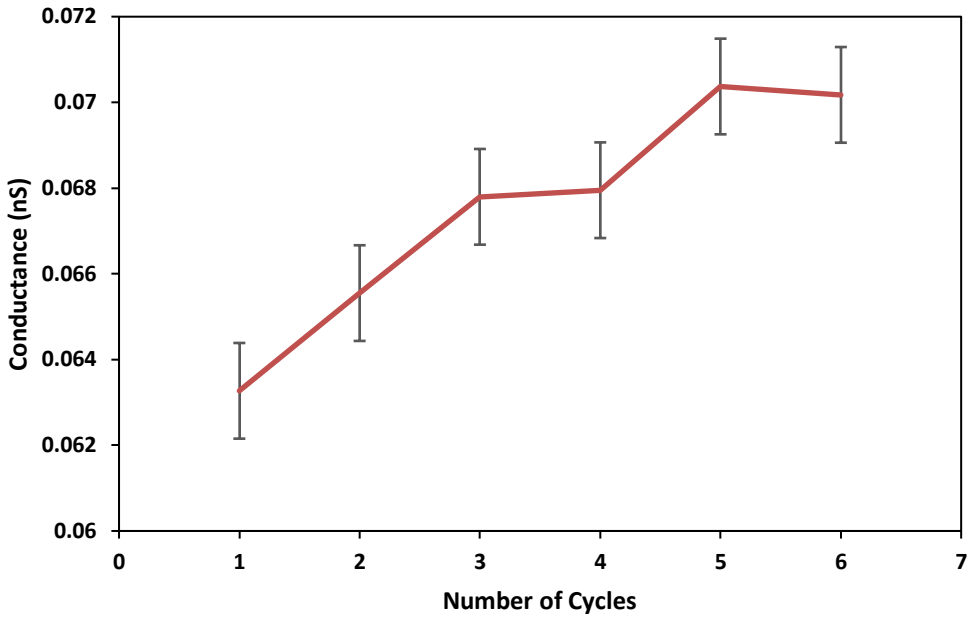

Figure 4-5: Average conductance value during each ON magnetic field three minute cycle for a low viscosity sample

A short cycle time, within a ten-second frame, deemed more appropriate because the material responds within milliseconds when the magnetic field is turned on as well as the most dynamic change occurring within ten seconds. For the low viscosity fluid, five seconds cycles were applied to see the effect of a short cycle time on changes in conductance. Seven five second cycles were applied to the low viscosity sample as shown in figure 4-6. Similar to the three minute cycle, the biggest conductance change occurred within the first three seconds during an on magnetic field state. The average conductance stayed nearly constant in the first four cycles showing the particle remembering their previous state and returning to the same chain formation. The conductance then increased as particles retain magnetization, causing stronger chain formation and higher conducting states.

Moreover, three second cycles were applied to the sample to study the dynamic changes that occurred in the material as shown in figure 4-8. As opposed to the three minute and five second cycles, during each ON state cycle, there were no changes in conductance. The low drag forces due to the low viscosity of the carrier fluid did not hinder the motion of the particles which allowed it to form chains instantaneously. In addition, as the number of cycles increased, there was a smooth straight slope that corresponds to an increase in conductance (see figure 4-9). The increase in conductance is due to particles retaining their magnetization and inducing a magnetic dipole force in a greater number of adjacent particles thus forming stronger chains.

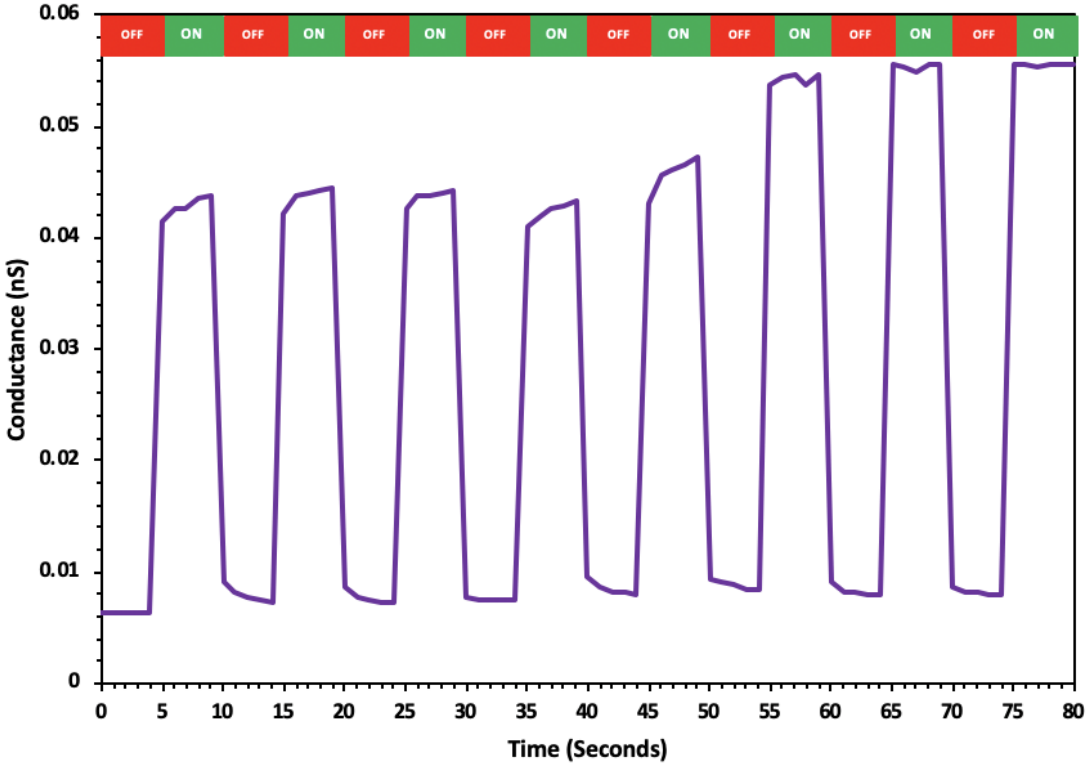

Figure 4-6: Conductance change of a low viscosity sample during five second cycles, with an on magnetic field indicated by the ON label and an off magnetic field off indicated by the OFF label

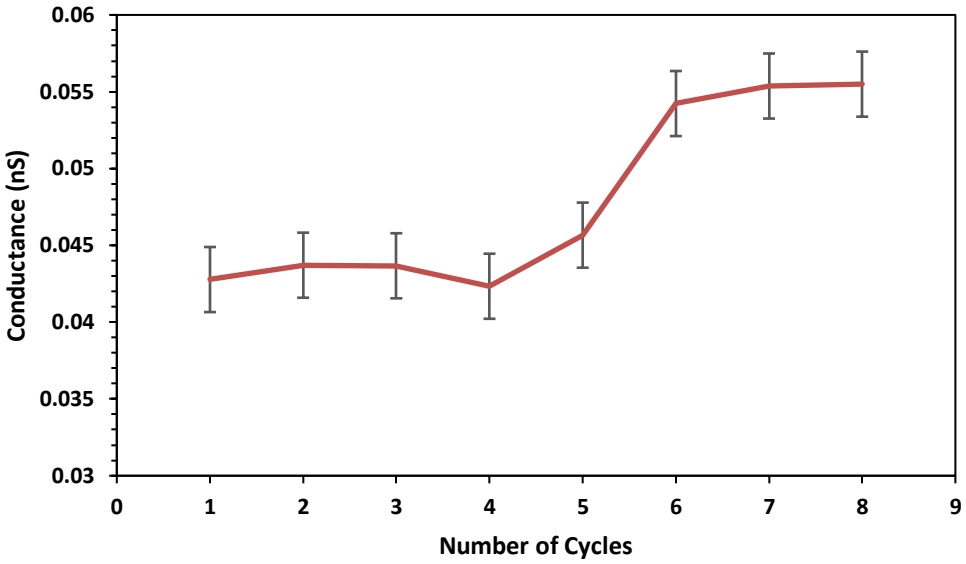

Figure 4-7: Average conductance value during each ON magnetic field five second cycle for a low viscosity sample

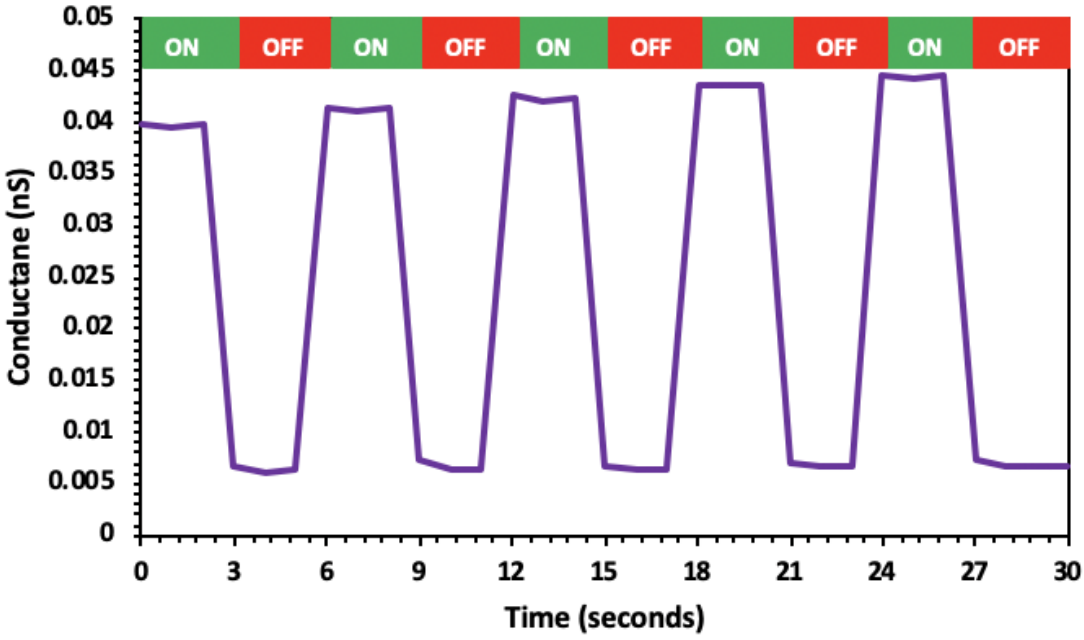

Figure 4-8: Conductance change of a low viscosity sample during three second cycles, with an on magnetic field indicated by the ON label and an off magnetic field off indicated by the OFF label

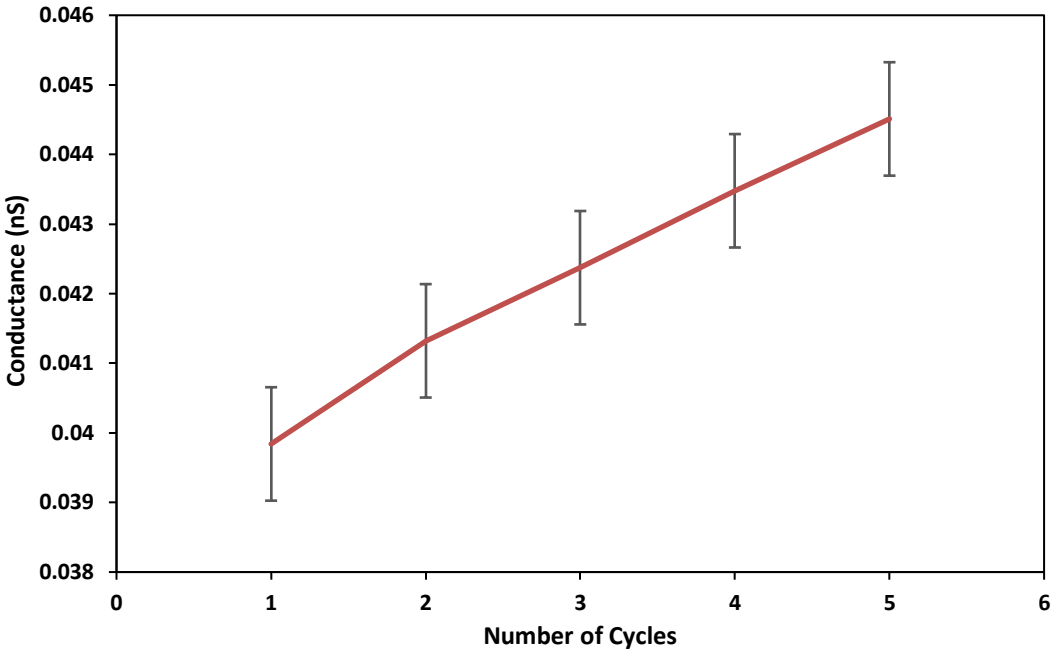

Figure 4-9: Average conductance value during each ON magnetic field three second cycle for a low viscosity sample

4.2 Medium Viscosity Carrier Fluid

4.2.1 Continuous Condition

A 10Vol% sample was fabricated using 100cst silicone oil, to test the effect of medium viscosity on the electrical properties of the magneto-responsive material. This sample started to sediment after 3 hours, and thus experimented with within the time frame before sedimentation. Under no magnetic field, the resistance of the sample averaged at 15 TΩ. After the magnetic field was turned on, the resistance of the sample dropped to 201 GΩ, corresponding to an overall decrease of 98.66% after 38 minutes (see figure 4.10). In terms of conductance, under no magnetic

field the conductance of the material was $6.67x10^{-5}$ GS. Within 38 minutes, the conductance value increased to 0.005 GS when a magnetic field was applied (see figure 4-11).

The effect of using medium viscosity for the carrier fluid displayed the interplay of two conflicting forces, magnetic dipole attraction and viscous drag. Compared to the low viscosity carrier fluid, the 100cst sample took longer to reach its minimum ON state resistance. By applying a constant uniform magnetic field, the magnetic moment of the particles aligned with the direction of the flux, allowing adjacent particles to be attracted to each other, thus forming chains. However, as the particles travel to form chains, the viscous forces act opposite to the motion of the particles slowing them down. The role of the viscous forces is crucial in understanding the longer time span it took for the material to achieve its minimum resistance state, or maximum conductance state; a mechanism that was not displayed significantly in low viscosity mediums.

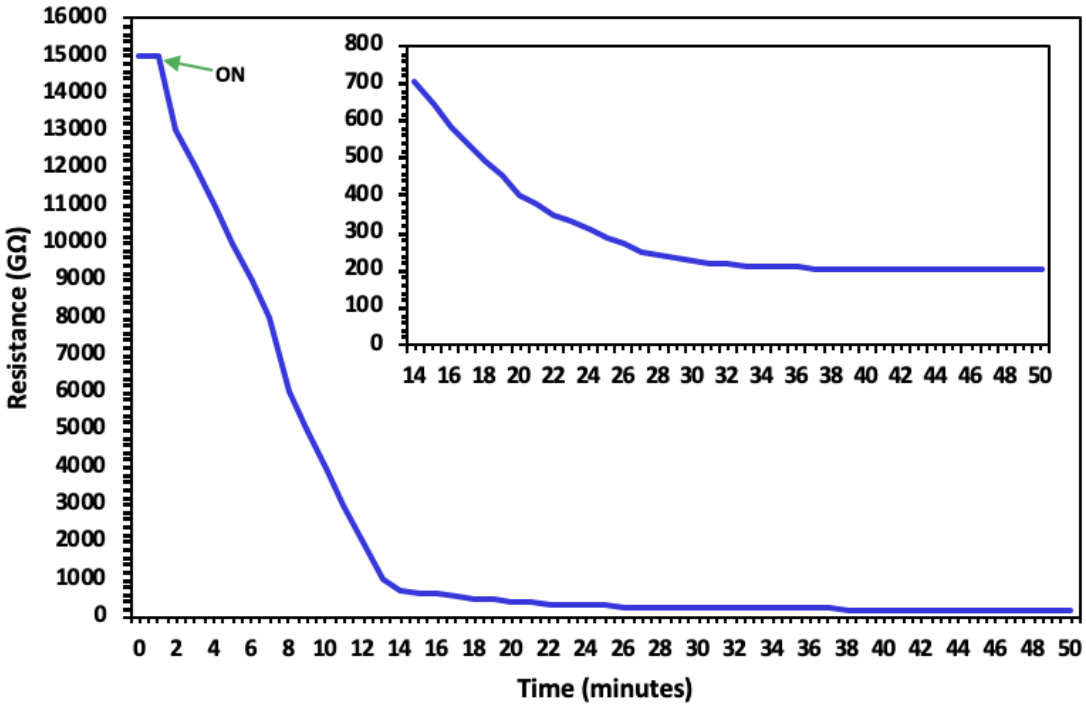

Figure 4-10: Resistance change over time for a medium viscosity sample under the constant application of a uniform 50mT magnetic field, with the magnetic field turned on 1 second, or as indicated by the ON label

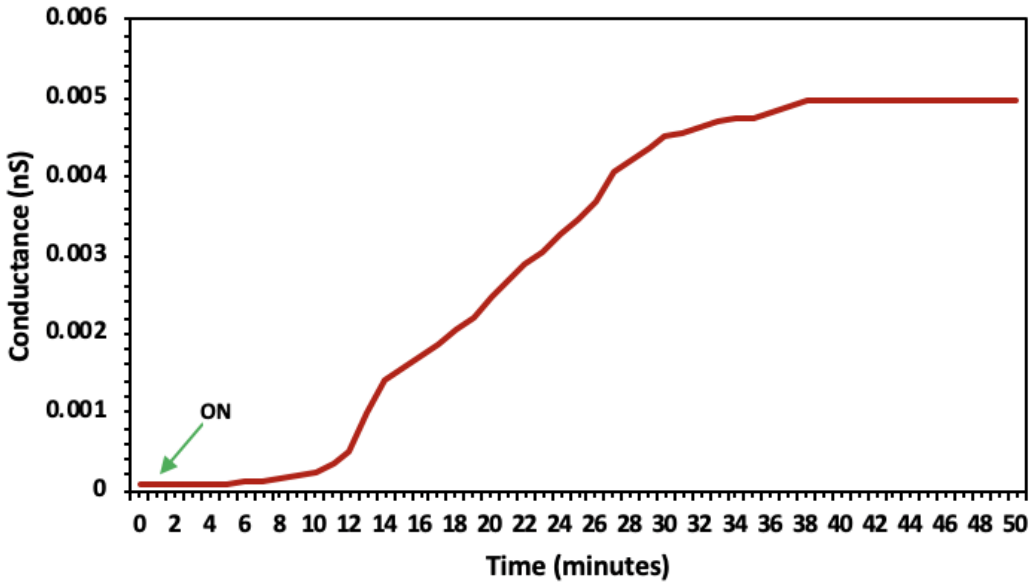

Figure 4-11: Conductance change over time for a medium viscosity sample under the constant application of a uniform 50mT magnetic field, with the magnetic field turned on 1 second, or as indicated by the ON label

4.2.2 Cyclic Condition

Two different cycle times were applied on the 10Vol% 100cst silicone oil sample to see the impact of medium viscosity on conductance. A longer time period was chosen based on the material's slower response to the external stimulus compared to the low viscosity carrier fluid as well as observations from the 10cst sample. The conflicting forces between the magnetic dipole and the viscous forces led to an irregular response of the material. First, a one-minute cycle was applied to the suspension as shown in figure 4-12. Unlike the low viscosity samples, when the magnetic field was turned on, the conductance initially decreased, and then increased (see figure 4-13). This can be explained by the particles trying to maintain their previous conductance state,

which lasted for one minute, when there was no magnetic field applied. However, the magnetic dipole realigns chains and enhances conductance as the magnetic field stayed on for sixty seconds. The magnetic dipoles are not as dominant as in the low viscosity carrier fluid, and thus it takes longer for particles to form chains and return to their magnetized state.

Moreover, a thirty second cycle was applied to the suspension to study the effect of a shorter cycle time on changes in conductance as shown in figure 4-15. Looking at the conductance state under the application of the magnetic field (ON label in figure 4-15), there was no significant variation per cycle like the one-minute cycle. This can be explained by the shorter time the particles are in the off state and thus don't try to maintain their previous conductance state.

In addition, both cycles exhibited a decrease in resistance as the cycle number increased (see figures 4-14 and 4-16). Under a magnetic field, the induced magnetic dipoles causes particles to get attracted to each other and form chains, similar to the low viscosity carrier fluid. However, with the medium viscosity carrier fluid, drag forces play a more prominent role, competing with the dipole forces. When the magnetic field is off, iron oxide particles re-disperse whilst also retaining some magnetization. When the magnetic field is turned on again, the particles attempt to form chains but the drag forces decrease motion. This conflicting force interacting at the microscale causes potential clustering as particles get attracted to adjacent ones due to remanence. The interplay of magnetic dipole and drag forces are displayed here as the particles attempt to form and break complete chains rapidly, which is disrupted by drag forces. This leads to particles

magnetizing and demagnetizing possibly causing separate chain groups to form that are incomplete and weak, thus reducing conductance with an increasing cycle number.

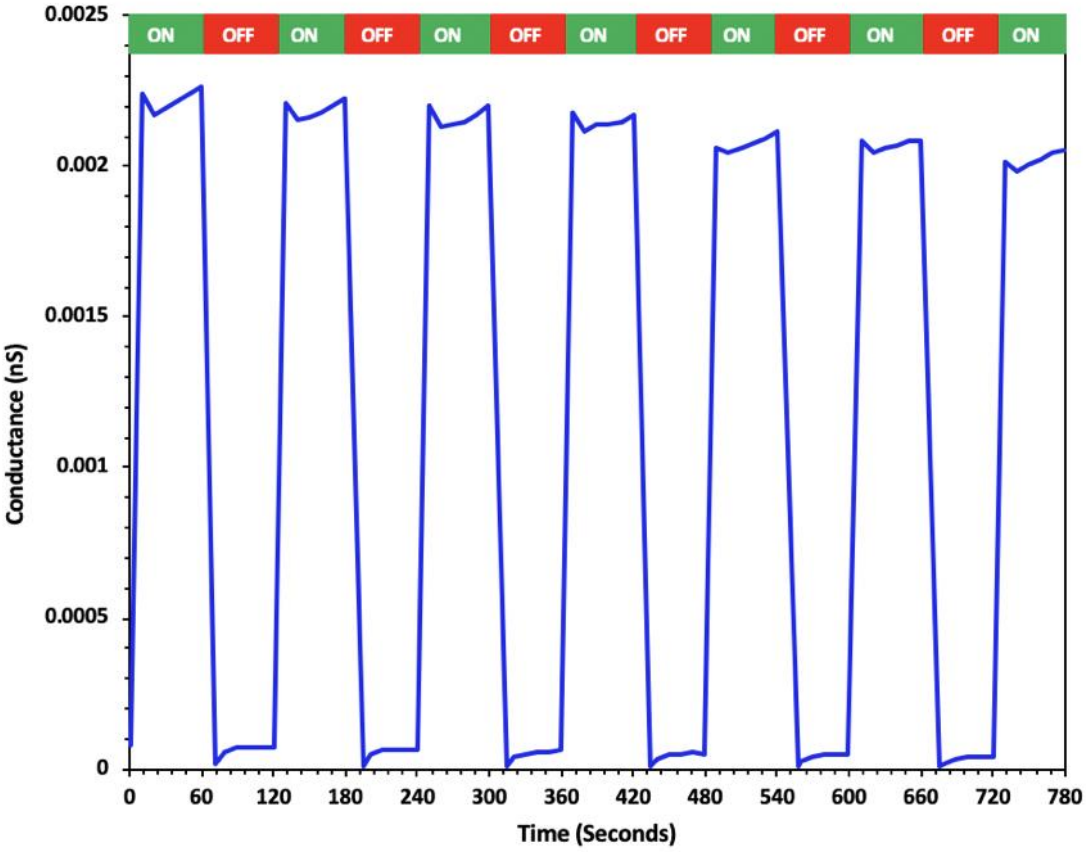

Figure 4-12: Conductance change of a medium viscosity sample during one minute cycles, with an on magnetic field indicated by the ON label and an off magnetic field off indicated by the OFF label

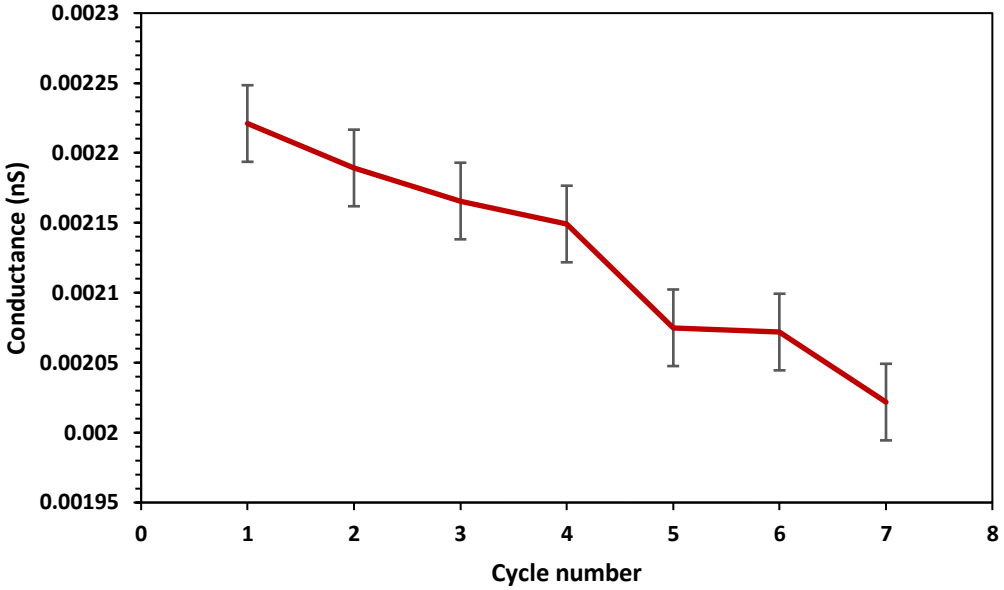

Figure 4-13: Average conductance value during each ON magnetic field one minute cycle for a medium viscosity sample

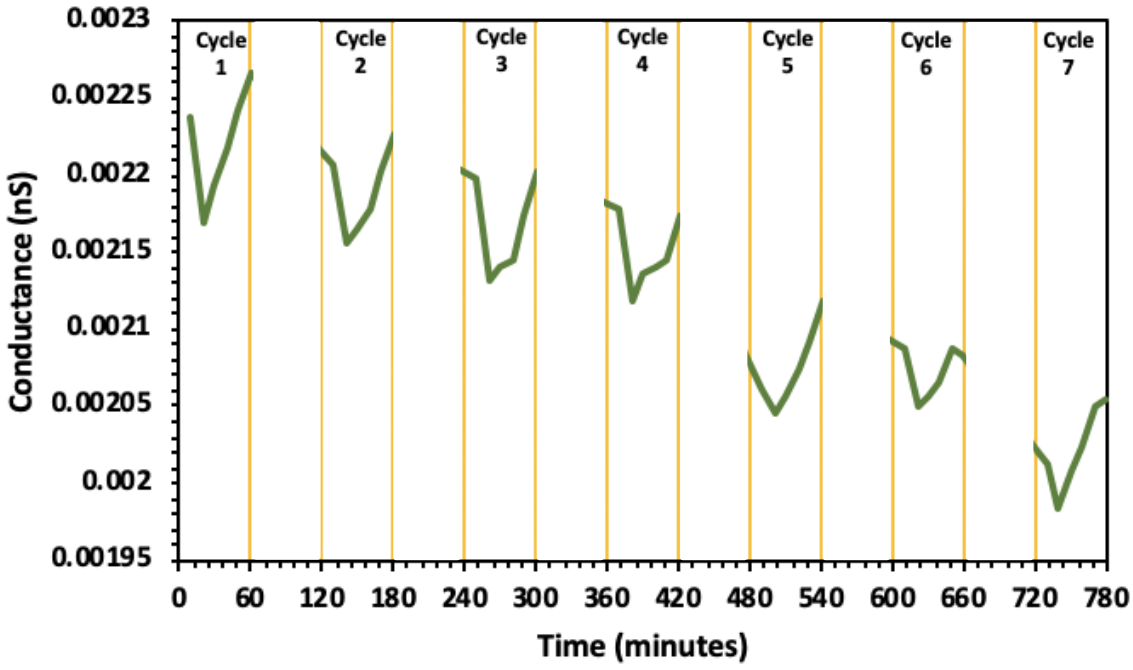

Figure 4-14: The conductance values during each 60 second cycle, when the magnetic field was turned on

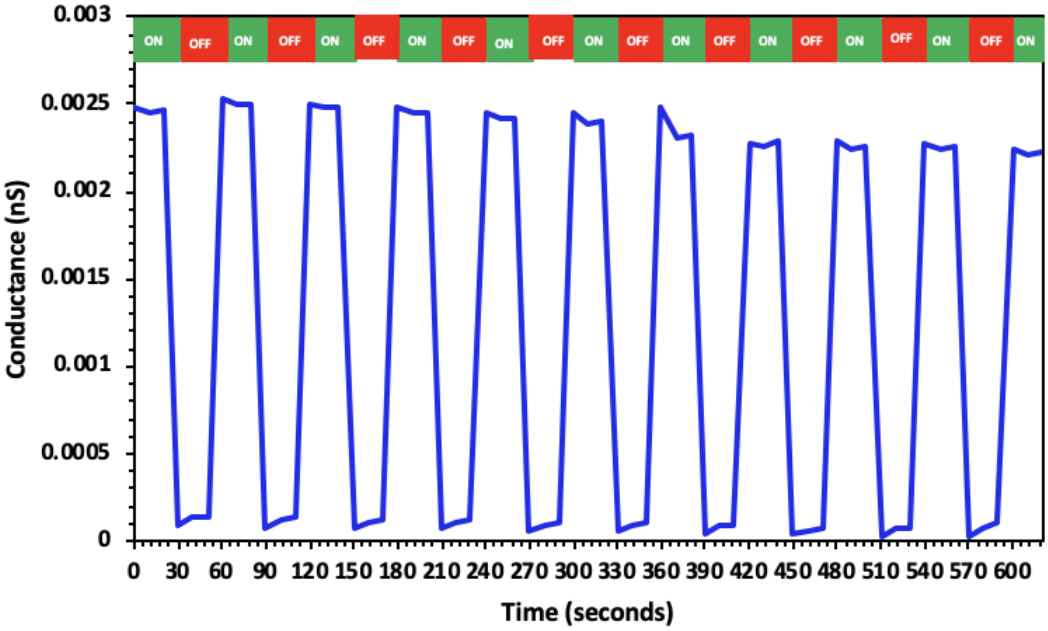

Figure 4-15: Conductance change of a medium viscosity sample during thirty second cycles, with an on magnetic field indicated by the ON label and an off magnetic field off indicated by the OFF label

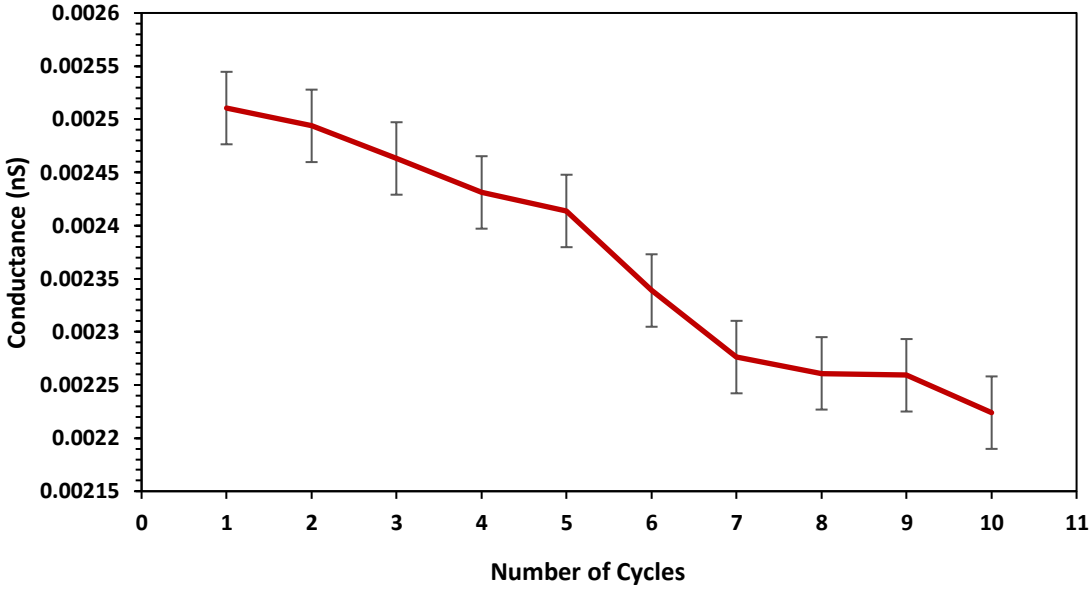

Figure 4-16: Average conductance value during each ON magnetic field thirty second cycle for a medium viscosity sample

4.3 High Viscosity Carrier Fluid

4.3.1 Continuous Condition

To test the effect of high viscosity on the electrical properties of the magneto-responsive material, a 10Vol% sample was fabricated using 5000cst silicone oil. The high viscosity suspension sample started to show sedimentation after 115 hours, and thus experiments were conducted before sedimentation occurred. Under no magnetic field, the resistance of the sample averaged at 235 GΩ. After the magnetic field was turned on, the resistance of the sample dropped to 67 GΩ, corresponding to an overall decrease of 71.49% after 94 minutes (see figure 4-17). The resistance then increased to 105GΩ, a 56.72% increase, after 155 minutes. In terms of conductance, under no magnetic field, the conductance of the material was 0.0043 nS. After 94 minutes the conductance value increased to 0.0015 nS, corresponding to an increase of 65.12%. The magnetic field was then turned off, and the conductance decreased to 0.0063nS after 155 minutes, parallel to a 320% increase (see figure 4-18).

The effect of using high viscosity for the carrier fluid displayed the dominant viscous forces acting on the particles. Compared to the low and medium viscosity carrier fluid, the 5000cst sample took the longest to reach its maximum ON state conductance when applying a constant uniform magnetic field. The particles formed chains slower due to higher drag forces that were inhibiting motion and reducing particle velocity, thus leading to a slow change in conductance over time.

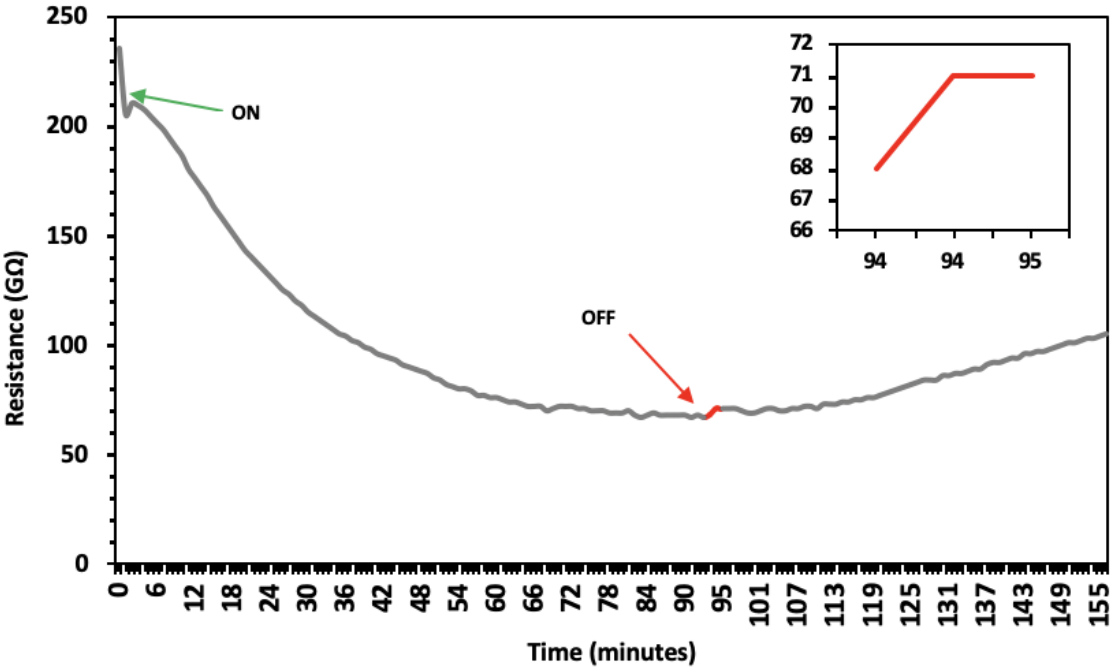

Figure 4-17: Resistance change over time for a high viscosity sample under the constant application of a uniform 50mT magnetic field, with the magnetic field turned on at 0 seconds (ON label), and then turned off at 94 minutes (OFF label).

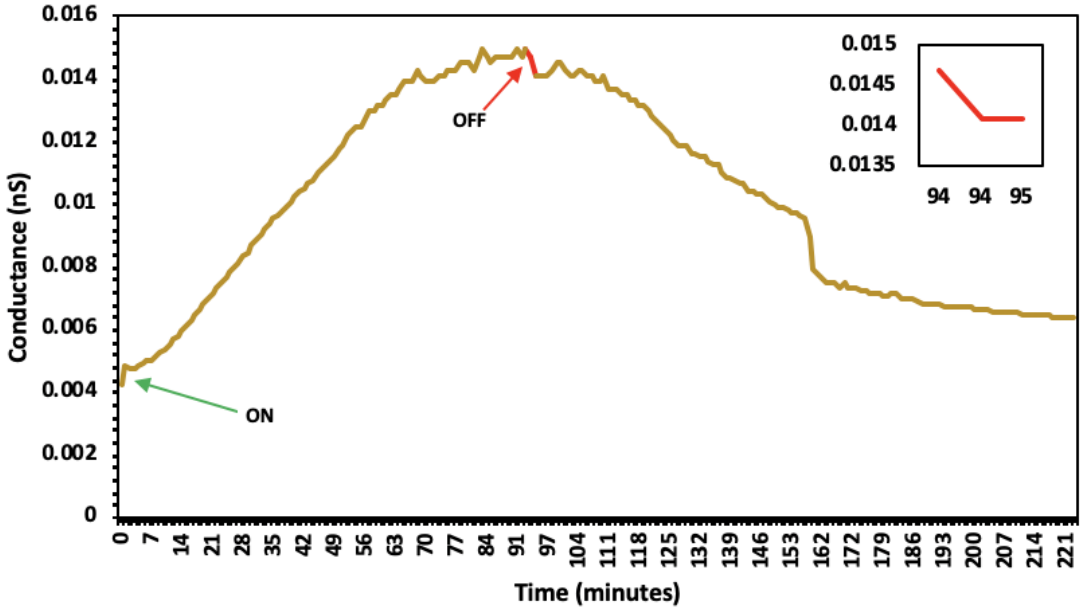

Figure 4-18: Conductance change over time for a high viscosity sample under the constant application of a uniform 50mT magnetic field, with the magnetic field turned on at 0 seconds (ON label), and then turned off at 94 minutes (OFF label).

4.3.2 Cyclic Condition

Moreover, five cycles, 15 minutes each, were applied to the 10Vol% 5000cst silicone oil sample to test the impact of cyclic conditions on conductance (see figure 4-19). Unlike the medium viscosity samples, the conductance of the material increased as the number of cycles increased. During an ON state, the particles moved to form chains aligned with the magnetic flux. Due to the dominating role of viscous forces, the particles experience high drag forces which slowed down motion, chain formation, and redistribution. As the number of cycles increased, more particles accumulated to form chains, and due to high viscosity and slow redispersion, the particles stayed in place when the magnetic field was off, forming stronger and more complete chains with each cycle. This mechanism led to an overall increase in conductance with each cycle (see figure 4-20). The changes in conductance are greater in the first cycles because there were a greater number of particles being magnetized form more incomplete chains. As higher cycle numbers, fewer particles get magnetized, and get added to the chains, strengthening it, thus increasing conductance but at a slower rate.

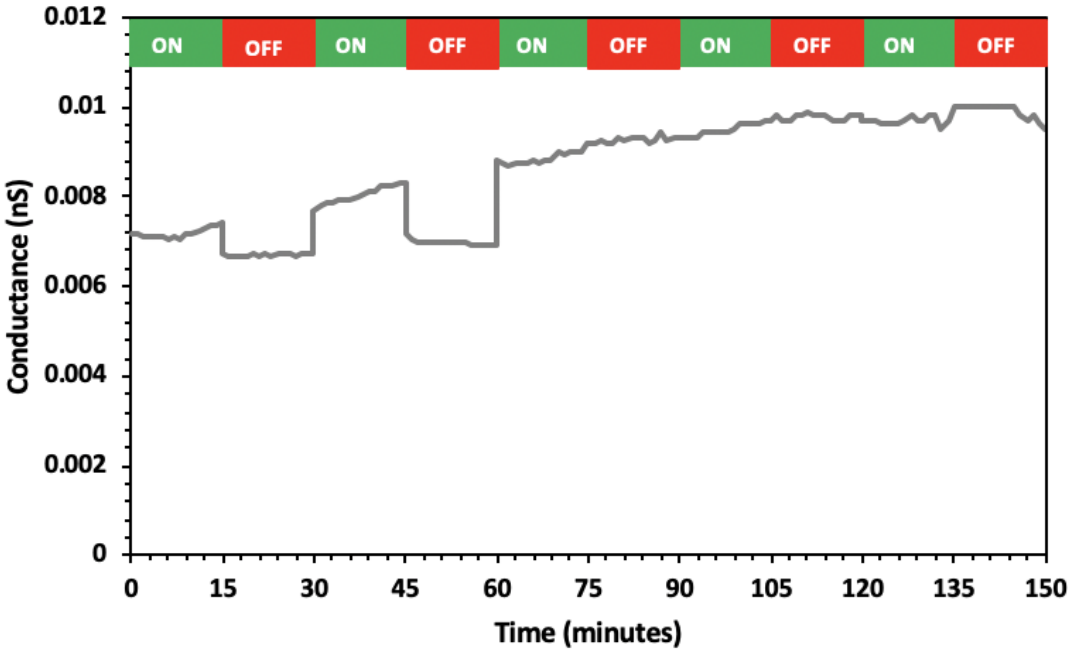

Figure 4-19: Conductance change of a high viscosity sample during fifteen minute long cycles

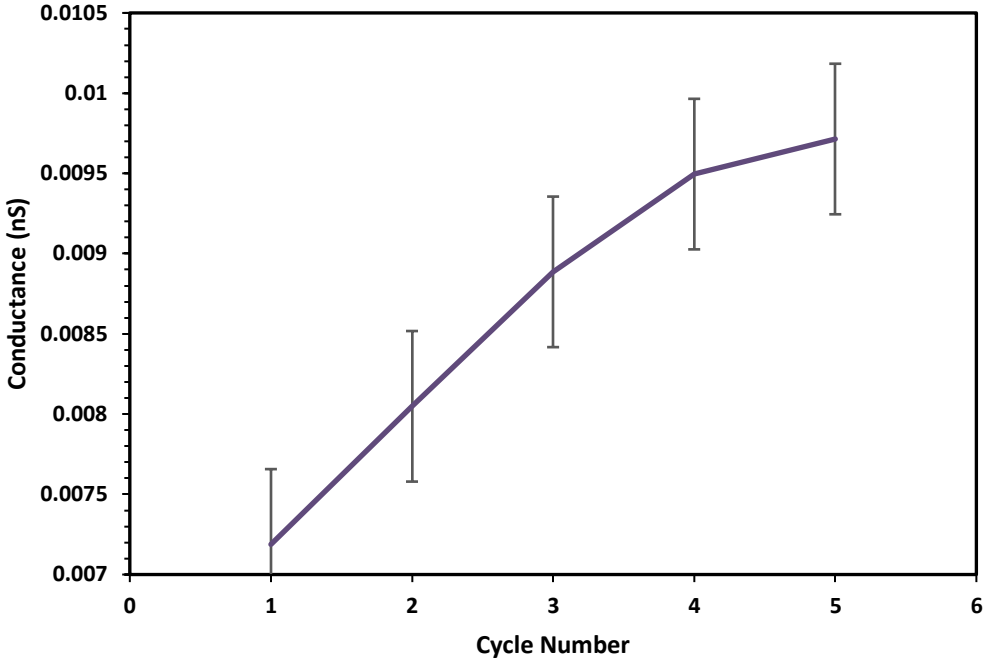

Figure 4-20: Average conductance value during each ON magnetic field fifteen minute cycle for a high viscosity sample

4.4 Link to Synaptic Plasticity

Neurons in the brain give rise to synaptic plasticity by firing repeated changes in voltages that act as an external stimulus, releasing neurotransmitters. Short term facilitation occurs when the repeated stimulus leads to more neurotransmitters being released across the synaptic junction. On the other hand, short term depression takes place when the repeated spikes leads to less neurotransmitters being released across the synaptic junction. The number of neurotransmitters released corresponds to the conducting paths that forms when particles form chains under the application of an external magnetic field.

The magneto-responsive material exhibited different behavior depending on the viscosity of the carrier fluid. The plots in figure 4-21 compares the effect of viscosity medium on the changes in conductance. The values were calibrated by dividing the conductance at each cycle with the

conductance from the first cycle, displaying changes in conductance with cycle number. For the low viscosity medium (three second cycle), as the stimuli was repeated, the conductance increased. This is due to remanence magnetization causing the particles to remember their previous states and form stronger chains as magnetic dipole is induced in adjacent particles. The low viscosity of the carrier fluid applied negligible drag forces; thus the plots demonstrated the role of magnetic dipole on the outcome.

For the high viscosity sample, as the stimuli was repeated, the conductance increased as well. As the number of cycles increases, more particles get magnetized and form stronger and more complete chains, leading to higher levels of conductance. As the number of cycles increased, more particles accumulated to form chains, and due to high viscosity and slow redispersion, the particles stayed in place when the magnetic field was off, forming stronger and more complete chains with each cycle. The larger changes in conductance that occurred for the high viscosity sample compared to the low viscosity sample demonstrated the significant role of carrier fluid viscosity. Due to the low magnetic field strength of 50mT, the magnetic dipoles induced in the particles are weak. However, the viscosity of the carrier fluid is high leading to its more prominent role in creating changes in conductance in the material. The increase in conductance demonstrated by both low and high viscosity samples are parallel to short-term facilitation, where more neurotransmitters are being released leading to a stronger synaptic response.

Conversely, for medium viscosity samples, due to the interplay of magnetic dipole and viscosity forces competing, the particles form incomplete chains. The particles attempt to get attracted to each other and form chains aligned with the flux, whilst also experiencing drag forces that inhibit motion and slows down particles from forming chains. As the drag forces act on the particles, adjacent iron oxide particles cluster together due to remanence magnetization. This causes incomplete or separate chains forming which leads to a decrease on conductance. Although remanence magnetization is present in low viscosity samples, the low drag forces causes particles

to re-distribute and form chains within millisecond, which reduces clustering. The decrease in conductance with repeated spikes is analogous to short term depression because of the weaker conducting paths, where less neurotransmitters are being released leading to a weaker synaptic response.

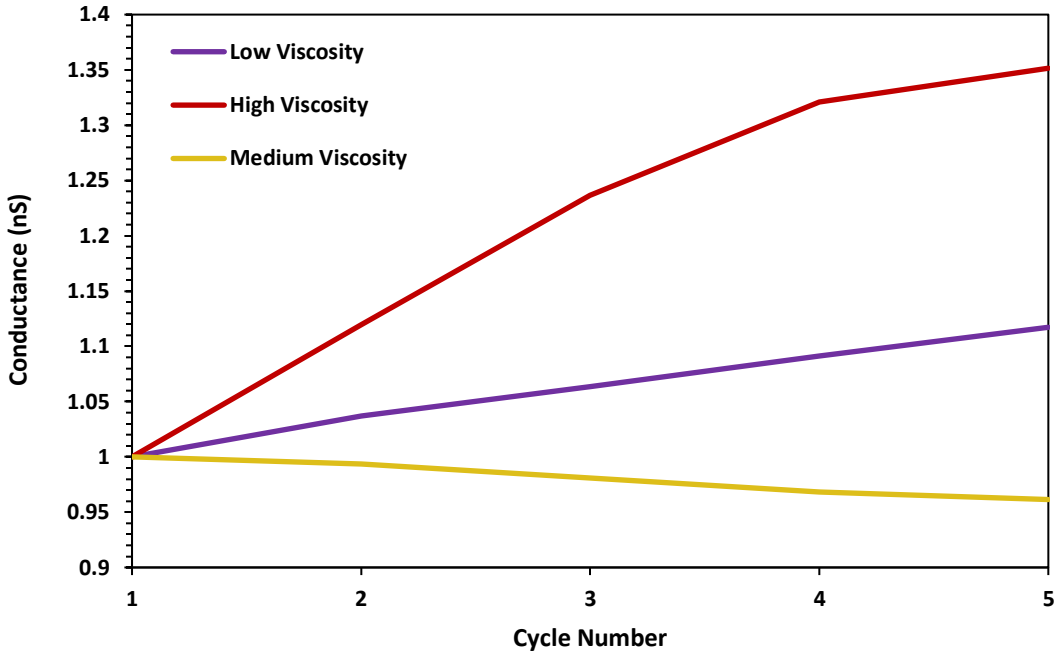

Figure 4-21: Comparison of the average conductance values during each ON magnetic field cycle for low, medium and high viscosity samples

5 Conclusion and Future Work

5.1 Conclusion

Magneto-responsive materials enables a variety of applications (see section 1.1), due to their ability to reversibly change their properties under the application of an external magnetic field. The magnetoactive particles align with the magnetic flux, forming chains that increases electrical conductance, mechanical stiffness, and viscosity of the material. When the magnetic field is turned off, the particles lose their magnetization and re-disperse, returning to their initial electrical and rheological state (see section 1.2). Despite their various applications, there is a lack of focus that links the changes in the material's properties to synaptic functions and short-term plasticity (see section 1.3). This is an important initial step in designing artificial synapses and memristors using magneto-responsive material.

The thesis was designed around three important research questions and many related objectives, to relate the property changes of stable magneto-responsive materials to synaptic functions (see section 1.4) . By studying the microscopic and macroscopic behavior of magneto-active particles in different carrier fluid viscosities, responsive materials can be designed and adjusted to achieve synaptic functions.

Research question 1: What synthesis method is most suitable to fabricate a stable magneto-responsive material that can exhibit synaptic functions?

For this research, iron oxide microparticles were found to be the most suitable magnetoactive size and type of particle to for emulating synaptic functions. This choice for the particle phase was motivated after conducting a vibrating sample magnetometer test on the micro

and nano-sized particles. The microparticles, unlike the nanoparticles, exhibited remanence magnetization which is an important characteristic in memory learning (see section 2.2.2). Moreover, the dry powder form of the particle was placed in a low-strength magnetic field and macroscopic chain formation were observed, crucial to changes in conductance.

Iron oxide microparticles are not frequently used in fabricating magneto-responsive material because of their low magnetic saturation and high sedimentation rate. Both mentioned factors make it difficult to synthesize a material that is both stable and has a large response to a strong magnetic field. However, iron oxide microparticles have the capability to retain their magnetization, giving rise to a memory-based material, and making them suitable for synaptic functions in contrast to nanoparticles. In addition, the low magnetic saturation of iron oxide microparticles make it suitable for applying low magnetic field strengths. This means the particles require a smaller magnetic field to form complete chains. Also, the rise of short-term synaptic plasticity states occurs due to the interplay of magnetic dipole forces and viscous forces acting on the material. At high magnetic field strengths which is required for particles with high magnetic saturation, the magnetic dipole would be much more significant than the drag forces, resulting in no variation in synaptic plasticity states. A low magnetic field strength would slow down chain formation in high viscosity carrier fluids as the drag forces becomes more dominant than the magnetic dipole forces. Thus, using particles with a low magnetic saturation is important in emulating synaptic functions as opposed to more commonly used microparticles in magneto-responsive materials with high magnetic saturation (see section 1.2.3 and 1.3.1).

The carrier fluid used ranged between very low to very high viscosities, which are 10cst, 100cst and 5000cst. Using a low viscosity carrier fluid is common in magneto-responsive materials mentioned in literature. This is because materials with a low viscosity carrier fluid leads to an instantaneous property change when exposed to an external stimulus. However, carrier fluids of high viscosity apply larger drag forces to the suspension, leading to better stability in the material.

The higher drag forces also reduce the material's response to the magnetic field, making it non-applicable to current applications in literature such as for drug delivery, brakes and vibration systems. However, high viscosity carrier fluids show promising applications in creating a magneto-responsive material that can mimic synaptic behavior and be used as artificial synapses. This fluid medium will introduce higher drag forces which will compete with the magnetic dipole forces and exhibit synaptic plasticity.

Moreover, fabricating a magneto-responsive material with low sedimentation rates and good dispersion is important to its stability and functioning. Multiple factors affect sedimentation rate such as particle size, viscosity of carrier fluid, volume fraction, dispersion method, surfactant ration and more. This study investigated different surfactant ratio (0.225, 0.45, 0.89, 1.45, 1.8, 2.7) mixing method (mechanical stirring, homogenizer, probe sonication), volume fraction (5Vol%, 10Vol%, 20Vol%) and carrier fluid viscosity(10cst,100cst,350cst,1000cst,5000cst) to determine the most optimum composition and synthesizing process in obtaining a stable suspension. By using mechanical stirring, an iron oxide to oleic acid weight ratio of 0.45, and the higher the viscosity medium and volume fraction, dispersion was enhanced.

To reduce sedimentation rate when working with iron oxide microparticles, they were coated with oleic acid. Oleic acid acts as a surfactant by increasing the electrical repulsion between microparticles and reducing clustering due to magnetic dipole-dipole interactions. The surfactant plays a very important role in the stability of the material (see section 1.2.4 and 1.3.2). By carrying out sedimentation tests on the six different rations, an optimum iron oxide to surfactant weight ratio is determined (see section 2.3). For our study, an iron oxide to oleic acid weight ratio of 0.45 was the most optimum which took 4 hours for the particles to start settling and 43.5 hours to reach full sedimentation (see section 3.2). Above and below the ideal ratio, the particles tend to agglomerate and increase sedimentation rate. Most past studies focus on nanoparticles, however iron oxide microparticles have a smaller surface area to volume ratio and require less surfactant to be

completely coated. Therefore, the focus on microparticle dispersion and the role of surfactant was important to initiate and advance research on the stability of magneto-responsive material for artificial synapses use.

Stability of the material was also affected by varying the viscosity of the carrier fluid and the volume fraction. Increasing carrier fluid viscosity or volume fraction of the material led to lower sedimentation rates as the stronger drag forces keep the particles suspended in the base fluid longer. Understanding the effect of viscosity and volume fraction on sedimentation rate is important when trying to emulate synaptic functions without compromising stability. The sedimentation tests under different viscosities and volume fractions provide initial insight into the conflicting role of drag forces and magnetic-dipole interaction acting on the material. Sedimentation tests also demonstrate the time frame in which the material is stable so that experiments are performed without being affected by particles settling (see section 3.3 and 3.4). For example, for the 10Vol% 10cst suspension, experiments had to be carried out in 15 minutes, for the 10Vol% 100cst suspension it was 3 hours, and for the 10Vol% 5000cst it was 390 hours.

Furthermore, based on past literature and multiple conducted experiments, mechanical mixing is most suitable to coat particles with the surfactant regardless of particle size and type. However, most literature papers work with nanoparticles and thus employ ultrasonication to disperse the functionalized particles in the carrier fluid. In this study, after experimenting with three different dispersion methods, and due to the larger size of microparticles, mechanical stirring led to most stable suspensions, as measured by changes in sedimentation over time (see section 3.1).

Research question 2: How can the composition of a stable magneto-responsive material and external stimulus be altered to allow the material to emulate synaptic behavior and become more intelligent and complex?

By applying continuous and cyclic magnetic fields to the material, different changes of conductance were attained and correlated to synaptic plasticity. The magnetic field, or external stimulus provided by the electromagnet, causes magnetic particles to align their induced magnetic dipole moments in the direction of the magnetic flux (see section 2.5.3). The magnetized particles induce attractive magnetic dipole forces in adjacent particles, forming chains and reversible electrical, mechanical and rheological changes in properties (see section 1.2). Commonly, high magnetic field strengths and no cyclic conditions are applied to magneto-responsive material so that complete chains and a maximum change in conductance occurs. However, by applying a low strength continuous and cyclic magnetic field conditions, different responses can arise from the same material. The response can thus be controlled by an external stimulus to emulate synaptic behavior. Low strength magnetic field conditions bring to light the material's initial response to the stimulus. By slowing down chain formation, the microscale changes that occur in the material before it achieves complete formation can be observed resulting in increases or decrease in conductance with each repeated stimulus.

Continuous magnetic field conditions with no relaxation time display chain growing in the material over a period of time that vary depending on the viscosity of the carrier fluid. Cyclic magnetic field conditions provide a method to stimulate the repeated spikes experienced by synapses (see section 1.2.1). Through experimental trial and error and observation, a starting cycle time was chosen for the material. The cycles applied had significant relaxation time, or infrequent voltage impulses correlating to infrequent magnetic field, so chains form and break continuously giving rise to short-term memory. The infrequent voltages lead to a series of incoming voltage spikes that results in an avalanche effect, locally triggering transition to a conductive state. By

varying cycle time, different responses of the material to the external stimulus can be achieved. For the 10cst suspension, as the cycle time decreases from three minutes to five seconds and then three seconds, the increase in conductance becomes more linear. Chain form and break under external stimuli. However, the extent to which it breaks or forms, and whether each cycle will improve or disrupt chain formation will depend on remanence magnetization, magnetic dipole forces and viscous drag.

Moreover, when applying high magnetic field strengths and using materials with low viscosity like the literature, drag forces are not very significant and have a negligible role. Dipole forces are most dominant in low viscosity materials. At high viscosities drag forces are more dominant, whilst at medium viscosity both conflicting forces play a role. At low strength stimulus and different viscosities, the role of the forces and which one is dominant can be controlled by varying the viscosity of the carrier fluid, which is not an option at high magnetic field strengths.

Research 3: How can the response of the material under different external magnetic field conditions mimic short-term facilitation and depression states of plasticity?

By varying viscosity of carrier fluid and cyclic conditions, in this case three viscous states at 10Vol%, the material exhibited different forms of plasticity due to the interplay of drag and dipole forces on particle motion.

At low viscosity, or 10cst base fluid, there was an instantaneous change in electrical properties displaying the dominant role of magnetic dipole forces on the material. During each cycle application, the particles form and break within milliseconds. However, due to remanence magnetization and the particle's ability to retain its memory and learn from history. This leads to chains form faster and using less energy as they remember their previous state, as can be seen in short cyclic time like 3 seconds and 5 seconds. Low viscosity materials displayed facilitation, as conductance increased with increasing cycle application (see section 4.1 and 4.4).

At medium viscosity, or 100cst base fluid, the interplay of drag and magnetic dipole-dipole are most obvious. Under the application of a continuous magnetic field the resistance drop was slower than low viscosity fluid. The particles try to form and break chains quickly, but remanence magnetization maintains some level of attraction between the particles, whilst the drag forces slows down motion. These conflicting forces lead to separate clusters of particles forming. There is no one force significantly more dominant that another, leading to a decrease in conductance with each cycle, and depression (see section 4.2 and 4.4).

At high viscosity, or 5000cst base fluid, the drag forces are much more dominant than the dipole forces stimulated by the low magnetic field strength. The particles motion is very slow, so once they magnetize and form chains, it is very difficult to re-disperse them as particles are too slow to break away from the chain. Hence, as the cycle number increases, more particles get magnetized, adding up to the chain, strengthening it and increasing conductance. This leads to the facilitation state observed in synapses (see section 4.3 and 4.4).

5.2 Future work

There are four different paths that this research can follow to advance understanding of magneto-responsive material as potential artificial synapses is summarized in figure 5.1.

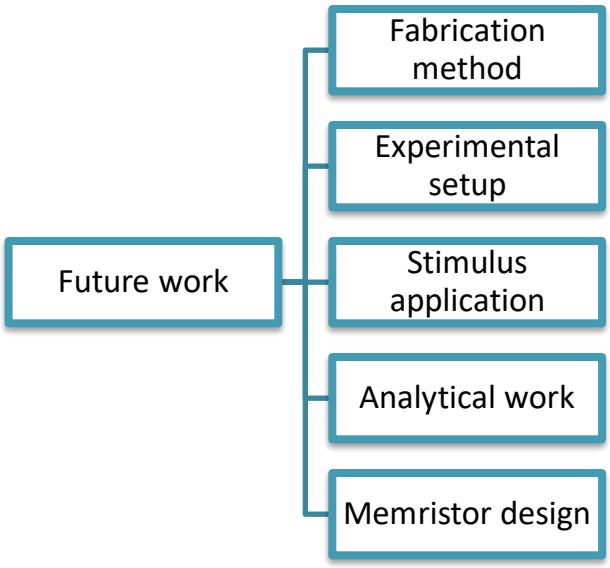

Figure 5-1: Summary of four different paths research can follow to advance understanding of magneto-responsive material as potential artificial synapses

5.2.1 Fabrication Method

It is crucial to the functioning and short-term and long-term use of the magneto-responsive material that the dispersion in the solution remains stable. There are several ways that can be investigated to enhance the current fabrication method further and increase the material's use as potential artificial synapses. First, different mixing times can be explored for the second step in the fabrication process (see section 2.3). The current time of one hour to disperse the coated iron oxide microparticles in oil was adapted from past work on nanoparticles and motor oil. Thus, a longer mixing time might be better for lower viscosity silicone oil and microparticles as they lead to more

sedimentation than high viscosity oil like motor oil and nanoparticles. Another improvement to the fabrication method is to explore using nanoparticles as additives to enhance stability. By employing both nanoparticles and microparticles, the stability and chain formation can be improved. The nanoparticles will fill smaller gaps between microparticles leading to lower conductance. The low viscosity material exhibited the fastest sedimentation rate and response to a magnetic field. Altering the current fabrication method to be specifically for low viscosity fluid can lead to better stability of the material. One example is reducing the mixing temperature, as higher temperature lowers the viscosity of the material. Other smaller objectives and improvements can include experimenting with a larger viscosity and volume fraction range to understand the effect on stability.

5.2.2 Experimental Setup

The current setup uses a low strength electromagnet and a high resistance electrometer to manually measure changes in resistance. The first improvement is to digitally measure changes in resistance to get a higher reading frequency. Secondly, although a low strength electromagnet seemed crucial to the mimicking of synaptic functions in the material, a slightly higher magnetic strength could lead to larger changes in conductance. This could be achieved by using a stronger electromagnet or permanent magnets placed in holders that are mechanically translated to achieve different strength based on distance from the sample. At higher magnetic field strengths, the first electrical setup described in section 2.6 can be employed to plot real-time changes in resistance on MATLAB.

5.2.3 External Magnetic Field Application

Firstly, a slightly higher strength (100mT or 200mT) should be explored using the same suspensions and cyclic times, to understand whether the material behaves in the same way. If the material behaves similarly and exhibits comparable synaptic functions as the low-strength magnet application, then higher changes in conductance can be achieved. However, if the synaptic functions at each viscosity changes, then the external stimulus can be used to control the synaptic functions of the material. At higher strengths, the timing it takes for particles to form chains and breaks may vary, thus it also becomes a factor in controlling chain formation. Moreover, at each viscosity, different cyclic times needs to be investigated, including shorter and longer time than the ones in this thesis. This task is imperative in seeing if the conductance change in the same suspension can switch from facilitation to depression or vice versa based on the cyclic time. Another objective is to carry out longer cyclic changes at higher viscosity materials to see if the particles would re-disperse, leading to different synaptic plasticity states. In addition, this current project applies cycles with significant relaxation time which leads to short term memory. The next step would be experimenting with relaxation time or cycle time to give rise to long term memory. Moreover, smaller aims to advance research in the field is to experiment with volume fractions higher than 10%, different viscosities especially between 100cst and 5000cst, to see if the material will transition from depression to facilitation at a specific viscosity.

5.2.4 Further Theoretical Analysis

One factor that has an effect on sedimentation rate, conductance change and material properties is the volume fraction of the sample. It is important to vary the volume fraction of the sample at each viscosity and analyze the resulting sedimentation ratio and changes in

conductance under a magnetic field. This will allow the determination of whether or not, volume fraction of particles like viscosity of carrier fluid, can be a factor that controls changes in synaptic behavior. A preliminary study was carried out by fabricating a 20Vol% in 10cst silicone oil sample. An external magnetic field of strength 50mT was applied on the material, and the resulting conductance did not change. Even after applying cyclic magnetic field conditions, the conductance changes were insignificant. Based on observation of the material under ON and OFF magnetic field conditions, incomplete chains and clusters were forming. Unlike the 10Vol%, the magnetic field strength was too low to overcome clustering and align chains parallel to the magnetic flux. Thus, a stronger magnetic field strengths is required at higher volume fractions.

Furthermore, analyzed work and explanations in this project is from a the magnetic particle perspective. An important step when moving forward with this project is to carry out theoretical and experimental work on the fluid being used. Fluid properties beyond viscosity can be affecting changes in conductance, and thus in-depth theoretical work such as non-dimensional numbers and experimental fluid analysis can help explain the material's response. This includes conducting experimental tests such as rheology tests on the carrier fluid and mass spectrometer of diffusion column. By determining the storage/loss properties and molecular distribution of the fluid, further understanding of the system will be achieved, and more in-depth explanations to describe the results.

5.2.5 Memristors

After understanding how the material composition and external stimulus can control and achieve desired synaptic functions, the complexity can be increased. A current vs voltage graph should be plotted to obtain a pinched hysteresis loop; a characteristic feature of memristors. Expansion of the analytical and theoretical part of a memristor should be done to link the device to

a model material. Existing artificial synapses are filament forming memristors and they show resemblance to magneto-responsive material. The conductance changes are due to formation and rupture of an electron conducting path triggered by ion migration. In magneto-responsive materials, the electron conducting path are formed and broken by magnetoactive particles that is triggered by an external magnetic field. The filament device achieves various tunable channel conductivities, which can be achieved in the magneto-responsive material by varying carrier fluid viscosity, volume fraction, cyclic time and external stimulus. Thus all four factors can be studied in depth to understand its effect on achieving tunable channel conductive, stepping closer to memristors. Moreover, neurons in the brain are connected to each other in parallel. Thus, a next step could be designing a sample holder for the material that will allow multiple chains to form in the same material and connected through one point , replicating the multiple connections between neurons and synapses.

References

[1] J. Jiang *et al.*, “2D MoS2 Neuromorphic Devices for Brain-Like Computational Systems,” *Small*, vol. 13, no. 29, pp. 1–11, 2017, doi: 10.1002/smll.201700933.

[2] K. Gacem *et al.*, “Neuromorphic function learning with carbon nanotube based synapses,” *Nanotechnology*, vol. 24, no. 38, 2013, doi: 10.1088/0957-4484/24/38/384013.

[3] S. Lequeux *et al.*, “A magnetic synapse: Multilevel spin-torque memristor with perpendicular anisotropy,” *Sci. Rep.*, vol. 6, pp. 3–5, 2016, doi: 10.1038/srep31510.

[4] C. Zamarreño-Ramos, L. A. Camuñas-Mesa, J. A. Perez-Carrasco, T. Masquelier, T. Serrano-Gotarredona, and B. Linares-Barranco, “On spike-timing-dependent-plasticity, memristive devices, and building a self-learning visual cortex,” *Front. Neurosci.*, no. MAR, 2011, doi: 10.3389/fnins.2011.00026.

[5] G. W. Burr *et al.*, “Neuromorphic computing using non-volatile memory,” *Adv. Phys. X*, vol. 2, no. 1, pp. 89–124, 2017, doi: 10.1080/23746149.2016.1259585.

[6] J.-S. Park, Youngjun, Lee, “Artificial Synapses with Short- and Long-Term Memory for Spiking Neural Networks Based on Renewable Materials,” *ASC Nano*, vol. 11, no. 9, pp. 8692–8696, 2017, doi: 10.1021/acsnano.7b03347.SEM.

[7] A. Citri and R. C. Malenka, “Synaptic Plasticity : Multiple Forms , Functions , and Mechanisms,” *Neuropsychopharmacol*, vol. 33, pp. 18–41, 2008.

[8] L. Q. Zhu, C. J. Wan, L. Q. Guo, Y. Shi, and Q. Wan, “Artificial synapse network on inorganic proton conductor for neuromorphic systems,” *Nat. Commun.*, vol. 5, pp. 6–8, 2014, doi: 10.1038/ncomms4158.

[9] M. H. Hennig, “Theoretical models of synaptic short term plasticity,” *Front. Comput. Neurosci.*, no. APR 2013, pp. 13–14, 2013, doi: 10.3389/fncom.2013.00045.

[10] X. Zhang *et al.*, “Emulating short-term and long-term plasticity of bio-synapse based on

cu/a-si/pt memristor," *IEEE Electron Device Lett.*, vol. 38, no. 9, pp. 1208–1211, 2017, doi: 10.1109/LED.2017.2722463.

[11] W. G. Zucker, Robert S, Regehr, "Short-Term Synaptic Plasticity," *Annu. Rev. Physiol.*, vol. 64, pp. 355–405, 2002.

[12] A. Ramirez and M. R. Arbuckle, "Synaptic Plasticity: The Role of Learning and Unlearning in Addiction and Beyond," *Biol. Psychiatry*, vol. 80, no. 9, pp. e73–e75, 2016, doi: 10.1016/j.biopsych.2016.09.002.

[13] K. M. MacLeod, T. K. Horiuchi, and C. E. Carr, "A role for short-term synaptic facilitation and depression in the processing of intensity information in the auditory brain stem," *J. Neurophysiol.*, vol. 97, no. 4, pp. 2863–2874, 2007, doi: 10.1152/jn.01030.2006.

[14] J. R. Whitlock, A. J. Heynen, M. G. Shuler, and M. F. Bear, "Learning induces long-term potentiation in the hippocampus," *Science (80-.).*, vol. 313, no. 5790, pp. 1093–1097, 2006, doi: 10.1038/375400a0.PMID.

[15] T. Ohno, T. Hasegawa, T. Tsuruoka, K. Terabe, J. K. Gimzewski, and M. Aono, "Short-term plasticity and long-term potentiation mimicked in single inorganic synapses," *Nat. Mater.*, vol. 10, no. 8, pp. 591–595, 2011, doi: 10.1038/nmat3054.

[16] A. J. Arnold, A. Razavieh, J. R. Nasr, D. S. Schulman, C. M. Eichfeld, and S. Das, "Mimicking Neurotransmitter Release in Chemical Synapses via Hysteresis Engineering in MoS2 Transistors," *ACS Nano*, vol. 11, no. 3, pp. 3110–3118, 2017, doi: 10.1021/acsnano.7b00113.

[17] S. L. Jackman and W. G. Regehr, "The Mechanisms and Functions of Synaptic Facilitation," *Neuron*, vol. 94, no. 3, pp. 447–464, 2017, doi: 10.1016/j.neuron.2017.02.047.

[18] P. Y. Deng and V. A. Klyachko, "The diverse functions of short-term plasticity components in synaptic computations," *Commun. Integr. Biol.*, vol. 4, no. 5, pp. 543–548,

2011, doi: 10.4161/cib.15870.

[19] W. G. Regehr, “Short-term presynaptic plasticity,” *Cold Spring Harb. Perspect. Biol.*, vol. 4, no. 7, pp. 1–19, 2012, doi: 10.1101/cshperspect.a005702.

[20] H. Lavian and A. Korngreen, “Short term depression shapes information transmission in a constitutively active GABAergic synapse,” *Sci. Rep.*, vol. 9, pp. 0–2, 2019, doi: 10.1101/370833.

[21] A. Ghanbari, A. Malyshev, M. Volgushev, and I. H. Stevenson, “Estimating short-term synaptic plasticity from pre- And postsynaptic spiking,” *PLOS Comput. Biol.*, 2017, doi: 10.1101/156687.

[22] D. B. Strukov, G. S. Snider, D. R. Stewart, and R. S. Williams, “The missing memristor found,” *Nature*, vol. 459, no. 7250, p. 1154, 2009, doi: 10.1038/nature08166.

[23] M. E. Fouda, A. S. Elwakil, and A. G. Radwan, “Pinched hysteresis with inverse-memristor frequency characteristics in some nonlinear circuit elements,” *Microelectronics J.*, vol. 46, no. 9, pp. 834–838, 2015, doi: 10.1016/j.mejo.2015.06.019.

[24] Y. Van De Burgt *et al.*, “A non-volatile organic electrochemical device as a low-voltage artificial synapse for neuromorphic computing,” *Nat. Mater.*, vol. 16, no. 4, pp. 414–418, 2017, doi: 10.1038/NMAT4856.

[25] C. Sen Yang *et al.*, “A Synaptic Transistor based on Quasi-2D Molybdenum Oxide,” *Adv. Mater.*, vol. 29, no. 27, p. 19262647, 2017, doi: 10.1002/adma.201700906.

[26] Z. Lv, Y. Zhou, S. Han, and V. A. L. Roy, “From biomaterial-based data storage to bio-inspired artificial synapse,” *Mater. day*, vol. 21, no. 5, pp. 537–552, 2018.

[27] L. Chua, “Resistance switching memories are memristors,” *Appl. Phys. A*, vol. 102, pp. 765–783, 2011, doi: 10.1007/978-3-319-76375-0_6.

[28] S. H. Jo, T. Chang, I. Ebong, B. B. Bhadviya, P. Mazumder, and W. Lu, “Nanoscale memristor device as synapse in neuromorphic systems,” *Nano Lett.*, vol. 10, no. 4, pp.

1297–1301, 2010, doi: 10.1021/nl904092h.

[29] J. J. Wang, Zhongrui, Joshi, Saumil, Saval'ev, Sergey E., Jiang, Hao, Midya, Rivu, Lin, Peng, Hu, Miao, Ge, Ning, Strachen, John Paul, Li, Zhiyong, Wu, Qing, Barnell, Mark, Li, Geng-Lin, Xin, Huolin L., Williams, R.Stanley, Xia, Qiangei, Yang, "Memristors with diffusive dynamics as synaptic emulators for neuromorphic computing," *Nat. Mater.*, vol. 16, pp. 101–108, 2016.

[30] Y. Van De Burgt, A. Melianas, S. T. Keene, G. Malliaras, and A. Salleo, "Organic electronics for neuromorphic computing," *Nat. Electron.*, vol. 1, no. 7, pp. 386–397, 2018, doi: 10.1038/s41928-018-0103-3.

[31] S. Yu, B. Gao, Z. Fang, H. Yu, J. Kang, and H. S. P. Wong, "A low energy oxide-based electronic synaptic device for neuromorphic visual systems with tolerance to device variation," *Adv. Mater.*, vol. 25, no. 12, pp. 1774–1779, 2013, doi: 10.1002/adma.201203680.

[32] M. S. Lee, J. W. Lee, C. H. Kim, B. G. Park, and J. H. Lee, "Implementation of short-term plasticity and long-term potentiation in a synapse using si-based type of charge-trap memory," *IEEE Trans. Electron Devices*, vol. 62, no. 2, pp. 569–573, 2015, doi: 10.1109/TED.2014.2378758.

[33] D. J. Inman, "Smart Materials and Structures," *CISM Int. Cent. Mech. Sci. Courses Lect.*, vol. 488, pp. 139–149, 2007, doi: 10.1007/978-3-211-70963-4_8.

[34] Y. Kim *et al.*, "A bioinspired flexible organic artificial afferent nerve," *Science (80-.).*, vol. 360, no. 6392, pp. 998–1003, 2018, doi: 10.1126/science.aao0098.

[35] A. G. Olabi and A. Grunwald, "Design and application of magneto-rheological fluid," *Mater. Des.*, vol. 28, no. 10, pp. 2658–2664, 2007, doi: 10.1016/j.matdes.2006.10.009.

[36] V. V. Mody, A. Singh, and B. Wesley, "Basics of magnetic nanoparticles for their application in the field of magnetic fluid hyperthermia," *Eur. J. Nanomedicine*, vol. 5, no.

1, pp. 11–21, 2013, doi: 10.1515/ejnm-2012-0008.

[37] V. Marghussian, “Magnetic Properties of Nano-Glass Ceramics,” in *Nano-Glass Ceramics*, 2015, pp. 181–223.

[38] D. Maity, G. Kandasamy, and A. Sudame, “Superparamagnetic iron oxide nanoparticles for cancer theranostic applications,” *Nanotheranostics Appl. Limitations*, pp. 245–276, 2019, doi: 10.1007/978-3-030-29768-8_12.

[39] T. D. Clemons, R. H. Kerr, and A. Joos, “Multifunctional magnetic nanoparticles: Design, synthesis, and biomedical applications,” in *Comprehensive Nanoscience and Nanotechnology*, vol. 3, 2019, pp. 193–210.

[40] K. Them, “On magnetic dipole-dipole interactions of nanoparticles in magnetic particle imaging,” *Phys. Med. Biol.*, vol. 62, no. 14, pp. 5623–5639, 2017, doi: 10.1088/1361-6560/aa70ca.

[41] B. K. Kumbhar, S. R. Patil, and S. M. Sawant, “Synthesis and characterization of magneto-rheological (MR) fluids for MR brake application,” *Eng. Sci. Technol. an Int. J.*, vol. 18, no. 3, pp. 432–438, 2015, doi: 10.1016/j.jestch.2015.03.002.

[42] R. Zhao, Y. Kim, S. A. Chester, P. Sharma, and X. Zhao, “Mechanics of hard-magnetic soft materials,” *J. Mech. Phys. Solids*, vol. 124, pp. 244–263, 2019, doi: 10.1016/j.jmps.2018.10.008.

[43] M. Ashtiani, S. H. Hashemabadi, and A. Ghaffari, “A review on the magnetorheological fluid preparation and stabilization,” *J. Magn. Magn. Mater.*, vol. 374, pp. 711–715, 2015, doi: 10.1016/j.jmmm.2014.09.020.

[44] I. Bica, “Influence of the transverse magnetic field intensity upon the electric resistance of the magnetorheological elastomer containing graphite microparticles,” *Mater. Lett.*, vol. 63, no. 26, pp. 2230–2232, 2009, doi: 10.1016/j.matlet.2009.07.032.

[45] T. Liu and Y. Xu, “Magnetorheological Elastomers: Materials and Applications,” *Smart*

Funct. Soft Mater., vol. 9, 2019, doi: 10.5772/intechopen.85083.

[46] T. Bloemen, Maarten, Brullot, Ward, Luong, Tai Thien, Geukens, Nick, Gils, Ann, Verbiest, M. J. Mondrinos, X. Chen, M. R. Gandhi, F. K. Ko, and P. I. Lelkes, "Improved functionalization of oleic acid-coated iron oxide nanoparticles for biomedical applications," *J. Nanoparticle Res.*, vol. 14, no. 9, 2012, doi: 10.1002/jbm.a.

[47] M. Machovsky, M. Mrlik, I. Kuritka, V. Pavlinek, and V. Babayan, "Novel synthesis of core-shell urchin-like ZnO coated carbonyl iron microparticles and their magnetorheological activity," *RSC Adv.*, vol. 4, no. 2, pp. 996–1003, 2014, doi: 10.1039/c3ra44982c.

[48] X. Dong, Y. Tong, N. Ma, M. Qi, and J. Ou, "Properties of cobalt nanofiber-based magnetorheological fluids," *RSC Adv.*, vol. 5, no. 18, pp. 13958–13963, 2015, doi: 10.1039/c4ra14149k.

[49] J. Soares, Paula, Alver, Ana, Pereira, Laura, Coutinho, Joana, Ferreira, Isabel, Novo, Carlos, Borges, "Effects of surfactants on the magnetic properties of iron oxide colloids," *J. Colloid Interface Sci.*, vol. 419, pp. 46–51, 2014.

[50] Q. Wang, Daoming, Zi, Bin, Zeng, Yishan, Hou, Youfu, Meng, "Temperature-dependant material properties of the components of magnetorheological fluids," *J. Mater. Sci.*, vol. 49, pp. 8459–8470, 2014, doi: 10.1007/s10853-009-3417-8.

[51] M. Abe, Hiroya, Naka, Takashi, Sato, Kazuyoshi, Suzuki, Yoshikazu, Nakano, "Shape-Controlled Syntheses of Magnetite Microparticles and Their Magnetorheology," *Int. J. Mol. Sci.*, vol. 20, no. 15, 2019, doi: 10.1122/1.550614.

[52] M. Mohamed, Norzilawati, Ubaidallah, Mazlan, Saiful Amri, Choi, Seung-bok, Abdul Aziz, Siti Aishah, Sugimoto, "The effect of particle shapes on the field-dependant rheological properties of magnetorheological greases," *Int. J. Mol. Sci.*, vol. 20, no. 7, 2019, doi: 10.1039/b906505a.

[53] Z. Laherisheth, K. Parekh, and R. V. Upadhyay, “Role of inter-particle force between micro and nano magnetic particles on the stability of magnetorheological fluid,” *AIP Adv.*, vol. 7, no. 2, pp. 2–3, 2017, doi: 10.1063/1.4975635.

[54] G. Dassisti, Michele, Brunetti, *Materials Science and Materials Engineering*. 2021.

[55] M. Wang, L. He, and Y. Yin, “Magnetic field guided colloidal assembly,” *Mater. Today*, vol. 16, no. 4, pp. 110–116, 2013, doi: 10.1016/j.mattod.2013.04.008.

[56] X. Yang, Y. Huang, Y. Hou, H. Wu, R. Xu, and P. K. Chu, “An experimental study of magnetorheological fluids on electrical conductivity property,” *J. Mater. Sci. Mater. Electron.*, vol. 28, no. 11, pp. 8130–8135, 2017, doi: 10.1007/s10854-017-6519-0.

[57] F. F. Fang, I. B. Jang, and H. J. Choi, “Single-walled carbon nanotube added carbonyl iron suspension and its magnetorheology,” *Diam. Relat. Mater.*, vol. 16, no. 4-7 SPEC. ISS., pp. 1167–1169, 2007, doi: 10.1016/j.diamond.2006.11.069.

[58] B. J. Park, K. H. Song, and H. J. Choi, “Magnetic carbonyl iron nanoparticle based magnetorheological suspension and its characteristics,” *Mater. Lett.*, vol. 63, no. 15, pp. 1350–1352, 2009, doi: 10.1016/j.matlet.2009.03.013.

[59] S. T. Lim, M. S. Cho, I. B. Jang, and H. J. Choi, “Magnetorheological characterization of carbonyl iron based suspension stabilized by fumed silica,” *J. Magn. Magn. Mater.*, vol. 282, pp. 170–173, 2004, doi: 10.1016/j.jmmm.2004.04.040.

[60] J. S. Choi, B. J. Park, M. S. Cho, and H. J. Choi, “Preparation and magnetorheological characteristics of polymer coated carbonyl iron suspensions,” *J. Magn. Magn. Mater.*, vol. 304, no. 1, pp. 374–376, 2006, doi: 10.1016/j.jmmm.2006.02.055.

[61] E. Esmaeilnezhad, H. Jin Choi, M. Schaffie, M. Gholizadeh, M. Ranjbar, and S. Hyuk Kwon, “Rheological analysis of magnetite added carbonyl iron based magnetorheological fluid,” *J. Magn. Magn. Mater.*, vol. 444, pp. 161–167, 2017, doi: 10.1016/j.jmmm.2017.08.023.

[62] I. B. Jang, H. B. Kim, J. Y. Lee, J. L. You, H. J. Choi, and M. S. Jhon, “Role of organic coating on carbonyl iron suspended particles in magnetorheological fluids,” *J. Appl. Phys.*, vol. 97, no. 10, p. 2020, 2005, doi: 10.1063/1.1853835.

[63] O. T. Sandler, Sarah E., Fellows, Benjamin, Mefford, “Best Practices for Characterization of Magnetic Nanoparticles for Biomedical Applications,” *Anal. Chem.*, vol. 91, no. 22, pp. 14159–14169, 2019, doi: 10.1038/nmat3558.

[64] H. A. Fonseca, E. Gonzalez, J. Restrepo, C. A. Parra, and C. Ortiz, “Magnetic effect in viscosity of magnetorheological fluids,” *J. Phys. Conf. Ser.*, vol. 687, no. 1, 2016, doi: 10.1088/1742-6596/687/1/012102.

[65] A. Ali *et al.*, “Synthesis, characterization, applications, and challenges of iron oxide nanoparticles,” *Nanotechnol. Sci. Appl.*, vol. 9, pp. 49–67, 2016, doi: 10.2147/NSA.S99986.

[66] J. Gupta, Ranjeetkumar, Pancholi, Ketan, De Sa, Rulston, Murray, Duncan, Huo, Dehong, Droubi, Ghazi, White, Maggie, Njuguna, “Effect of Oleic Acid Coating of Iron Oxide Nanoparticles on Properties of Magnetic Polyamide-6 Nanocomposite,” *Adv. Process. Manuf. Appl. Magn. Mater.*, no. 71, pp. 3119–3128, 2019.

[67] A. Bu, “Iron Oxide Nanoparticles, Characteristics and Applications | Sigma-Aldrich,” pp. 2–3, 2018, [Online]. Available: http://www.sigmaaldrich.com/technical-documents/articles/technology-spotlights/iron-oxide-nanoparticles-characteristics-and-applications.html.

[68] B. Sodipo and A. Abdulaziz, “A sonochemical approach to the direct surface functionalization of superparamagnetic iron oxide nanoparticles with (3-aminopropyl)triethoxysilane,” *Beilstein J. Nanotechnol.*, vol. 5, pp. 1472–1476, 2014, doi: 10.1021/cm050280n.

[69] S. Masur, B. Zingsem, T. Marzi, R. Meckenstock, and M. Farle, “Characterization of the

oleic acid/iron oxide nanoparticle interface by magnetic resonance," *J. Magn. Magn. Mater.*, vol. 415, pp. 8–12, 2016, doi: 10.1016/j.jmmm.2016.03.045.

[70] D. Cruze, H. Gladston, S. Loganathan, T. Dharmaraj, and S. M. Solomon, "Study on Magnatec oil-based MR fluid and its damping efficiency using MR damper with various annular gap configurations," *Energy, Ecol. Environ.*, vol. 6, no. 1, pp. 44–54, 2021, doi: 10.1007/s40974-020-00170-6.

[71] A. Ronzova, M. Sedlacik, and M. Cvek, "Magnetorheological fluids based on core–shell carbonyl iron particles modified by various organosilanes: synthesis, stability and performance," *Soft Matter*, vol. 17, no. 5, pp. 1299–1306, 2021, doi: 10.1039/d0sm01785j.

[72] M. A. Willard and M. Daniil, "Nanocrystalline Soft Magnetic Alloys Two Decades of Progress," *Handb. Magn. Mater.*, vol. 21, pp. 173–342, 2013, doi: 10.1016/B978-0-444-59593-5.00004-0.

[73] M. Imran *et al.*, "Synthesis of highly stable γ-Fe2O3 ferrofluid dispersed in liquid paraffin, motor oil and sunflower oil for heat transfer applications," *RSC Adv.*, vol. 8, no. 25, pp. 13970–13975, 2018, doi: 10.1039/c7ra13467c.

[74] R. N. Laurent, Sophie, Forge, Delphine, Port, Marc, Roch, Alain, Robic, Caroline, Elst, Luce Vander, Muller, "Magnetic iron oxide nanoparticles : Synthesis, Stabilization,Vectorization,Physicochemical Characterizations,and Biological Applications," *Chemcial Rev.*, vol. 108, no. 6, pp. 2064–2110, 2008.

[75] K. Petcharoen and A. Sirivat, "Synthesis and characterization of magnetite nanoparticles via the chemical co-precipitation method," *Mater. Sci. Eng. B Solid-State Mater. Adv. Technol.*, vol. 177, no. 5, pp. 421–427, 2012, doi: 10.1016/j.mseb.2012.01.003.

[76] W. Wei and Z. Wang, "Investigation of Magnetic Nanoparticle Motion under a Gradient Magnetic Field by an Electromagnet," *J. Nanomater.*, vol. 2018, p. 19, 2018, doi: 10.1155/2018/6246917.

[77] M. T. López-López, J. D. G. Durán, A. V. Delgado, and F. González-Caballero, “Stability and magnetic characterization of oleate-covered magnetite ferrofluids in different nonpolar carriers,” *J. Colloid Interface Sci.*, vol. 291, no. 1, pp. 144–151, 2005, doi: 10.1016/j.jcis.2005.04.099.

[78] M. Hajiyan, S. Ebadi, S. Mahmud, M. Biglarbegian, and H. Abdullah, “Experimental investigation of the effect of an external magnetic field on the thermal conductivity and viscosity of Fe 3 O 4 –glycerol,” *J. Therm. Anal. Calorim.*, vol. 135, no. 2, pp. 1451–1464, 2019, doi: 10.1007/s10973-018-7531-1.

[79] Q. Li, C. W. Kartikowati, S. Horie, T. Ogi, T. Iwaki, and K. Okuyama, “Correlation between particle size/domain structure and magnetic properties of highly crystalline Fe3O4 nanoparticles,” *Sci. Rep.*, vol. 7, no. 1, pp. 23–24, 2017, doi: 10.1038/s41598-017-09897-5.

[80] N. Usov and B. Liubimov, “Magnetic nanoparticle traveling in external magnetic field,” *arXiv Prepr. arXiv1407.3964*, pp. 1–14, 2014, [Online]. Available: http://arxiv.org/abs/1407.3964.

[81] A. Asadi *et al.*, “Effect of sonication characteristics on stability, thermophysical properties, and heat transfer of nanofluids: A comprehensive review,” *Ultrason. Sonochem.*, vol. 58, pp. 5–7, 2019, doi: 10.1016/j.ultsonch.2019.104701.

[82] V. V. Deshmane and A. V. Patil, “Study of Relation Between Particle Size And Magnetic Saturation of Synthesized Undoped Iron Oxide,” *Int. J. Chem. Phys. Sci.*, vol. 7, no. 2, 2018, doi: 10.30731/ijcps.7.2.2018.8-12.

[83] N. Caterino, B. M. Azmoodeh, and A. Occhiuzzi, “Medium to long term behavior of MR dampers for structural control,” *Smart Mater. Struct.*, vol. 23, no. 11, pp. 6–7, 2014, doi: 10.1088/0964-1726/23/11/117005.

[84] X. G. Huang, Z. Y. Yan, C. Liu, G. H. Li, and J. Wang, “Study on the resistance

properties of magnetorheological elastomer," *Mater. Res. Innov.*, vol. 19, pp. S5924–S5928, 2015, doi: 10.1179/1432891714Z.0000000001223.

[85] M. A. Portillo and G. R. Iglesias, "Magnetic Nanoparticles as a Redispersing Additive in Magnetorheological Fluid," *J. Nanomater.*, vol. 2017, pp. 8–9, 2017, doi: 10.1155/2017/9026219.

[86] Y. Wang, Daoming, Zi, Bin, Zeng, Yishan, Xie, Fangwei, Hou, "Measurement of temperature-dependant mechanical properties of magnetorheological fluids using a parallel disk shear stress tesrin," *J. Mech. Eng. Sci.*, 2015, doi: 10.1177/0954406211402139.

[87] C. Anderson, "Presenting and evaluating qualitative research," *Am. J. Pharm. Educ.*, vol. 74, no. 8, p. 141, 2010, doi: 10.5688/aj7408141.

[88] R. V. Upadhyay, Z. Laherisheth, and K. Shah, "Rheological properties of soft magnetic flake shaped iron particle based magnetorheological fluid in dynamic mode," *Smart Mater. Struct.*, vol. 23, no. 1, p. 2021, 2014, doi: 10.1088/0964-1726/23/1/015002.

[89] G. Wang, Y. Ma, Y. Tong, and X. Dong, "Development of manganese ferrite/graphene oxide nanocomposites for magnetorheological fluid with enhanced sedimentation stability," *J. Ind. Eng. Chem.*, vol. 48, pp. 142–150, 2017, doi: 10.1016/j.jiec.2016.12.032.

[90] J. Roupec *et al.*, "A novel method for measurement of MR fluid sedimentation and its experimental verification," *Smart Mater. Struct.*, vol. 26, no. 10, 2017, doi: 10.1088/1361-665X/aa83f2.

[91] T. D. Truong, V. Q. Nguyen, B. T. Diep, D. H. Q. Le, D. T. Le, and Q. H. Nguyen, "Speed control of rotary shaft at different loading torque using MR clutch," vol. 33, no. 11, p. 57, 2019, doi: 10.1117/12.2515309.

[92] K. Shah, D. Xuan Phu, and S. B. Choi, "Rheological properties of bi-dispersed magnetorheological fluids based on plate-like iron particles with application to a small-

sized damper," *J. Appl. Phys.*, vol. 115, no. 20, pp. 1–3, 2014, doi: 10.1063/1.4879681.

[93] D. S. Jang, Y. D. Liu, J. H. Kim, and H. J. Choi, "Enhanced magnetorheology of soft magnetic carbonyl iron suspension with hard magnetic γ-Fe2O3 nanoparticle additive," *Colloid Polym. Sci.*, vol. 293, no. 2, pp. 641–647, 2015, doi: 10.1007/s00396-014-3475-6.

[94] G. R. Iglesias, M. T. López-López, J. D. G. Durán, F. González-Caballero, and A. V. Delgado, "Dynamic characterization of extremely bidisperse magnetorheological fluids," *J. Colloid Interface Sci.*, vol. 377, no. 1, pp. 153–159, 2012, doi: 10.1016/j.jcis.2012.03.077.

[95] H. Bin Cheng, J. M. Wang, Q. J. Zhang, and N. M. Wereley, "Preparation of composite magnetic particles and aqueous magnetorheological fluids," *Smart Mater. Struct.*, vol. 18, no. 8, p. 2021, 2009, doi: 10.1088/0964-1726/18/8/085009.

[96] F. Barca, T. Caporossi, and S. Rizzo, "Silicone Oil : Different Physical Proprieties and Clinical Applications," *Biomed Res. Int.*, 2014, doi: 10.1155/2014/502143.

[97] L. Aziz, Tariq, Fan, Hong, Khan, Farman Ullah, Haroon, Muhammad, Cheng, "Modified silicone oil types , mechanical properties and applications," *Polym. Bull.*, vol. 76, pp. 2129–2145, 2019.

[98] Y. Xu, G. Liao, and T. Liu, "Magneto-Sensitive Smart Materials and Magnetorheological Mechanism," *Nanofluid Flow Porous Media*, 2020, doi: 10.5772/intechopen.84742.

[99] J. Kwon, Seung Kwon, Jung, Hyo Seung, Choi, Hyoung Jin, Strecker, Zbynek, Roupec, "Effect of octahedral typed iron oxide particles on magnetorheological behavior of carbonyl iron dispersion," *Colloids Surfaces A Physicochem. Eng. Asp.*, vol. 555, pp. 685–590, 2018.